TIME EVOLUTION OF THE XXZ HEISENBERG MODEL

By

WENSHUO LIU

A dissertation submitted to the
Graduate School—New Brunswick
Rutgers, The State University of New Jersey
in partial fulfillment of the requirements
for the degree of
Doctor of Philosophy
Graduate Program in Physics and Astronomy
written under the direction of
Prof. Natan Andrei
and approved by

_____

_____

_____

_____

_____

New Brunswick, New Jersey

October, 2014

ABSTRACT OF THE DISSERTATION

Time Evolution of the XXZ Heisenberg Model

By WENSHUO LIU

Dissertation Director:

Prof. Natan Andrei

The recent advance of techniques in controlling ultracold gases in optical lattice provides a ideal experimental platform to study quantum many-body physics. The almost isolated and highly tunable systems created in these experimental setups are perfect for studying coherent time evolution of closed quantum many-body systems. In this thesis I present an analytical approach on the time evolution of the anisotropic Heisenberg spin chain (XXZ model), which is a fundamental model but has rich dynamics. This approach is developed through generalizing the Yudson contour representation. With this approach I obtain the exact time-dependent wave functions after a quantum quench in an integral form for generic initial states and for any anisotropy Δ. I reformulate the integrals and show their physical interpretation as propagating magnons and their bound states, which were predicted by the "string" solutions of Bethe Ansatz equations. To apply the new approach to specific problems, I calculate the quench dynamics of various observables from some particular initial states: starting from a local Néel state I calculate the time evolution of the antiferromagnetic order parameter–staggered magnetization; starting from a state with consecutive flipped spins I calculate the evolution of the local magnetization, and predict the evolution of the induced spin currents. These results and predictions can be confronted with recently experiments in ultracold gases in optical lattices, and are expected to contribute to the understanding of non-equilibrium physics of isolated many-body systems.

Preface

The main results of this thesis is published in Ref [1, 2]. The work of this thesis was done under the supervision of my advisor, Natan Andrei.

Acknowledgments

I am grateful to my advisor Prof. Natan Andrei, who taught me not only physics itself, but also how to think and research. From him, I got the knowledge of Bethe ansatz, as well as consistent encouragement.

I am grateful to Prof. Joel Lebowitz, who gave much useful, interesting discussion and support to my research.

I am grateful to the friends in my group, specifically Deepak Iyer, Huijie Guan, Garry Goldstein and Paata Kakashvili. The discussion with them were inspiring.

I am also grateful to all those professors who taught me in classes during my graduate study, specifically K. Haule, D. Vanderbilt, L. Ioffe, S. Cheong, E. Yuzbashyan and P Coleman. Particularly for K. Haule, the numerical skills I acquired from his class tuned out to be important for my research. I am also grateful to the NSF research grants that supports my work.

I also want to say thanks to all my friends at Rutgers, who shared the classes, hot pots and basketball court with me. With them the graduate life here is not that tough any more.

I am especially grateful to my wonderful wife Dr. Yajuan Si, who has always been there for me.

Dedication

For my father: Jianqiang Liu

Table of Contents

List of Tables

List of Figures

Chapter 1
Introduction

One of the most important tasks of modern condensed matter physics is to understand the interacting quantum many-body systems. For equilibrium systems, many concepts and theories have been well developed for decades, for example the quasi-particles from Fermi-liquid theory and the universality in phase transition based on renormalization group. One the other hand, the understanding of systems far from equilibrium is still limited nowadays, especially in low dimension where quantum fluctuation is enhanced. There is not even a unified framework available and each direction or problem requires its own set of ideas. Understanding of the non-equilibrium many-body systems are not only theoretically fundamental, but also important for potential applications such as quantum information processing and quantum computation [8]. They are also related to non-equilibrium questions in other areas of physics, e.g., the preheating of the early universe in cosmology [9].

As a very generic scenario, a physical system can be driven out of equilibrium in many different ways, leading to totally different phenomenon. As an example, in the classical transport problem, the system is driven by a small external field and generate currents. It was well understood under the framework of linear response theory [10], because it can be considered as a perturbation from equilibrium situation. However, it is of less interest because in this process coherent dynamics is destroyed by dissipation. When coherent dynamics comes into play, thing becomes much more interesting. There are recent works on non-equilibrium phase transition driven by current flow across the system [11, 12], where the unitary Hamiltonian dynamics and dissipative Liouvillian dynamics compete and lead to highly non-trivial physics [13]. In this thesis, I will mostly discuss the coherent dynamics of closed many-body systems, the study of which was largely enriched by the achievement of ultracold atoms in experiments.

1.1 Ultracold Gases in Optical Lattice

In the last two decades, breakthroughs in experimental techniques have allowed people to produce, control and observe dilute ultracold atomic gases in optical lattice [3]. At the beginning, aiming to experimentally study the Bose-Einstein condensate(BEC) [14, 15, 16], the dilute gases of alkali atoms

were cooled down by laser and evaporative cooling techniques to temperature in the nanokelvin range, sufficiently below the transition. Since then, a few crucial techniques were developed eventually, equipping the ultracold gas systems to be a perfect platform to study isolated many-body systems.

1.1.1 Feshbach Resonance

The first important technique is to tune the atom-atom interaction strength by Feshbach resonances [17, 18].

Let's start with the two atom scattering process. Under the low temperature of ultracold atoms, the typical kinetic energy of relative motion of atoms is much lower than the centrifugal barrier due to the angular momentum $l \neq 0$. So the scattering of atoms is dominated by the lowest-angular-momentum collisions, typically the s-wave scattering. Under this condition, it is commonly assumed the atoms scatter with a pseudopotential,

$$V(\mathbf{r})(\dots) = \frac{4\pi\hbar^2 a}{2M_r}\delta(\mathbf{r})\frac{\partial}{\partial r}(r\dots), \tag{1.1}$$

where M_r is the reduced mass of the relative motion, and a is called the scattering length, usually taken as an experimentally determined parameter. This so-called *pseudopotential approximation* gives the exact scattering amplitude

$$f(k) = -\frac{a}{1+ika} \tag{1.2}$$

of s-wave scattering, and is valid in a wide range of experimental situations. With this approximation, the interaction strength between atoms

$$g = \frac{4\pi\hbar^2 a}{2M_r} \tag{1.3}$$

is fixed by one parameter: the scattering length.

Under the low density of ultracold gases, the interaction between atoms is generally expected to be very week (considering the ratio between the scattering length and the mean-inter-atom distance). But when Feshbach resonance occurs, the interaction can be largely enhanced. Consider the collision of two atoms. For different spin configurations of the two atoms (including the electron spins and the nuclear spins), the inter-atom potentials are different. They are called different collision channels. Consider a simple situation with two channels shown in Fig. 1.1. The two atoms are prepared in the open channel with a small incident energy. In the course of the collision, if one of the bound state energies in the closed channel is close to the incident energy, a scattering resonance occurs. The relative position of the closed channel with respect to the open channel can be tuned by varying the external magnetic field. On a phenomenology level, the scattering length in a Feshbach resonance

can be described by

$$a(B) = a_{bg}(1 - \frac{\Delta B}{B - B_0}) \tag{1.4}$$

where a_{bg} is the off-resonance background scattering length given by the open channel alone. The parameters ΔB and B_0 describe the width and position of the resonance. The positive and negative scattering length represent repulsive and attractive interaction respectively. At the resonance magnetic field B_0, the scattering length diverges, indicating the tunability of the interaction strength to over several orders of magnitude.

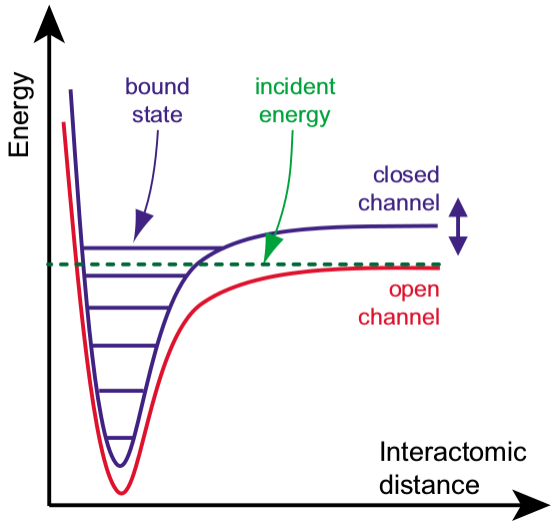

Figure 1.1: Mechanism of Feshbach resonance. Reproduced from Ref. [3].

Above I sketch the basic physics of the Feshbach resonance. For a detailed review on this topic, see Ref. [19]. The ability to artificially tune the interaction strength of ultracold atoms is obviously a very useful technique to probe different regimes of quantum many-body systems. Some famous examples include the BEC-BCS crossover for fermionic liquid [20] and the transition between superfluid and Mott-insulator for bosons in a lattice [21].

1.1.2 Optical Lattice

The second influential technique is to confine the gases in optical lattices, which open the path of simulating a series of condensed-matter models with ultracold atoms. The confinement of laser on neutral atoms originates from the dipole force

$$\mathbf{F} = \frac{1}{2}\alpha(\omega_L)\nabla[|\mathbf{E}(r)|^2] \tag{1.5}$$

due to a spatially varying ac Stark shift. Here $|\mathbf{E}(r)|^2$ is the time-averaged light intensity and $\alpha(\omega_L)$ is the polarizability. The laser frequency ω_L should be tuned away from any atomic resonances

to avoid atomic transitions. With proper approximation under the experimental conditions, the potential of the dipole force is proportional to the intensity of the laser $V_{dip}(\mathbf{r}) \sim I(\mathbf{r})$. Then by overlapping two contour-propagating laser beams, an optical standing wave can be formed, and a periodic potential experienced by the atoms with period $\lambda/2$ can be set up. Furthermore, by superimposing two or three orthogonal standing waves of lasers, the ultracold atoms can be confined within either 1-dimensional tubes or 0-dimensional quantum dots, as shown schematically in Fig. 1.2. It should be emphasized that by enlarging the detuning from an atomic frequency, the optical potential can be considered purely conservative and defect-free, so an isolated system on lattice is achievable. The hyperfine states of alkali atoms such as ^{87}Rb can be identified with a pseudo-spin degree of freedom, leading to even richer physics.

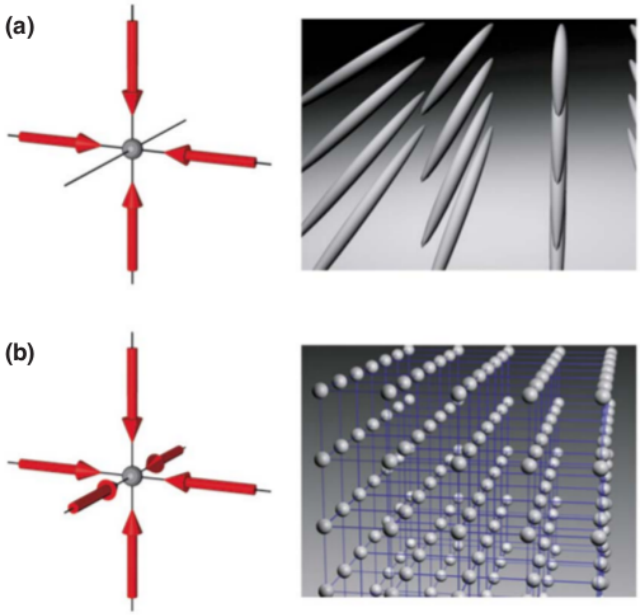

Figure 1.2: Schematic optical lattice. Reproduced from Ref. [3].

With the tunable periodic potential, a lattice model with many-body interaction can be easily set up. In the center of a 3-D optical lattice, for distance much smaller than the laser beam waist, the trapping potential can be approximated as

$$V_p(x, y, z) = V_0(\sin^2 kx + \sin^2 ky + \sin^2 kz), \tag{1.6}$$

where $k = 2\pi/\lambda$ is the wave vector of the laser, and V_0 is the tunable parameter characterizing the trapping depth. The recoil energy $E_r = \hbar^2 k^2/2m$ provides a natural measure of the energy scale in the optical lattice. And the deep lattice limit refers to $V_0 \gg E_r$. Within a sinusoidal potential like (1.6), the single-particle eigenstate is the Bloch wave $\psi_{n,\mathbf{q}}(\mathbf{r})$. Under the ultralow temperature,

considering only the lowest band, its energy is

$$E(\mathbf{q}) = -2J(\cos q_x d + \cos q_y d + \cos q_z d) + \text{const.}, \tag{1.7}$$

where $d = \lambda/2$ is the lattice constant, and the band width parameter J can be calculated by the 1-D Mathieu equation,

$$J \approx \frac{4}{\sqrt{\pi}} E_r \left(\frac{V_0}{E_r}\right)^{3/4} \exp\left[-2\left(\frac{V_0}{E_r}\right)^{1/2}\right]. \tag{1.8}$$

For a deep lattice, it is convenient to use the Wannier functions $w_{\mathbf{R}}(\mathbf{r})$ as a basis, which are centered at lattice sites $\mathbf{R}$, and related with the Bloch wave by

$$\psi_{0,\mathbf{q}}(\mathbf{r}) = \sum_{\mathbf{R}} w_{\mathbf{R}}(\mathbf{r}) e^{i\mathbf{q}\cdot\mathbf{R}}. \tag{1.9}$$

Denote the annihilation operator on the Wannier state to be $\hat{a}_{\mathbf{R}}$. Then the free particles on the lattice is captured by the Hamiltonian

$$\hat{H} = \sum_{\mathbf{R},\mathbf{R}'} J(\mathbf{R}-\mathbf{R}') \hat{a}^\dagger_{\mathbf{R}} \hat{a}_{\mathbf{R}'}. \tag{1.10}$$

In the limit $V_0 \gg E_r$, $J(\mathbf{R}-\mathbf{R}')$ is non-zero only for nearest neighbors, and equal to J given by (1.8). Next, let's add interaction. Within the pseudopotential approximation (1.1), the interaction between bosons takes the form

$$\hat{V} = \frac{g}{2} \int dr^3 \hat{\psi}^\dagger(\mathbf{r}) \hat{\psi}^\dagger(\mathbf{r}) \hat{\psi}(\mathbf{r}) \hat{\psi}(\mathbf{r}), \tag{1.11}$$

where $\hat{\psi}(\mathbf{r}) = \sum_{\mathbf{R}} w(\mathbf{r}-\mathbf{R}) \hat{a}_{\mathbf{R}}$ is the annihilation operator at point $\mathbf{r}$. Written in the Wannier basis, the interaction is dominated by the on-site term

$$\hat{V} = \sum_{\mathbf{R}} \frac{U}{2} \hat{n}_{\mathbf{R}} (\hat{n}_{\mathbf{R}} - 1), \tag{1.12}$$

where $\hat{n}_{\mathbf{R}} = \hat{a}^\dagger_{\mathbf{R}} \hat{a}_{\mathbf{R}}$, and

$$U = g \int dr^3 |w_{\mathbf{R}}(\mathbf{r})|^4 = \sqrt{\frac{8}{\pi}} k a E_r \left(\frac{V_0}{E_r}\right)^{3/4}. \tag{1.13}$$

The many-body Hamiltonian $\hat{H} + \hat{V}$ we introduced above is apparently the Bose-Hubbard model.

The optical lattice not only reduces the dimensions of ultracold gases and thus enhances interactions, but also provide a new way of tuning the parameters of the ultracold atomic systems. By adjusting the laser intensity, the depth of the potential wells can be changed, and therefore the tunneling rate of atoms between adjacent wells, as a typical parameter of a Hamiltonian, can be controlled. As an example, the Bose-Hubbard model undergoes a quantum phase transition from

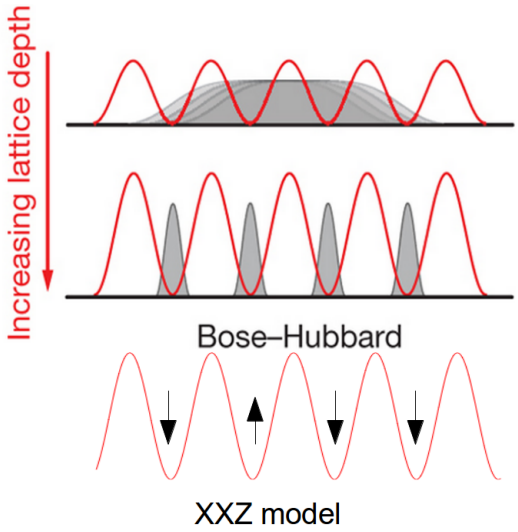

Figure 1.3: The anisotropic Heisenberg model can be realized by suppressing the charge fluctuation of the Bose-Hubbard model, in experiments with ultracold atomic gases.

superfluid to Mott-insulator when the ratio of the on-site interaction to the tunneling rate U/J is tuned up [22]. This can be achieved in two ways: enlarge the scattering length and therefore increase the interaction U by Feshbach resonance, or raise the optical potential and therefore decrease the tunneling rate t. Both of the methods have been used in experiment to drive the transition. Generally, the laser frequency is off-resonant to the hyperfine-structure splitting. But since the hyperfine states are identified as pseudo-spins, a near-resonant light field can lead to the situation where different magnetic sublevels experience different potentials. The spin-dependent optical lattice potential offers more freedoms to tune the model parameters for different spin states. It is particularly useful in adjusting the isotropy of the Heisenberg model, as discussed later.

1.1.3 Experimental Realization of a Quantum Spin Chains

In experiments with ultracold gases, the Heisenberg spin chain can be implemented by freezing the charge fluctuation of a Bose-Hubbard model. As introduced before, a Bose-Eistein condensate can be loaded into a 1-D optical lattice, realized by the Bose-Hubbard model

$$H_{BH} = \sum_{ij\sigma}[t_{ij\sigma}a^{\dagger}_{i\sigma}a_{j\sigma} + h.c.] + \sum_{i} U_{\uparrow\downarrow}n_{i\uparrow}n_{i\downarrow} + \frac{1}{2}\sum_{i\sigma} U_{\sigma\sigma}(n_{i\sigma}-1)n_{i\sigma} - \sum_{i}\mu_{i\sigma}n_{i\sigma} \qquad (1.14)$$

where $a^{\dagger}_{i\sigma}/a_{i\sigma}$ is the bosonic creation/annihilation operator in the Wannier basis. $n_{i\sigma} = a^{\dagger}_{i\sigma}a_{i\sigma}$ is the corresponding occupation number. σ represents the internal hyperfine states, identifying a (pseudo) spin, $\sigma = \uparrow, \downarrow$. The hopping and interaction parameters $t_{ij\sigma}$ and $U_{\sigma\sigma'}$ are given by overlaps of Wannier orbitals. Making use of superposition of polarized laser beams, the spin-dependent

potentials [23, 24, 25] are generated. In the strong-interaction limit $t_{ij\sigma} \ll U_{\sigma\sigma'}$ and unit filling, the charge fluctuation is suppressed, and the model is equivalently mapped onto the anisotropic Heisenberg model (XXZ model) [26, 27]

$$H_{XXZ} = \sum_{ij} [J_{\perp}^{ij}(S_i^x S_j^x + S_i^y S_j^y) + J_z^{ij} S_i^z S_j^z] \tag{1.15}$$

with the superexchange parameters given by

$$\begin{aligned} J_z &= \frac{2t_\uparrow^2 + 2t_\downarrow^2}{U_{\uparrow\downarrow}} - \frac{4t_\uparrow^2}{U_{\uparrow\uparrow}} - \frac{4t_\downarrow^2}{U_{\downarrow\downarrow}} \\ J_\perp &= -\frac{4t_\uparrow t_\downarrow}{U_{\uparrow\downarrow}} \end{aligned} \tag{1.16}$$

This realization of the Heisenberg spin chain is depicted in Fig. 1.3. The anisotropy $\Delta_{ij} = J_z^{ij}/J_\perp^{ij}$ can be tuned to a large extent by properly choosing the lattice and interaction parameters. Besides, the sign of J_z^{ij} can also be changed between ferromagnetic ($J_z^{ij} < 0$) and antiferromagnetic ($J_z^{ij} > 0$) using the double-well potentials [28]. In some very recent work, the time-dependent configuration of the whole spin chain can even be monitored [29, 5] thanks to the techniques of single-atom-resolved detection [30, 31].

Recent Developed Techniques

The techniques I mentioned above build up the foundation of the experiments with ultracold atoms. Recently, more techniques are developed to detect more exotic properties. Let me mention a few of them. First, in the past few years, a numbers of high-resolution imaging techniques, including high-resolution absorption, fluorescence and electron microscope-based image, were established. They can provides snapshots of single-atom resolved particle distribution on a lattice, revealing complex spatial correlations between particles. Second, by rotating a ultracold gas confined in a 2-D harmonic well with the frequency close to the trapping frequency, a Landau-like single-particle spectrum can be obtained. Such a method is proposed to mimic the quantum Hall effect and therefore study the topological properties. Last but not the least, using a tightly focused laser beam together with a microwave field, the spin of a single atom can be flipped at a predetermined lattice site [32]. With this technique, arbitrary spin patterns can be created on a lattice, providing a ideal way to prepare the initial state of a quantum quench, as discussed later. For a review of the recent development on techniques with ultracold quantum gases, see Ref. [33].

Above I depict a picture of artificially engineered quantum systems with high controllability, which almost fulfill Feynman's idea of quantum simulator [34]: instead of solving the highly complex theory on quantum many-body systems, the model could be tested directly by the artificial system. Unlike the conventional subjects of condensed matter physics such as electrons in solids

who inevitably couples to environment, the ultracold gases are almost isolated with a long coherent time, and can be described by fundamental models (e.g. Hubbard, Lie-Liniger etc.) with high accuracy, thus are perfect playgrounds for understanding non-equilibrium dynamics. One remarkable feature of the ultracold gases is their controllability, from geometry structure to strength of interaction. It drastically changed the interplay between theories and experiments. The theoretical models are not only devised from complex physical reality with approximation as before, but can also be designed and simulated in artificial systems. This controllability on one hand leads to direct application such as building quantum computers, on the other hand provides the access to particular physics phenomenons that are of interest.

1.2 Quantum Quench

Given the complexity of the non-equilibrium problems, people usually start with simple protocol. One of these protocols is to prepare the system in its ground state and then slowly change some parameter of the Hamiltonian. In some cases, this process is kept adiabatic like in the quantum adiabatic algorithm to solve the NP-complete problem [8]. In more interesting cases, the system is driven through a quantum critical point. Such a dynamic phase transition, e.g. from superfluid to Mott-insulator, is observed in some groundbreaking experimental work [21]. Adiabaticity is violated in these process and excitations are inevitably generated. Some theoretical studies are naturally extended from the equilibrium universality [11], discussing the scaling the the excitations as a function of the parameter-changing rate [35, 36]. For a review in this topic see the colloquium Ref. [37].

In this thesis, I will focus on another widely-applied protocol to drive the system out of equilibrium –the quantum quench. A quantum quench is defined to instantaneously change some parameter of the Hamiltonian, and follow the subsequent unitary time evolution of the system under the new Hamiltonian. Theoretically it can be written as

$$H(t) = H_0 + \theta(t)H_1, \tag{1.17}$$

where $\theta(t)$ is the standard Heaviside step function. Typically when $t < 0$, the system is prepared in the ground state $|\Psi_0\rangle$ of H_0, and people are interested in the subsequent state

$$|\Psi(t)\rangle = e^{-i(H_0+H_1)t}|\Psi_0\rangle \tag{1.18}$$

and more importantly the evolution of the observable

$$\langle\hat{O}(t)\rangle = \langle\Psi(t)|\hat{O}|\Psi(t)\rangle \tag{1.19}$$

In some typical scenarios, one can prepare the system in the non-interacting ground state and then suddenly turn on the interaction where H_1 represents the interaction term of the Hamiltonian, or one can apply or remove an external field abruptly where the H_1 includes the field term. Experimentally the abruptness means the changing of the parameter is much faster than any time scale related to the relaxation of the system. Because of this abruptness, high energy excitations will be stimulated, and thus the low energy theory in equilibrium fails to apply in this situation. When one considers the time-evolution problem in the standard way, the whole spectrum need to be taken into account. It on the one hand makes the problem even harder to approach, on the other hand reveals new phenomenons unaccessible by other means. I need to point out in some reference like [37], a slow change of parameter is also called "quench". But in this thesis, I will follow the narrow sense of the quantum quench as introduced above.

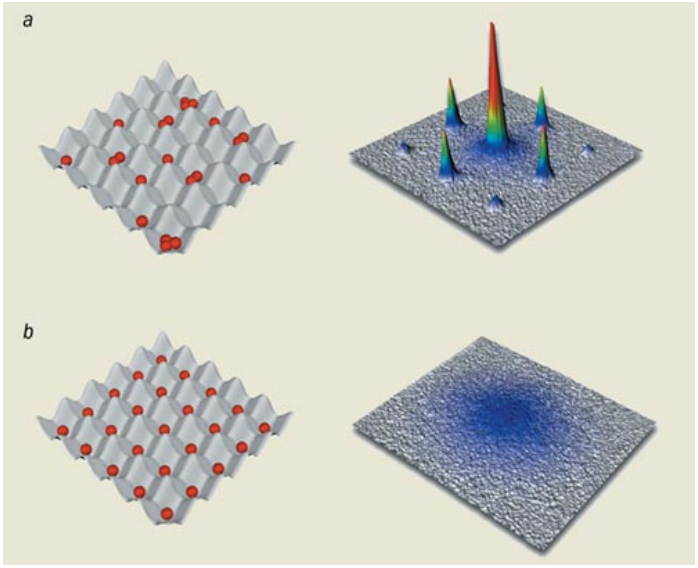

Figure 1.4: The quantum quench of bosons in an optical lattice from the superfluid phase to Mott-insulator. In **a**, the system is in the superfluid phase. Each atom is in a state flowing over all lattice sites. There is a perfect coherence between sites. In **b**, the system is quenched to Mott-insulator phase. The coherence between sites is lost, as shown on the right.

Ultracold atomic gases is perfect to realize the unitary time evolution experimentally. As an typical and famous example, let's consider bosonic gases in an optical lattice, which can be described by the Bose-Hubbard model

$$H = -J \sum_{\langle i,j \rangle} (a_i^\dagger a_j + h.c.) + U \sum_i \hat{n}_i(\hat{n}_i - 1) \tag{1.20}$$

where $a_i^\dagger / a_i$ is the bosonic creation/annihilation operator in a Wannier basis on site i, and $\hat{n}_i$ is the number operator on site i. At the beginning the system is prepared such that the tunneling rate J is much larger than the on-site interaction U, so it is in the ground state of the superfluid phase. The

wave function on different sites are phase coherent, with constant relative phases between lattice sites. Then the potential well is suddenly raised so that the parameters falls into the Mott insulator regime $J \ll U$. Approximately, each lattice site can be considered decoupled. One can obtain the time evolution by expanding the coherent wave function as a superposition of eigenstates of a single site Hamiltonian, and evolving them. It can be derived that the coherence between lattice sites will be lost and then revive after a certain time. This phenomenon was observed experimentally in Ref. [38], as shown in Fig. 1.4. The theoretical analysis is rather simple because the quench is considered only from the limit $U/J \to 0$ to another limit $U/J \to \infty$. A generic quench like that would be a complex problem. Some experimental works on similar quantum quenches include the dephasing of the superfluid phase [39] and quench of a ferromagnetic spinor BEC [40].

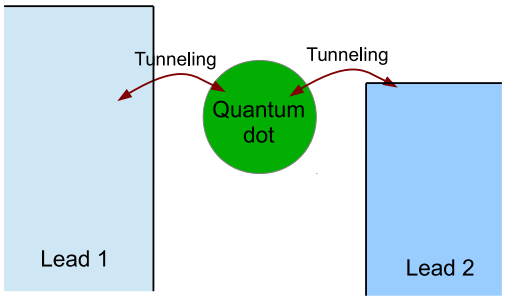

Figure 1.5: A quench problem with quantum dot.

Ultracold atoms is not the only experimental tool to approach quantum quench problem. Modern techniques with quantum dots, molecular electronics and photonics can also reveal interesting phenomenon of quantum quenches. A typical set up with a quantum dot is depicted in Fig. 1.5. At the beginning the two leads and the quantum dot are decoupled. Then at a certain time, the tunnelings are suddenly tuned on. The evolution and particularly the long-time limit of the current is of great interest. A general review on this topic is given in Ref. [41].

The experimental works inspire extensive theoretical study on quench dynamics. Some of them focuses on particular fundamental models, including the Bose-Hubbard model [42], the transverse field Ising model [43], XY-1/2 model [44], interacting fermions on lattice [45] and many others [46, 47]. In some other works, the generic quantum quenches of field-theoretical models, such as the Luttinger model and sine-Gordon model, are studied by applying the renormalization group ideas to non-equilibrium situtations [48, 49, 50, 51, 52, 53, 54]. Along this direction, the generic behavior of the correlation function is discussed through methods of boundary critical phenomena and conformal

field theory [55, 56]. But in general, the theoretical approaches so far all have shortages, and many interesting questions on quench dynamics are open. I will discuss them eventually.

1.3 Theoretical Approaches on Quantum Quenches

The theoretical approaches on quench dynamics can be roughly categorized as numerical methods and analytical methods.

It is worth mentioning many efficient and powerful numerical methods are well developed in the past few years, providing good testing tools for many assumptions and hypothesis. For small systems, the exact diagonalization [4] can be used to calculate evolution for quite long time. For larger but one dimensional systems, recently developed time-dependent density-matrix renormalization group (t-DMRG) [57, 58, 59] can be applied. Even for infinite system, there is the infinite-size time-evolving block decimation algorithm (iTEBD) [60, 6], which is base on the concepts of matrix product states (MPS) [61, 62] and the consideration of translational invariance. Recently, the non-equilibrium dynamical mean-field theory (DMFT) was also applied to the quench dynamics of the fermionic Hubbard model [63]. These numerical approaches can provide accurate, unbiased simulations on the quench dynamics of various model. But they are usually constrained by the exponentially increasing computational cost. Besides, they don't give enough deep insights of the physics.

On the other hand, the analytical methods that focuses on physical insights are only developed for limited cases so far. One common analytical approach is mapping the model to non-interacting particles. It usually gives exact solutions of the dynamics, but has the disadvantage that the specific relaxation of these non-interacting particles can hardly represent the generic behavior of interacting systems. Another massively studied analytical direction is to apply the field-theoretical tools to the critical points of the models. It does provide generic features of quantum quenches, but it is not clear under what conditions and with what accuracy it can be applied to the lattice models implemented in experiments. Among the analytical approaches, the study of integrable models [64] provides a promising direction, because the integrable models have both accessible exact eigenstates and highly non-trivial interacting dynamics. Along this direction, the Yudson contour approach were applied to the Lieb-Liniger model and gave real time evolution [65, 66]. More recently, the quench action method [67] were developed by a generalization of the thermodynamic Bethe ansatz (TBA) and provide a good way to obtain the asymptotic states of integrable systems [68]. The main topic of this thesis is a particular progress in this area: to give the exact solution of time evolution of one fundamental but complicated integrable model –the anisotropic Heisenberg model.

From the study on quench dynamics arises a series of fundamental questions: After sufficiently

long time following a quantum quench, does the system evolve into a steady state? If it does, is this steady state related to the thermal equilibrium state of the new Hamiltonian? Does it carry any memory of the initial state? Answer of these questions centers around the concept thermalization, and brings back one of the fundamental elements of statistical mechanics –classical and quantum ergodicity [69, 70]. The integrable models, again, play a very special roles in these questions due to their conservation laws. All these questions will be discussed extensively in proceeding sections.

1.4 Outline of the Thesis

The remainder of the thesis is organized as the following.

In Chapter 2, I review the study on quench dynamics of isolated quantum systems. I start by introducing the fascinating experiment of quantum "Newton's cradle" in Section 2.1. In section 2.2 I explain the widely accepted thermalization mechanism for a generic system: the eigenstate thermalization hypothesis (ETH). In section 2.3, I briefly review the development and properties of quantum integrable systems. In section 2.4, I discuss the asymptotic states for integrable models, emphasizing the concept of Generalized Gibbs ensemble and its limitation. In section 2.5, I summarize more open questions on time evolution of quantum many-body systems. In section 2.6, I review specifically on quench dynamics of the quantum spin chain, as direct motivation of this thesis.

In Chapter 3, I review the solution of the isotropic Heisenberg model (XXZ model) by coordinate Bethe ansatz. In Section 3.1 I introduce the XXZ model and discuss its bipartite symmetry. In Section 3.2 I describe Bethe's idea of obtaining the eigenstates of the XXZ model. In Section 3.2 I introduce the widely-used parametrization which is convenient for both studying the thermodynamic limit and description of the new contour approach. In Section 3.3 I discuss the string solutions of the Bethe ansatz equations in the thermodynamic limit, which will be revisited later from the contour approach. In Section 3.4, the basic properties of the XXZ model in equilibrium is reviewed.

In Chapter 4, I generalize the Yudson contour approach so it can be applied to the XXZ model. In Section 4.1 I review the Yudson contour approach in the context of the Lieb-Liniger model. In Section 4.2 I show the mathematical proof of the contour representation of the initial state (called central theorem) for the XXZ model. I show it explicitly for one regime of the anisotropy. For the other regimes, I briefly describe the contour shapes, since the proof follow the same idea. In Section 4.3 I present the exact time-dependent wave function after a quench in a integral form, which is the main results of this thesis.

In Chapter 5, I reformulate the integral representation obtained in Chapter 4, and explain its physical interpretations. Two topics are covered: Section 5.1 explain how the string solution emerge

from the contour approach, and discussed the properties of the bound states. Section 5.2 introduce the Yudson representation in a finite system, and discuss its connection to the contour representation.

In Chapter 6, I show the time evolution of several observables evaluated by approximation and numerics. I first explain the details of the saddle point approximation which provides a feasible way to evaluate the integrals obtained in Chapter 4 in Section 6.1. The in Section 6.2 - 6.4, I show the results of time-dependent observables, including the local magnetization, the staggered magnetization as the antiferromagnetic order parameter, and the induced spin currents.

In Chapter 7 I summarize the theoretical improvement of the thesis and discuss some possible future direction to proceed.

Chapter 2

A Review of the Quench Dynamics of Strongly Correlated Systems

2.1 Quantum Newton's Cradle

Starting from a state far from equilibrium, a generic, closed, classical system with many degrees of freedom is expected to rapidly relax into thermal equilibrium –a state that can be described by the microcanonical ensemble. Initial states with different configurations will evolve into the same thermal state finally, with detailed information of the initial state seemingly lost in this process. This phenomenon is called thermalization, and explained by the classical ergodicity, a fundamental assumption of statistical mechanics: in the long time limit, the trajectory of the system in the phase space will traverse the constant-energy hyper-surface ergodically with the same probability, because of the chaotic dynamics of classical systems. This mechanism will apparently fail if the system has conservation laws other than the energy, because the trajectory of the system will be confined within a small area of the constant-energy surface by the conservation laws. There is a special category of systems, the integrable systems, who have a large number (comparable to the total degree of freedom) of conserved quantities and thus bring interesting questions on its asymptotic state. The study of non-ergodicity of classical integrable systems has a long history. As an significant example, the study on Fermi-Pasta-Ulam problem [71] eventually gives rise to the modern chaos theory.

Recently, this story was extended to the quantum realm mainly by the fascinating experimental work on the "quantum Newton's cradle" [72]. In this experiment, the optical lattice is prepared as a two dimensional array of parallel trapping "tubes", with negligible tunneling between them. So each of the tubes can be considered a 1-D system, and a weak parabola-like confinement is imposed along the axial direction. Then a Bose-Eistein condensate of ^{87}Rb atoms are loaded into this lattice, with each tube containing 40 to 250 atoms. Initially, these atoms are given a large momentum in opposite axial direction, and the subsequent evolution is monitored, as a typical quench problem. The atoms are expected to oscillate due to the weak axial confinement, and collide with a point-like

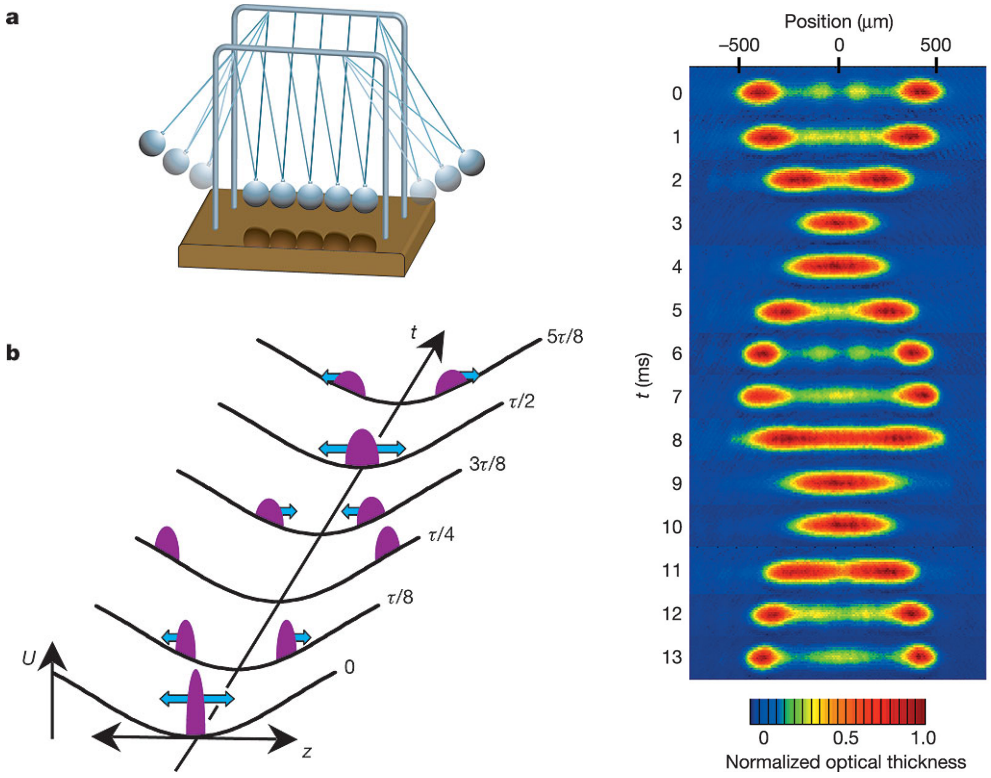

Figure 2.1: The quantum newton's cradle.

interaction. Bosons in such a set-up can be roughly described by the Lieb-Liniger model

$$H_{LL} = \int dx[\partial_x b^\dagger(x)\partial_x b(x) + cb^\dagger(x)b(x)b^\dagger(x)b(x)] \tag{2.1}$$

which turns out to be integrable (the quantum integrability has a slightly different meaning from classical integrability, as will be discussed later). The schematic picture and the measured absorption image of the atoms are shown in Fig. 2.1, reproduced from Ref. [72]. A remarkable result is that these atoms do not show any sign of thermalization in the time scale of the experiment, even after thousands of collisions. This result is attributed to the integrability of the Lieb-Liniger model. This phenomenon is compared with the Newton's cradle –a trivially integrable classical system which evolves with time in a simple way instead of touring ergodically over the constant-energy surface, no matter how many degrees of freedom it has. Classically, a large number of conservation laws are responsible for this non-ergodicity, since they significantly confine the dynamics of the system. But for a quantum integrable system, how to describe its time evolution, particularly the long time limit, was brought on table as a question.

This pioneering experimental work stimulated massive study on the mechanism of thermalization of quantum systems, which still has many open questions. The quantum integrable models surely play a special role in these studies. In this chapter I briefly review the topics of quantum

thermalization, quantum integrability, and asymptotic states of integrable systems.

2.2 Quantum Thermalization of Non-Integrable systems

In this section I discuss the thermalization of quantum non-integrable systems. I suppose there is only one conserved quantity of the system –its energy. Notice that the system with a few more conserved quantities like the total momentum or the particle numbers will fit in the same discussions below. Let's clarify some definitions first. Equilibration of a quantum system means that the expectation values of observables converge to a stationary value in the long time limit. Thermalization means these stationary values coincide with the ones predicted by thermal ensembles. In both of the definitions the system is considered to be infinite large, or in the thermodynamic limit, since a finite closed quantum system never equilibrates due to quantum revival.

First, it is easy to see the full system cannot thermalize. Consider a generic (non-integrable) quantum system starting from a generic initial state $|\Psi_0\rangle$, and evolves under the Hamiltonian $\hat{H}$. The eigenvalues and eigenstates of $\hat{H}$ are denoted by E_α and $|\Psi_\alpha\rangle$. Then the energy of the system (which is conserved) is given by

$$E_0 = \langle\Psi_0|\hat{H}|\Psi_0\rangle \tag{2.2}$$

The evolution of the state can be obtained by standard quantum mechanics as the following. The initial state can be expanded by the complete eigenstates

$$|\Psi_0\rangle = \sum_\alpha C_\alpha |\Psi_\alpha\rangle \tag{2.3}$$

where $C_\alpha = \langle\Psi_\alpha|\Psi_0\rangle$. Then the subsequent state is given by

$$|\Psi(t)\rangle = e^{-i\hat{H}t}|\Psi_0\rangle = \sum_\alpha e^{-itE_\alpha} C_\alpha |\Psi_\alpha\rangle \tag{2.4}$$

The long time limit of the density matrix will be

$$\begin{aligned}\hat{\rho}(t\to\infty) &= \lim_{t\to\infty} |\Psi(t)\rangle\langle\Psi(t)| \\ &= \lim_{t\to\infty} \sum_{\alpha,\beta} e^{-it(E_\alpha - E_\beta)} C_\alpha C_\beta^* |\Psi_\alpha\rangle\langle\Psi_\beta| \\ &= \sum_\alpha |C_\alpha|^2 |\Psi_\alpha\rangle\langle\Psi_\alpha|\end{aligned} \tag{2.5}$$

where I used the idea of saddle point approximation: the oscillatory phase $e^{-it(E_\alpha - E_\beta)}$ with infinite large t can only survive at $E_\alpha = E_\beta$. The density matrix above defines an ensemble called the diagonal ensemble [73, 4, 74]

$$\hat{\rho}_{diag} = \sum_\alpha |C_\alpha|^2 |\Psi_\alpha\rangle\langle\Psi_\alpha| \tag{2.6}$$

If a quantum system thermalizes at all, its long time limit will be characterized by this density matrix. This is equivalent to say any observable $\hat{O}$ will converge to a stationary value

$$\langle O(t \to \infty) \rangle = \mathrm{Tr}[\hat{\rho}_{diag} \hat{O}] = \sum_{\alpha} |C_\alpha|^2 O_{\alpha\alpha} \tag{2.7}$$

where $O_{\alpha\alpha} = \langle \Psi_\alpha | \hat{O} | \Psi_\alpha \rangle$ is expectation value of the observable $\hat{O}$ in the eigenstate $|\Psi_\alpha\rangle$.

On the other hand, the Gibbs canonical ensemble predicts the expectation value of the observable $\hat{O}$ to be

$$\langle O \rangle_T = \frac{1}{Z} \sum_{\alpha} e^{-E_\alpha / T} O_{\alpha\alpha} \tag{2.8}$$

where $Z = \sum_\alpha e^{-E_\alpha/T}$ is the partition function, and the temperature T is fixed by the requirement

$$\langle H \rangle_T = E_0 \tag{2.9}$$

Notice that the eigen energy E_α is proportional to the system size L. In the thermodynamic limit $L \to \infty$, the canonical ensemble goes to a microcanonical ensemble, so (2.8) becomes

$$\langle O \rangle_{mc} = \frac{1}{N(E_0, \Delta E)} \sum_{\substack{\alpha \\ |E_\alpha - E_0| < \Delta E}} O_{\alpha\alpha} \tag{2.10}$$

Here the energy shell of the spectrum is coarse grained. The shell width $2\Delta E$ is supposed to be much smaller than macroscopic scales, but large enough to contain many states. And $N(E_0, \Delta E)$ is the number of states in the energy shell. This can be equivalently describe by the microcanonical density matrix

$$\hat{\rho}_{mc} = \frac{1}{N(E_0, \Delta E)} \sum_{\substack{\alpha \\ |E_\alpha - E_0| < \Delta E}} |\Psi_\alpha\rangle\langle\Psi_\alpha| \tag{2.11}$$

Notice that the diagonal density matrix is a function of the initial state through the amplitudes C_α, while the microcanonical density matrix only "remember" the energy of the initial state. These two density matrix almost never agree with each other. This non-thermalization of a full quantum system was discussed long ago by J. von Neumann [69, 70]. It makes sense because a unitary evolution doesn't lose any information.

However, a finite subsystem can thermalize. This statement can be phased in two equivalent way: if the $\hat{\rho}$ is a reduce density matrix of a finite subsystem, then one can have

$$\hat{\rho}_{mc} = \hat{\rho}_{diag} \tag{2.12}$$

or, if $\hat{O}$ is an operator involving a few degrees of freedom of the system, then one can have

$$\frac{1}{N(E_0, \Delta E)} \sum_{\substack{\alpha \\ |E_\alpha - E_0| < \Delta E}} O_{\alpha\alpha} = \sum_{\alpha} |C_\alpha|^2 O_{\alpha\alpha} \tag{2.13}$$

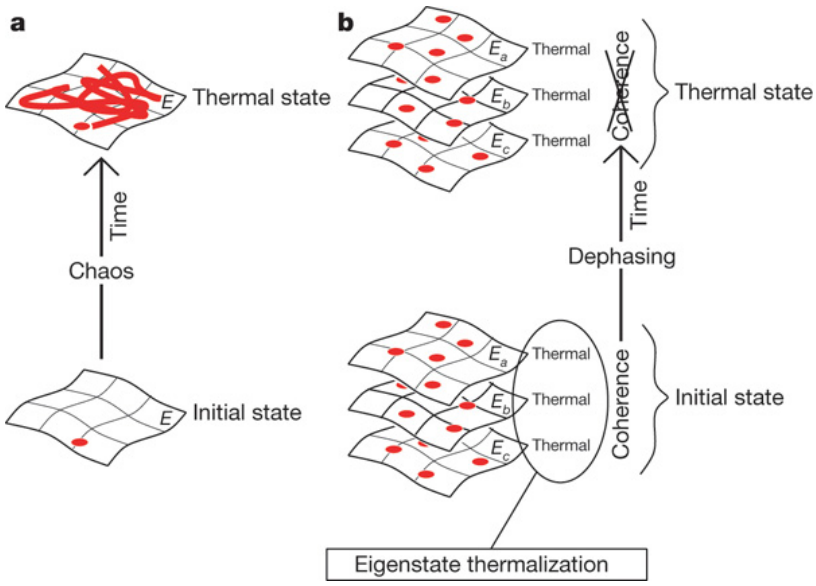

Figure 2.2: The mechanism of thermalization for classical and quantum systems. Borrowed from Ref. [4].

This is the generally expected result for generic systems. But how it happens still needs explanation. A widely accepted mechanism for thermalization is the *eigenstate thermalization hypothesis (ETH)*. It conjectures that $O_{\alpha\alpha}$ is a smooth function of α (thus approximately a constant on the energy shell), and the initial state is narrow in energy. So the $O_{\alpha\alpha}$ is roughly a constant for all $|\Psi_\alpha\rangle$ with non-negligible overlap with the initial state, and therefore (2.13) is satisfied. Notice the ETH conjecture means the expectation value in each eigenstate in the energy shell is the same, and equal to the thermal value given by the microcanonical ensemble. In another word, any eigenstate with energy close to the initial energy can play the role of thermal state. The time evolution merely plays the role of dephasing. This mechanism is sketched in Fig. 2.2. Physically, the ETH means the large remainder of the system acts as a thermal bath of the subsystem, thus the subsystem thermalizes.

The ETH was proposed by Deutsch [75] and Srednicki [76]. The general validity of ETH is not theoretically proved. There are only some indication of its correctness in particular circumstances ranging from nuclear physics [77] to semi-classical limit of quantum systems [78]. Recently there are numerical works verifying the ETH in particular models [4, 74, 79, 80], for some few-body observables. Generally, the condition for eigenstate thermalization to occur is still an open question. For integrable models, the ETH would not work but may be generalized, as will be discussed later. Recently, there are also some works [81, 82] showing that disorder can cause ETH to fail.

Up to here we are talking about non-integrable systems. For integrable systems, the story is totally different. Even classical integrable systems are not expected to thermalize because their conservation laws restrain the dynamics. On the other hand, the quantum version of integrability,

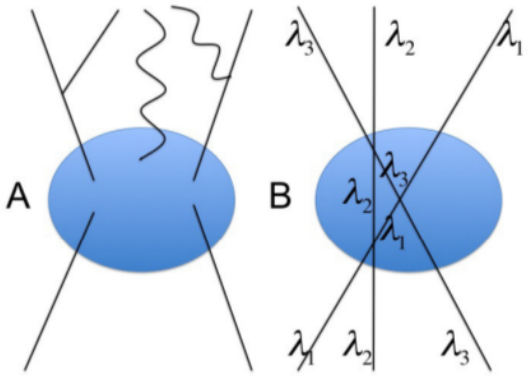

Figure 2.3: Conservation of bare momenta in a integrable model.

as a influential branch of modern mathematical physics, is worth an introduction itself.

2.3 Quantum Integrability

The quantum integrable systems are usually defined as the systems exactly solvable by Bethe Ansatz. In 1931, Hans Bethe proposed a method to obtain the exact eigenstates of the isotropic interacting quantum spin chain [83], known as the Heisenberg model [84]. This method, now realized as Bethe Ansatz, has been generalized and expanded over years, to exactly solve a series of 1-D quantum many-body systems. These systems, spanning over different fields of physics, include the Lieb-Liniger model [85], the Kondo model [86], the Anderson impurity model [87], the massive Thirring model [88], the Hubbard model [89], etc. Many classical statistical models on the 2-D lattice can also be solved by the Behte Ansatz, given their equivalence to the 1-D quantum models [90]. During the development of the Bethe Ansatz, many significant work by C.N. Yang and C.P. Yang [91, 92, 93, 94] need to be emphasized. In non-integrable models, the scattering of particles usually lead to particle production and decay, thus only the total momentum is expected to conserve. But in a model solvable by Bethe Ansatz, the Yang-Baxter consistency [92] indicates that the multi-particle scattering can be factorize into two-particle scattering, and each of the bare momenta is conserved, as sketched in Fig. 2.3. The Bethe Ansatz not only gives the whole spectrum and the complete eigenstates, but also can be applied to the calculation of the thermodynamics [64, 95]. In later Chapters, I will discuss more details of the coordinate Bethe Ansatz introduced by H. Bethe, in the context of the isotropic Heisenberg model.

The connection between classical and quantum integrability is established by the quantization of classical inverse scattering method [96]. The classical integrable systems was previous introduced as the systems with infinite number of conserved quantities. Their Hamiltonian evolution is captured

by the classical integrable differential equations, also know as soliton equations [97]. The modern way to solve these equations is called the classical inverse scattering method (CISM). The quantum generalization of CISM, known as the quantum inverse scattering method (QISM), was found to reproduce the results of the Bethe Ansatz. The approach to solve quantum integrable systems by QISM is now summarized under the name of *Algebraic Bethe Ansatz*. It has been developed to be a powerful tool to calculate various properties of generic integrable systems. For example, all the conserved charges can be found through a recursive way based on algebraic Behte ansatz. A general formulation of correlation functions can also be derived from it. The details of the Algebraic Bethe Ansatz and its connection to classical integrability are introduced in the book by V.E. Korepin *et al.* [98]. In this thesis, I will not go deep into this direction, but mostly make use of the coordinate Bethe Ansatz. But in Chapter 7, I will discuss the possibility to combine Algebraic Bethe Ansatz and our approach in future directions.

2.4 Asymptotic States of Integrable Systems

The experimental work [72] at the beginning of this chapter has shown the lack of thermalization of an quantum integrable system. It was expected because the infinite number of conserved charges (usually called integral of motion for classical case) of the systems drastically changed the dynamics. But the question is naturally extended: Does an integrable system relax into an asymptotic steady state after a quantum quench? If it does, is the asymptotic state described by some other ensemble, instead of the conventional Gibbs ensemble?

The *generalized Gibbs ensemble (GGE)*, first introduced by Jaynes [99], recently conjectured by Rigol to describe the asymptotic state of integrable models, opens a popular point of view to these questions. Rigol *et al.* conjectured [73] that the asymptotic state of a integrable system is characterized by the density matrix

$$\hat{\rho}_{GGE} = Z^{-1} \exp\left[-\sum_m \lambda_m \hat{\mathcal{I}}_m\right] \tag{2.14}$$

where the $\{\hat{\mathcal{I}}_m\}$ is the full set of conserved charges of the system, and $Z = \mathrm{Tr}[\exp(-\sum_m \lambda_m \hat{\mathcal{I}}_m)]$ is the partition function. The $\{\lambda_m\}$ are the Lagrange multipliers, determined by the initial state

$$\mathrm{Tr}[\rho_{GGE}\hat{\mathcal{I}}_m] = \langle\Psi_0|\hat{\mathcal{I}}_m|\Psi_0\rangle \tag{2.15}$$

The ensemble given by this density matrix is named the generalized Gibbs ensemble. It is a direct generalization of the Gibbs ensemble, since energy $\hat{H}$ is one of the conserved charges, and its corresponding Lagrange multiplier is $\beta = 1/T$.

The GGE can be derived by maximizing the entropy subject to the constrains imposed by the conserved charges –a standard prescription of statistical mechanics. That's why it is also known as the maximum entropy ensemble. The asymptotic state described by the GGE clearly carries more information of the initial state than the microcanonical ensemble, but still much less than the full information of dynamics. The microcanonical ensemble only "remember" the energy; the GGE "remember" all the conserved charges, which is typically of the size of the systems; while the full information of dynamics is of the size of the Hilbert space, typically exponential of the size of the system. In Rigol's work this conjecture is numerically tested on hard-core bosons on a 1-D lattice. The model can be mapped to free fermions, thus the conserved charges are easy to be found explicitly. Similar thing happens in Cazalilla's analytical work [48] on Luttinger model, in which the conserved charges are naturally chosen to be the occupation numbers of the mapped bosons, and the GGE is verified for some simple correlation functions.

The GGE reveals a simple and plausible way of looking at the thermalization problem of integrable models, and motivates a lot of theoretical work [100, 74, 101, 102]. In particular, it was proved to be valid for models equivalent to free fermions [103, 47, 104, 53, 105, 106]. But a central question it has to face is how to choose the set of conserved charges, especially for complicated integrable models that cannot be mapped to free particles. In some early work on this topic, the projection operators $\hat{P}_\alpha = |\Psi_\alpha\rangle\langle\Psi_\alpha|$ to the eigenstates of the Hamiltonian [48] and the powers of the Hamiltonian $\{\hat{H}^m\}$ [45] are both considered. But these choices of conserved charges are not local, and therefore cannot capture Yang-Baxter consistency of integrable models. The naturally choice of the conserved charges arises from the Bethe-Ansatz solution of the system. The Bethe Ansatz implies the existence of the well-defined quasi-particles which scatter elastically, without dissipation or creation of new particles. The conserved charges turns out to have eigen values of integer powers of the rapidities of these quasi-particles, and can be generated in a recursive way through algebraic Bethe ansatz [98].

Another important question on GGE is its mechanism. It was proposed by Cassidy *et al.* [102] that the GGE can be explained by a proper extension of the ETH, called the generalized eigenstate thermalization (GETH). They conjectured that if all the conserved charges of an eigenstate are close to the corresponding ones of another eigenstate, then expectation values of a local operator in these two eigenstates are also close. In another word, a set of conserved charges uniquely determines all correlations (expectation of local observables) of the state. It can be written as

$$\langle O(t\to\infty)\rangle = \sum_\alpha |C_\alpha|^2 O_{\alpha\alpha} = (\sum_\alpha |C_\alpha|^2) O_{\alpha_1\alpha_1} = \langle\alpha_1|O|\alpha_1\rangle \tag{2.16}$$

where α now denotes a series of quantum numbers of the conserved charges $\{\hat{\mathcal{I}}_m\}$, and α_1 is one set

of them. The right hand side of (2.16) is the prediction of the GGE in thermodynamic limit. So the GETH explains the GGE. The conjecture of GETH was checked for hard-core bosons in Ref. [102], but its correctness is questioned by later works.

Very recently, the quench action method [67] was proposed through a generalization of the thermodynamic Bethe ansatz (TBA). It calculates the asymptotic states of integrable models on first principles without any assumptions. Some very recent works based on it show that the GGE fails for the XXZ model [107, 68]. It is concluded by Goldstein *et al.* [108] and Pozsgay [109] that the GGE only works for integrable models without bound states, and fails for those with bound states: for integrable models with bound states, the eigen basis is fully represented by the distribution functions on arbitrary orders of strings given by TBA. A set of conserved charges is not enough to uniquely determine these distribution functions, therefore cannot uniquely determine all correlation functions –they are enough to determine the distribution function on one string, thus works for models without bound states.

It can be seen that the interplay between thermalization and integrability is far from conclusive. For example, there are works showing even non-integrable models can approach non-thermal steady state, depending on regimes of quenched parameters [42, 110, 111]. Conversely, some natural observable of physical interest in integrable models are believed to behave thermally [112], highly depending on the locality of the observable in the quasi-particle space of integrable system.

2.5 More Open Questions

As an actively developing area, the relaxation of strongly correlated systems has a lot of open questions. Let me name some of them.

One important question in this field is the crossover between ergodic and non-ergodic behaviors. In the classical FPU problem, it has been shown there is a finite threshold for chaotic behavior, i.e. the non-linear coupling that breaks integrability has to be strong enough to cause ergodicity [71]. The same question for quantum systems is still unclear. Rigol's numerical work [74, 79] shows a smooth breakdown of thermalization as one approaches integrability, in 1-D hard-core bosons. But he claim it could be the effect of the small size of the system.

So far most of the works focus on the asymptotic or time averaged states. The real time evolution after a quantum quench was studied much less. For fermionic Hubbard model, the existence of a intermediate quasi-steady regime before thermalization was found [113, 63], providing deeper understanding of the process of thermalization. In a much earlier work, the *prethermalization* [49] of equation of state and kinetic temperature much faster than thermal equilibration was studied in

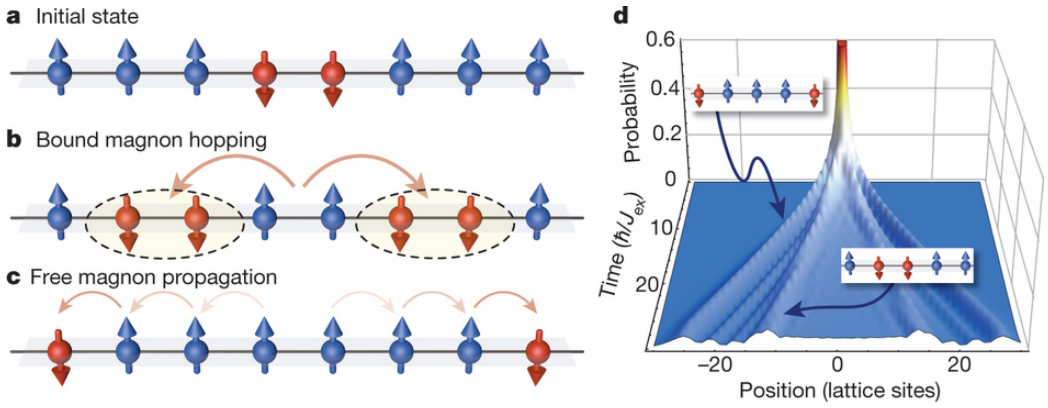

Figure 2.4: The experimental work by Fukuhara *et al.* [5] on local quench of the Heisenberg spin chain.

a more general sense. For the Heisenberg spin chain, Barmettler *et al.* [6, 7] studied the real time relaxation of the antiferromagnetic order parameter by numerics. Different time scales during the relaxation was discussed.

Because of so many open questions discussed above, an analytical, especially exact approach on the real time evolution for a non-trivial integrable model would help with clarification of many confusions. It will be the main subject of this thesis, as introduced gradually in proceeding chapters.

2.6 Quench Dynamics of the Quantum Spin Chain

The Heisenberg spin chain is a generic and fundamental model for 1-D spin order system. It characterizes rich physics that governs many strong-correlated systems. For example, its low-energy physics in the gapless phase can be described by the Luttinger liquid [114]; while around the critical point, it effectively becomes sine-Gordon model. Besides, the Heisenberg spin chain is integrable, but not trivially mapped to free particles. So its quench dynamics is expected to contribute to deep understanding of relaxation of generic integrable systems. In this section, I will review some recent works, both experimental and theoretical, on the quench dynamics of the Heisenberg spin chain. Some of them greatly motivates the work of this thesis.

2.6.1 Propagating Magnons after a Local Quench

A main motivation of this thesis is the fascinating experimental work by Fukuhara *et al.* [5], in which the propagation of magnons and their bound states are directly observed. They set up a quantum quench as follow, shown in Fig. 2.4: they start from an a fully magnetized chain with all spins "up" except for two neighboring spins in the center flipped "down". By "up" and "down" we mean in the eigenstates of the local z-direction spin operator σ_j^z. Then they let the system evolve under the

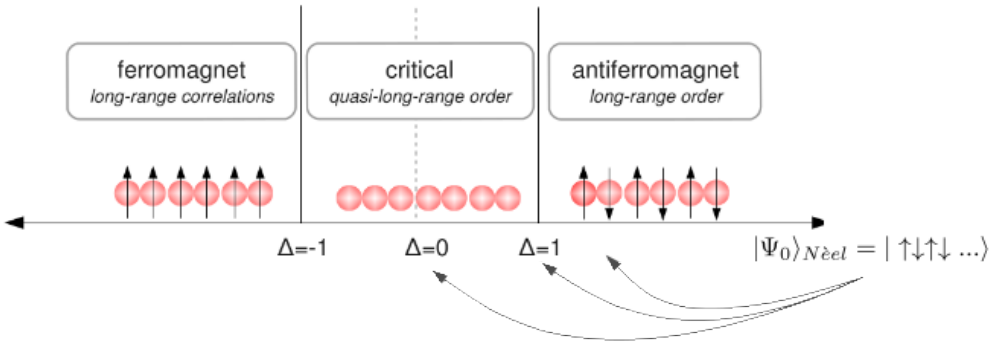

Figure 2.5: The numerical work by Barmettler *et al.* [6, 7] on the global quench of the Heisenberg spin chain through the critical point.

Hamiltonian (1.15), and monitor the system with their detection technique which has single-site and single-spin resolution. This theoretically ideal set-up surely requires sophisticated techniques. For example, the flipping of spins in the initial state is achieved by a line-shaped laser beam generated with a spatial light modulator that selectively shifted the addressed sites in resonance with the microwave radiation [29]. After a variable evolution time, all lattice confinement is rapidly ramped up to a very large value to freeze out the dynamics, so the single-site spin states can be detected. As results, the joint probability P_{ij} of simultaneously detecting atoms on lattice sites i and j can be extracted atom positions data, with sufficient consideration of fidelity (see Ref. [5] for details). Notice this joint probability is directly comparable to the norm square of the two-body wave function $|\Psi(i,j;t)|^2$, defined by

$$|\Psi(t)\rangle = \sum_{i,j} \Psi(i,j;t)\sigma_i^- \sigma_j^- |\Uparrow\rangle, \tag{2.17}$$

where σ_i^- is the spin-lowering operator on site i, and $|\Uparrow\rangle$ denotes the states with all spins up. We will calculate this quantity in extensive details and compare with the experimental results in Chapter 5. The physics picture of propagating magnons and their bound states can be extracted from the probability data. It can also be obtained by our new theoretical approach, which we will also discuss in details in Chapter 5.

It is worth mentioning the same set-up of a quantum quench in Heisenberg spin chained was studied numerically in the work by Ganahl *et al.* [115] using the time evolving block decimation algorithm. It will be shown that we provide more physics insights with our analytical approach.

2.6.2 Antiferromagnetic Order Parameter after a Global Quench

In the works above, a local quench of the Heisenberg spin chain is performed. As discussed in previous sections, the global quench through the critical point of the Heisenberg model is also of

great interest. It was studied in a numerical work by Barmettler *et al.* [6, 7]. As shown in Fig. 2.5, the spins chain is prepared initially in the Neél state, which has long-range antiferromagnetic order

$$|\Psi_0\rangle_{\text{Neél}} = |\uparrow\downarrow\uparrow\ldots\downarrow\uparrow\downarrow\rangle. \tag{2.18}$$

This initial state can be considered the ground state of the XXZ Hamiltonian (1.15) with the anisotropy $\Delta_0 = J_z/J_\perp \to \infty$. Then the system is evolved under the XXZ Hamiltonian with a finite anisotropy. The real time evolution after the quench is obtained by the infinite-size matrix product method [61, 62], and compared with different approximation methods in Ref. [7]. They particularly monitor the evolution of the staggered magnetization

$$m_s(t) = \frac{1}{N}\sum_j (-1)^j \langle\Psi(t)|S_j^z|\Psi(t)\rangle, \tag{2.19}$$

which characterizes the antiferromagnetic order, and the equal-time spin-spin correlation function

$$G_c^{zz}(l,t) = \frac{1}{N}\sum_i \langle S_{i+1}^z S_i^z\rangle(t) - \langle S_{i+1}^z\rangle(t)\langle S_i^z\rangle(t) \tag{2.20}$$

to describe non-local properties. Their basic observation is the decay and oscillation behavior of the order parameter depending on the values of Δ. This behavior can be roughly categorized into three regimes

$$\begin{aligned} &m_s(t) \sim t^{-1/2}\cos(2Jt - \pi/4) && \Delta = 0, \\ &m_s(t) \sim \exp(t/\tau_2)\cos(\omega t + \phi) && 0 \lesssim \Delta < 1, \\ &m_s(t) \sim \exp(t/\tau_1) && \Delta \gg 1. \end{aligned} \tag{2.21}$$

where the behavior for $\Delta = 0$ has a simple closed form, since it can be mapped to free fermions. Besides, the behavior around the critical point $\Delta \approx 1$ appears complicated and hard to fit into any simple functions. It is due to the "interplay of process of all energy scales".

The emergence of time scales ω^{-1}, τ_1 and τ_2 and their dependence on the parameters of the Hamiltonian are of great interest. In particular, they found ω to be very close to $2J$, its non-interacting counterpart. It is attributed to the Rabi oscillation: consider the dynamics of two coupled spins, starting from the initial state $|\psi_0\rangle = |\uparrow\downarrow\rangle$. A system like this would oscillate between $|\uparrow\downarrow\rangle$ and $|\downarrow\uparrow\rangle$, with the frequency independent of Δ:

$$|\psi(t)\rangle = \cos(\frac{Jt}{2})|\uparrow\downarrow\rangle + i\sin(\frac{Jt}{2})|\downarrow\uparrow\rangle. \tag{2.22}$$

And the staggered magnetization behaves like $m_s(t) = \frac{1}{2}\cos(Jt)$. So its oscillation frequency is set by the exchange coupling J. In the experimental work by Trotzky *et al.* [28], this oscillation frequency is observed, and the simple model above is investigated in detail. For the spin chain

model, Barmettler *et al.* observed very weak dependence of ω on Δ, i.e. $\omega \approx 2J$ for all values of Δ, according to their numerical simulation. On the other hand, the relaxation time τ_1 and τ_2 are emergent time scales generated from the highly correlated dynamics, and cannot be simply related to the model parameters. Only qualitative observation can be obtained from numerical data: $\tau_1 \to \infty$ as $\Delta \to \infty$, and $\tau_2 \to \infty$ as $\Delta \to 0$, namely the relaxation times diverge in these limit; both τ_1 and τ_2 goes to 0 as $\Delta \to 1$ from either side, namely the relaxation time vanishes around the critical points. These qualitative results were compared with approximative methods, such as mean field, Luttinger model and sine-Gordon model in Ref. [7].

We will discuss these results again and compare to our newly developed approach in Chapter 6.

Other Works

Besides the works we mentioned above, the quench dynamics of the Heisenberg spin chain attracts much attention from many other aspects due to its specially important role in both strongly correlated systems and integrability. For example, the Loschmidt echo, defined as

$$L(t) = |\langle \Psi_0 | \exp(-i\hat{H}t | \Psi_0 \rangle|^2, \tag{2.23}$$

was studied in a number of recent works on the XXZ model [116, 117]. It characterizes the work function during the quench. It is also interesting from the phase transition point of view because its logarithm per unit of length has a non-analytic behavior when the system is quenched across a critical point. Due to the integrability of the XXZ model, methods based on Bethe ansatz, eg. quantum transfer matrix formalism [118, 119] were recently applied to its quench problem. However, an analytical approach to give the full dynamics after a quench for the XXZ model is still missing. The main subject of this thesis is to present an approach like that, which is generically works for any initial state and any anisotropy Δ.

Chapter 3
Bethe Ansatz Solution of the XXZ Model

In this chapter, I review the solution of the XXZ model by coordinate Bethe ansatz. Many results of this chapter will be the foundation of the contour approach I introduce in the next chapter.

3.1 The XXZ Model and Its Symmetry

The anisotropic Heisenberg model (XXZ model) captures the physics of one-dimensional quantum spin chain with a nearest-neighbor exchange coupling

$$H = -J\sum_{j=1}^{L}[\sigma_j^x\sigma_{j+1}^x + \sigma_j^y\sigma_{j+1}^y + \Delta(\sigma_j^z\sigma_{j+1}^z - 1)], \tag{3.1}$$

where the σ_j^x, σ_j^y, σ_j^z are Pauli matrices of a particular site j and $\Delta = \frac{J_z}{J_{xy}}$ denotes the anisotropy. Here L is the size of the system. Usually I loosely write $\sum_j$ because sometimes I work on a infinite system. Here $\sigma_j^z\sigma_{j+1}^z$ is subtracted by 1 to make the ground state energy zero. For convenience, the Hamiltonian is also usually written as

$$H = -J\sum_{j}[2(\sigma_j^+\sigma_{j+1}^- + \sigma_j^-\sigma_{j+1}^+) + \Delta(\sigma_j^z\sigma_{j+1}^z - 1)], \tag{3.2}$$

through a transformation

$$\sigma_j^{\pm} \equiv \frac{\sigma_j^x \pm \sigma_j^y}{2}, \tag{3.3}$$

where the $\sigma_j^{\pm}$ are the spin-raising/lowering operator on one site. We choose the fully ferromagnetic ordered state $|\uparrow\uparrow\ldots\uparrow\rangle$ (the other one $|\downarrow\downarrow\ldots\downarrow\rangle$ gives equivalent results) to be the reference state, and regard the down spins as particles.

The XXZ Hamiltonian has a special symmetry when the size L is an even number. Under the unitary transformation

$$\mathcal{U} \equiv \prod_{j=\text{even}} \sigma_j^z = \mathcal{U}^{-1}, \tag{3.4}$$

every other spin is rotated by π along z-axis: $(\sigma_j^x, \sigma_j^y, \sigma_j^z) \to (-\sigma_j^x, -\sigma_j^y, \sigma_j^z)$ for j = even. So the Hamiltonian changes as $H(J,\Delta) \to H(-J,-\Delta) = -H(J,-\Delta)$. Usually J is chosen to be positive,

and Δ is the only parameter to determine the phase space, as shown in Fig.2.5. A lattice that can be split into even and odd sites like this is called *bipartite*. An interesting conclusion following this symmetry is that the Hamiltonians with opposite signs of Δ have the same time evolution. I will discuss it in the next chapter.

The complete eigenstates of this model is given by Hans Bethe [83], as I will review below.

3.2 Coordinate Bethe Ansatz

3.2.1 Physics Intuition and Scattering-Matrix

It is easy to see the total magnetization (the number of flipped spins) $\hat{N} = \sum_j \sigma_j^z$ is conserved. To find the eigenstates of the XXZ Hamiltonian (3.2), let's start with the simplest one particle (namely one down-spin) case. It's easy to see a simple plane wave is the eigenstate for one particle case:

$$|k\rangle = \sum_m e^{ikm}\sigma_m^-|\Uparrow\rangle. \tag{3.5}$$

It is labeled by the (bare) momentum k. Its eigen energy can be calculated from the Schrödinger's equation $H|k\rangle = E(k)|k\rangle$, and is given by

$$E(k) = 4J(\Delta - \cos k). \tag{3.6}$$

For two-particle case, Hans Bethe proposed the ansatz that the eigenstate is given by

$$|k_1, k_2\rangle = \sum_{m_1,m_2} e^{ik_1m_1+ik_2m_2}[\theta(m_1 - m_2) + s(k_1, k_2)\theta(m_2 - m_1)]\sigma_{m_1}^-\sigma_{m_2}^-|\Uparrow\rangle, \tag{3.7}$$

where $\theta(m)$ is the Heaveside step function

$$\theta(m) = \begin{cases} 1 & \text{if } m > 0 \\ 0 & \text{if } m < 0. \end{cases} \tag{3.8}$$

Because $\sigma_m^-\sigma_m^- = 0$, $\theta(0)$ never comes into the question, and thus doesn't need to be defined. Intuitively, this eigenstate means that when the two particles are far apart, the wave function is just a product of single-particle wave functions; only when the two particle get through each other, the wave function gains a extra phase $s(k_1, k_2)$, which is called the scattering matrix, or S-matrix. Bethe further assumes the eigen energy of the two particle eigenstate is the summation of single-particle eigen energies:

$$E(k_1, k_2) = 4J(2\Delta - \cos k_1 - \cos k_2). \tag{3.9}$$

Then from the Schrödinger's equation $H|k_1, k_2\rangle = E(k_1, k_2)|k_1, k_2\rangle$, one can derive the form of the S-matrix:

$$s(k_1, k_2) = -\frac{1 + e^{ik_1+ik_2} - 2\Delta e^{ik_1}}{1 + e^{ik_1+ik_2} - 2\Delta e^{ik_2}}. \tag{3.10}$$

I give this derivation in Appendix A.

For many-particle case, it is assumed that the multi-particle scattering process can be decomposed into two-particle scatterings, and the eigenstate can be written as

$$|\vec{k}\rangle = \sum_{\{m_j\}} \prod_{i<j} [\theta(m_i - m_j) + s(k_i, k_j)\theta(m_j - m_i)] \prod_j e^{ik_j m_j} \sigma^-_{m_j} |\Uparrow\rangle. \tag{3.11}$$

Here $\vec{k}$ denotes k_1, $k_2 \ldots k_M$. Every m_j, with $j = 1, 2, \ldots, M$, is summed from 1 to L (length of the chain), and $s(k_i, k_j)$ is the two-particle S-matrix (3.10). It can be considered that the theta functions divide the coordinate space into $M!$ regions according to different permutations of the coordinates, and each region has a different amplitude consisting of product of S-matrices. The validity of this eigenstate is guaranteed by the Yang-Baxter equations (YBE) [92]

$$\begin{aligned} &s^{12}s^{21} = I, \\ &s^{12}s^{13}s^{23} = s^{23}s^{13}s^{12}, \\ &s^{12}s^{34} = s^{34}s^{12}, \end{aligned} \tag{3.12}$$

which are written with a general notation. In the case of XXZ, $s^{ij} = s(k_i, k_j)$ and the YBE is trivially satisfied. But in a more complicated situation where the S-matrices don't necessarily commute, it needs to be verified. For example, in the Hubbard model, S-matrices are functions of both momenta and spins, and the Yang-Baxter consistency is not trivial at all. As shown schematically in Fig. 3.1, the second equation of (3.12) guarantees the amplitudes obtained through different paths for a certain region are the same. Physically, it means the three particle scattering can be decomposed into two-particle scatterings, and the order of the two-particle scattering doesn't matter (Right hand side of Fig. 3.1). Systems with this property are called integrable systems, featuring infinite number of conserved quantities, and shows special non-equilibrium behavior as discussed in the previous chapters.

Note that one has to symmetrize the wave function

$$\Psi_{\vec{k}}(\{m_j\}) = \mathcal{S} \prod_{i<j} [\theta(m_i - m_j) + s(k_i, k_j)\theta(m_j - m_i)] \prod_j e^{ik_j m_j}. \tag{3.13}$$

since σ^-_m and σ^-_n commute. But if one deals with the state directly, symmetrization is not necessary because the unsymmetrized part will be canceled by $\prod_j \sigma^-_{m_j}$ sooner or later. As a matter of fact,

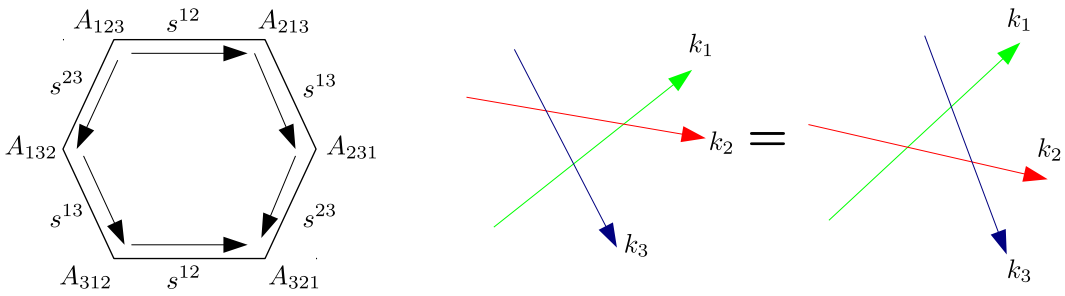

Figure 3.1: The Yang-Baxter consistency.

the unsymmetrized state (3.11) is the form we will use in Yudson's contour approach in the next chapter. The eigen energy is still given by the summation of single-particle energies:

$$E = 4J\sum_{j=1}^{M}(\Delta - \cos k_j). \tag{3.14}$$

The form of the eigenstate (3.11) is necessary for our discussion of Yudson's contour approach later, but in different books and references people usually follow some other forms. So it's necessary to clarify these different conventions.

3.2.2 Relation of Different Conventions

In my convention, which favors the Yudson's approach, the two particle Bethe Ansatz state is written as

$$|k_1, k_2\rangle = \sum_{m_1,m_2} [\theta(m_1 - m_2) + s(k_1, k_2)\theta(m_2 - m_1)]e^{ik_1m_1+ik_2m_2}\sigma^-_{m_1}\sigma^-_{m_2}|\Uparrow\rangle. \tag{3.15}$$

Notice that when you write down the state, it doesn't matter whether you symmetrize the wave function or not, namely

$$\begin{aligned} |k_1, k_2\rangle &= \sum_{m_1,m_2} [\theta(m_1 - m_2) + s(k_1, k_2)\theta(m_2 - m_1)]e^{ik_1m_1+ik_2m_2}\sigma^-_{m_1}\sigma^-_{m_2}|\Uparrow\rangle \\ &= \sum_{m_1,m_2} \mathcal{S}[\theta(m_1 - m_2) + s(k_1, k_2)\theta(m_2 - m_1)]e^{ik_1m_1+ik_2m_2}\sigma^-_{m_1}\sigma^-_{m_2}|\Uparrow\rangle. \end{aligned} \tag{3.16}$$

It's easy to check the identity above using the fact $[\sigma^-_{m_1}, \sigma^-_{m_2}] = 0$. But if one wants to manipulate the wave functions themselves, it is necessary to do the symmetrization. Also notice that the summation in (3.15) actually doesn't include $m_1 = m_2$, since $\sigma^-_m\sigma^-_m = 0$. So we can have another convention of

writing (3.15):

$$
\begin{aligned}
|k_1,k_2\rangle &= \sum_{m_1\neq m_2}[\theta(m_1-m_2)+s(k_1,k_2)\theta(m_2-m_1)]e^{ik_1m_1+ik_2m_2}\sigma^-_{m_1}\sigma^-_{m_2}|\Uparrow\rangle \\
&= (\sum_{m_1<m_2}+\sum_{m_1>m_2})[\theta(m_1-m_2)+s(k_1,k_2)\theta(m_2-m_1)]e^{ik_1m_1+ik_2m_2}\sigma^-_{m_1}\sigma^-_{m_2}|\Uparrow\rangle \\
&= \sum_{m_1<m_2}s(k_1,k_2)e^{ik_1m_1+ik_2m_2}\sigma^-_{m_1}\sigma^-_{m_2}|\Uparrow\rangle+\sum_{m_1>m_2}e^{ik_1m_1+ik_2m_2}\sigma^-_{m_1}\sigma^-_{m_2}|\Uparrow\rangle \\
&= \sum_{m_1>m_2}[e^{ik_1m_1+ik_2m_2}+s(k_1,k_2)e^{ik_1m_2+ik_2m_1}]\sigma^-_{m_1}\sigma^-_{m_2}|\Uparrow\rangle. \qquad (3.17)
\end{aligned}
$$

In the last step, I redefine the variables: $m_1 \leftrightarrow m_2$ for the second term. Following the same strategy, the general Bethe eigenstate (3.11) can be written in another form

$$
|\vec{k}\rangle = \sum_{m_1>m_2>\cdots>m_M}\sum_P A_P(\vec{k})\prod_j e^{ik_{P_j}m_j}\sigma^-_{m_j}|\Uparrow\rangle. \qquad (3.18)
$$

This is the convention used by Sutherland's book [64] and many papers: instead of summing over all m_j's and giving a step function term, they do summation in only one quadrant of the coordinates and sum over all permutations of the k_j's, each permutation with a different amplitude. Under their convention, the two-particle S-matrix is defined as the ratio between amplitudes with adjacent permutations. The two conventions can be connected by

$$
A_P(\vec{k}) = \prod_{\substack{i<j \\ P_i>P_j}} s(k_i,k_j). \qquad (3.19)
$$

Note that the amplitude of the unpermuted $\{k_j\}$ is one –this determines the normalizing factor of the state (3.11). As a supplement I like to point out, it's easy to check if we start from the symmetrized state (3.16), we still get (3.17).

3.3 Change of Variables – from Momentum to Rapidity

It is convenient to label the eigenstates with rapidity α instead of momentum k, so that the S-matrices have a civilized structure [64]. Later we will see the Yudson's contour approach is also more intuitive in the α language. This reparametrization takes different form for different values of Δ, as discussed below.

- $-1<\Delta<1$. In this region, the reparametrization is defined as:

$$
e^{ik} = \frac{e^{i\mu}-e^{\alpha}}{e^{i\mu+\alpha}-1},
$$
$$
\text{where } \Delta = -\cos\mu. \qquad (3.20)
$$

It is usually written in other forms. Two useful ones are

$$k = 2\arctan[\frac{\tanh(\alpha/2)}{\tan(\mu/2)}], \tag{3.21}$$

$$e^{ik} = \frac{\sinh(\frac{i\mu-\alpha}{2})}{\sinh(\frac{i\mu+\alpha}{2})}. \tag{3.22}$$

From (3.21) we see that $-\infty < \alpha < +\infty$ only covers the range $-\pi+\mu < k < \pi-\mu$. The range $-\pi < k < -\pi+\mu$ and $\pi-\mu < k < \pi$ are covered by $-\infty+i\pi < \alpha < i\pi$ and $i\pi < \alpha < +\infty+i\pi$, respectively. From (3.22), it is easy to see the position of the poles of α, which will play an important role in the contour approach. Under this change of variable, the S-matrix becomes

$$s(k_i, k_j) = s(\alpha_i, \alpha_j) = \frac{\sinh(\frac{\alpha_i-\alpha_j}{2} - i\mu)}{\sinh(\frac{\alpha_i-\alpha_j}{2} + i\mu)}. \tag{3.23}$$

So the Bethe eigenstate becomes

$$|\vec{\alpha}\rangle = \sum_{\{m_j\}} \prod_{i<j} [\theta(m_i - m_j) + s(\alpha_i, \alpha_j)\theta(m_j - m_i)] \prod_j [\frac{\sinh(\frac{i\mu-\alpha}{2})}{\sinh(\frac{i\mu+\alpha}{2})}]^{m_j} \sigma^-_{m_j} |\Uparrow\rangle. \tag{3.24}$$

Its eigen energy is also translated into a function of α:

$$E = 4J\sum_{j=1}^{M}(\Delta - \cos k_j) = -4J\sum_j \frac{\sin^2\mu}{\cosh\alpha - \cos\mu}. \tag{3.25}$$

Here we see that every function of α_j is periodic in the imaginary direction, with period $2\pi i$. It will affect our choice of contours significantly. Later we need to integrate over continuous k. Here it becomes integration over the α correspondingly. So the weight between dk and $d\alpha$ is useful:

$$\frac{dk}{d\alpha} = \frac{\sin\mu}{\cosh\alpha - \cos\mu} = \frac{\sin\mu}{2\sinh\frac{\alpha+i\mu}{2}\sinh\frac{\alpha-i\mu}{2}}. \tag{3.26}$$

- $\Delta < -1$. In this region, we change the the variable $k \to \alpha$ as follow:

$$e^{ik} = \frac{\sin\frac{i\lambda-\alpha}{2}}{\sin\frac{i\lambda+\alpha}{2}},$$

$$\text{where } \Delta = -\cosh\lambda \text{ , with} \lambda > 0. \tag{3.27}$$

Correspondingly, the S-matrix and eigen energy take the form of

$$S(\alpha_1, \alpha_2) = \frac{\sin(\frac{\alpha_1-\alpha_2}{2} - i\lambda)}{\sin(\frac{\alpha_1-\alpha_2}{2} + i\lambda)}, \tag{3.28}$$

$$E(\alpha) = \frac{4J\sinh^2\lambda}{\cos\alpha - \cosh\lambda}. \tag{3.29}$$

The weight between dk and $d\alpha$ becomes

$$\frac{dk}{d\alpha} = \frac{\sinh\lambda}{\cosh\lambda - \cos\alpha} = \frac{-\sinh\lambda}{2\sin\frac{i\lambda-\alpha}{2}\sin\frac{i\lambda+\alpha}{2}}. \tag{3.30}$$

- $\Delta > 1$. This region is very similar to $\Delta < -1$:

$$e^{ik} = -\frac{\sin\frac{i\lambda-\alpha}{2}}{\sin\frac{i\lambda+\alpha}{2}},$$
$$\text{where } \Delta = \cosh\lambda \text{ , with} \lambda > 0. \tag{3.31}$$

The S-matrix and eigen energy:

$$S(\alpha_1, \alpha_2) = \frac{\sin(\frac{\alpha_1-\alpha_2}{2} - i\lambda)}{\sin(\frac{\alpha_1-\alpha_2}{2} + i\lambda)}, \tag{3.32}$$
$$E(\alpha) = -\frac{4J\sinh^2\lambda}{\cos\alpha - \cosh\lambda}. \tag{3.33}$$

The weight between dk and $d\alpha$:

$$\frac{dk}{d\alpha} = \frac{\sinh\lambda}{\cosh\lambda - \cos\alpha} = \frac{-\sinh\lambda}{2\sin\frac{i\lambda-\alpha}{2}\sin\frac{i\lambda+\alpha}{2}}. \tag{3.34}$$

- $\Delta = -1$. The reparametrization takes the form

$$e^{ik} = \frac{\alpha + \frac{i}{2}}{\alpha - \frac{i}{2}}. \tag{3.35}$$

The S-matrix, eigen energy and weight function:

$$S(\alpha_1, \alpha_2) = \frac{\alpha_1 - \alpha_2 + i}{\alpha_1 - \alpha_2 - i}, \tag{3.36}$$
$$E(\alpha) = \frac{2J}{\alpha^2 + \frac{1}{4}}, \tag{3.37}$$
$$\frac{dk}{d\alpha} = \frac{1}{\alpha^2 + \frac{1}{4}}. \tag{3.38}$$

Here I summarize the different parametrization in Table 3.1. Later I will give an argument that Δ's with opposite sign give the same time evolution. So actually, the discussion on the regime $\Delta < 0$ is general enough.

3.4 Thermodynamic Limit and String Solutions

For (3.11) to be a valid eigenstate, the momentum k need to be quantized. Or equivalently, the rapidity α need to be quantized. It is conventional to impose a periodic boundary condition on the system [95], which leads to the Bethe Ansatz equations (BAE) that restrict the k (or α):

$$e^{ik_j L} = \prod_{l\neq j} s(k_l, k_j) \text{ for } j = 1, 2, \ldots, M. \tag{3.39}$$

where the L is the size of the system. Intuitively, it means that if one particle is moved through all the other particles and comes back to the original position, the wave function gets a extra phase of

Table 3.1: Parametrizations in different region of Δ. In this table we also define the functions $P(\alpha)$, $S(\alpha_1,\alpha_2)$, $\epsilon(\alpha)$ and $W(\alpha)$ as functions of the rapidity.

	Plane wave	S-matrix	Eigen energy	Weight$\equiv \frac{1}{2\pi}\frac{dk}{d\alpha}$
In k-language	e^{ik}	$-\frac{1-e^{ik_1+ik_2}-2\Delta e^{ik_1}}{1-e^{ik_1+ik_2}-2\Delta e^{ik_2}}$	$4J(\Delta-\cos k)$	
Functions in α-language	$P(\alpha)$	$S(\alpha_1,\alpha_2)$	$\epsilon(\alpha)$	$W(\alpha)$
$\Delta=-\cosh\lambda<-1$	$\frac{\sin\frac{i\lambda-\alpha}{2}}{\sin\frac{i\lambda+\alpha}{2}}$	$\frac{\sin(\frac{\alpha_1-\alpha_2}{2}-i\lambda)}{\sin(\frac{\alpha_1-\alpha_2}{2}+i\lambda)}$	$\frac{4J\sinh^2\lambda}{\cos\alpha-\cosh\lambda}$	$\frac{1}{2\pi}\frac{\sinh\lambda}{\cosh\lambda-\cos\alpha}$
$\Delta=-1$	$\frac{\alpha+i/2}{\alpha-i/2}$	$\frac{\alpha_1-\alpha_2+i}{\alpha_1-\alpha_2-i}$	$\frac{2J}{\alpha^2+1/4}$	$\frac{1}{2\pi}\frac{1}{\alpha^2+1/4}$
$-1<\Delta=-\cos\mu<1$	$\frac{\sinh(\frac{i\mu-\alpha}{2})}{\sinh(\frac{i\mu+\alpha}{2})}$	$\frac{\sinh(\frac{\alpha_i-\alpha_j}{2}-i\mu)}{\sinh(\frac{\alpha_i-\alpha_j}{2}+i\mu)}$	$-\frac{4J\sin^2\mu}{\cosh\alpha-\cos\mu}$	$\frac{1}{2\pi}\frac{\sin\mu}{\cosh\alpha-\cos\mu}$
$\Delta=\cosh\lambda>1$	$-\frac{\sin\frac{i\lambda-\alpha}{2}}{\sin\frac{i\lambda+\alpha}{2}}$	$\frac{\sin(\frac{\alpha_1-\alpha_2}{2}-i\lambda)}{\sin(\frac{\alpha_1-\alpha_2}{2}+i\lambda)}$	$-\frac{4J\sinh^2\lambda}{\cos\alpha-\cosh\lambda}$	$\frac{1}{2\pi}\frac{\sinh\lambda}{\cosh\lambda-\cos\alpha}$

e^{ik_jL}. Taking the logarithm, it becomes more familiar:

$$k_j=\frac{2\pi n_j}{L}-\frac{i}{L}\sum_l \ln[s(k_l,k_j)] \text{ for } j=1,2,\ldots,M. \tag{3.40}$$

Here n_j's are the quantum numbers. Without the last term, it is the standard way to quantize k for free particles. The last term captures the interaction through S-matrices.

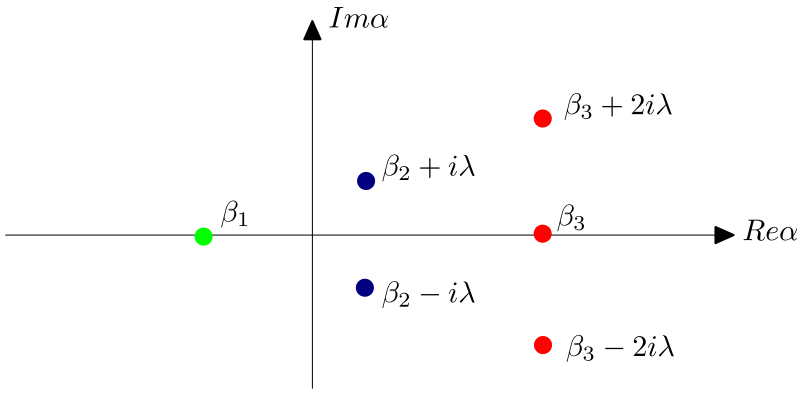

Figure 3.2: String solutions of Bethe Ansatz Equations

In general it is difficult to find the solutions of (3.39). In the thermodynamic limit, namely the size and particle number of the system $L,M\to\infty$ with $M/L=const.$, the *string hypothesis* states that solutions of the BAE will form equally spaced strings in the complex α-plane. As an example, for the regime $\Delta<-1$, the BAE (3.39) are reparametrized as

$$\left(\frac{\sin\frac{\alpha_j+i\lambda}{2}}{\sin\frac{\alpha_j-i\lambda}{2}}\right)^L\prod_{l\neq j}\frac{\sin(\frac{\alpha_j-\alpha_l}{2}-i\lambda)}{\sin(\frac{\alpha_j-\alpha_l}{2}+i\lambda)}=1. \tag{3.41}$$

A string of order n (usually written as n-string) of its solutions can be written as

$$\{\alpha\}_n = \beta_n - (n-1)i\lambda + i\delta_1, \beta_n - (n-3)i\lambda + i\delta_2, \ldots, \beta_n + (n-1)i\lambda + i\delta_n, \tag{3.42}$$

where β_n is the real part (usually called "center" of the string), δ_j's are the deviations which goes to 0 as $e^{-const\cdot L}$, and $\lambda = \cosh(-\Delta)$ as defined in Table. 3.1. Figure 3.2 shows three strings of order 1, 2 and 3. Under this hypothesis, the BAE (3.39) can be rewritten as equations of the distribution functions of the centers $\rho_n(\beta)$. Any observable in the thermodynamic limit is given as a functional of these distribution functions. E.g. the total magnetization is given by

$$\langle s^z \rangle = \frac{1}{2}\frac{L-2M}{L} = \frac{1}{2} - \sum_{n=1}^{\infty} n \int \frac{d\beta}{2\pi}\rho_n(\beta). \tag{3.43}$$

To get the thermal values of observables, one sums over all possible eigenstates with the Gibbs weight $e^{H/T-S}$, and gets a functional integral over the functions $\{\rho_n(\beta)\}$, which can be simplified by saddle point approximation at last. This formalism is know as the *thermodynamic Bethe ansatz (TBA)*. The book [95] explains the gory details of it. Recently it has been generalized to study the asymptotic states of integrable models [67], as introduced in Section 2.4.

Physically, the real solutions of the BAE (3.39) are identified as propagating states, while the complex solutions are realized as bound states –in those states the wave function decays exponentially when particles are far apart. Later we will show this string structure emerges naturally from the our contour approach, and are independent of the periodic boundary condition.

Chapter 4
Methodology – Generalized Yudson's Contour Approach

In this chapter, I generalize the Yudson contour representation, and show explicitly how to get the exact time-dependent wave function in an integral form for the XXZ model.

4.1 Introduction to Yudson's Contour Approach

The conventional way to calculate the time evolution of a quantum system is to expand the initial state by the complete eigenstate basis of the full Hamiltonian

$$|\Psi_0\rangle = \sum_{\{k_j\}} |\vec{k}\rangle\langle\vec{k}|\Psi_0\rangle, \tag{4.1}$$

where the summation over $\{k_j\}$ means over all the possible set of quantized k_j's, or equivalently for the XXZ model, over all the possible solutions of the BAE (3.39). Then the time dependent state is given by

$$|\Psi(t)\rangle = e^{-i\hat{H}t} \sum_{\{k_j\}} |\vec{k}\rangle\langle\vec{k}|\Psi_0\rangle = \sum_{\{k_j\}} e^{-iE(\vec{k})t}|\vec{k}\rangle\langle\vec{k}|\Psi_0\rangle. \tag{4.2}$$

Due to the complexity of the Bethe eigenstates, both the overlap $\langle\vec{k}|\Psi_0\rangle$ and the summation over all possible k_j's are difficulty to calculate. Until very recently there are some developments following this direction [67, 107, 68]. On the other hand, V. I. Yudson proposed a method to calculate the time evolution of integrable system in 1985, in the context of Dicke model [120]. The basic idea is to work on an infinite line directly, so the summation in the expansion (4.1) can be replaced by an integral on the complex plane

$$|\Psi_0\rangle = \int_\gamma d\vec{k}|\vec{k}\rangle(\vec{k}|\Psi_0\rangle, \tag{4.3}$$

where the $|\vec{k})$, called Yudson's auxiliary state, has a simple overlap with a generic physical state. The contours of integrals need to be chosen cleverly to make the identity above valid. With this expansion, the time-dependent state is given by

$$|\Psi(t)\rangle = \int_\gamma d\vec{k}e^{-iE(\vec{k})t}|\vec{k}\rangle(\vec{k}|\Psi_0\rangle, \tag{4.4}$$

and the observables follow from it. We call the expansion of the initial state (4.3) the central theorem, as it plays the central role in this contour approach. This approach is shown to be successful in Lieb-Liniger model [65, 66], which has an simple-structured S-matrix almost identical to Dicke model. In the next section I will show that a generalized version of the Yudson's contour approach can be applied to the XXZ model, which has a more complicated S-matrix. Before that, let me briefly review the proof of the central theorem for the Lieb-liniger model (the proof is almost identical to that of the Dicke model), as a comparison of the generalized version in the next section.

4.1.1 Proof of the Central Theorem in the Lieb-Liniger Model

The Lieb-Liniger model describes the 1-D boson gas with a Delta-function interaction:

$$H = \int dx[\partial_x b^\dagger(x)\partial_x b(x) + cb^\dagger(x)b(x)b^\dagger(x)b(x)]. \tag{4.5}$$

Its Bethe eigenstate, in a similar notation as (3.11), is given by

$$|\vec{k}\rangle = \int d\vec{y}\prod_{i<j}[\theta(y_i - y_j) + s(k_i, k_j)\theta(y_j - y_i)]\prod_j e^{ik_j y_j}b^\dagger(y_j)|0\rangle, \tag{4.6}$$

where the $|0\rangle$ is the vacuum state, and the S-matrix is given by

$$s(k_1, k_2) = \frac{k_1 - k_2 + ic}{k_1 - k_2 - ic}. \tag{4.7}$$

We choose the initial state with N bosons to be

$$|\vec{x}\rangle = \theta(\vec{x})\prod_j b^\dagger(x_j)|0\rangle, \tag{4.8}$$

where the notation $\theta(\vec{x})$ means $\theta(x_1 > x_2 > \cdots > x_N)$. A generic initial state can be written as a expansion of it. And the Yudson's auxiliary state is defined as

$$|\vec{k}) = \int d\vec{y}\theta(\vec{y})\prod_j e^{ik_j y_j}b^\dagger(y_j)|0\rangle. \tag{4.9}$$

Note that we use y's to denote the numb coordinates that will be integrated out, and x's to denote the initial coordinates. The overlap between the auxiliary state and the initial state is trivial: $(\vec{k}|\vec{x}\rangle = \prod_j e^{-ik_j x_j}$. With these notations, the central theorem is written explicitly as

$$\begin{aligned}
|\vec{x}\rangle &= \int_{\gamma_j} d\vec{k}|\vec{k}\rangle(\vec{k}|\vec{x}\rangle \\
&= \int_{\gamma_j} d\vec{k}\int d\vec{y}\prod_{i<j}[\theta(y_i - y_j) + \frac{k_i - k_j + ic}{k_i - k_j - ic}\theta(y_j - y_i)]\prod_j e^{ik_j(y_j - x_j)}b^\dagger(y_j)|0\rangle \\
&= \int_{\gamma_j} d\vec{k}\int d\vec{y}\prod_{i<j}[1 + \frac{2ic}{k_i - k_j - ic}\theta(y_j - y_i)]\prod_j e^{ik_j(y_j - x_j)}b^\dagger(y_j)|0\rangle.
\end{aligned} \tag{4.10}$$

In the last line we use the fact $\theta(y_i - y_j) + \theta(y_j - y_i) = 1$. The term 1 in the bracket [] will give us the identity we want. So we just need to prove

$$\int_{\gamma_j} d\vec{k} \int d\vec{y} \prod_{i<j} \frac{2ic}{k_i - k_j - ic} \theta(y_j - y_i) \prod_j e^{ik_j(y_j - x_j)} b^\dagger(y_j)|0\rangle = 0. \tag{4.11}$$

For the repulsive case $c > 0$, the contours γ_j can be chosen as along the real axis from $-\infty$ to ∞, shown in Fig. 4.1 (a). The identity (4.11) can be proved following Yudson's logic [120] as below:

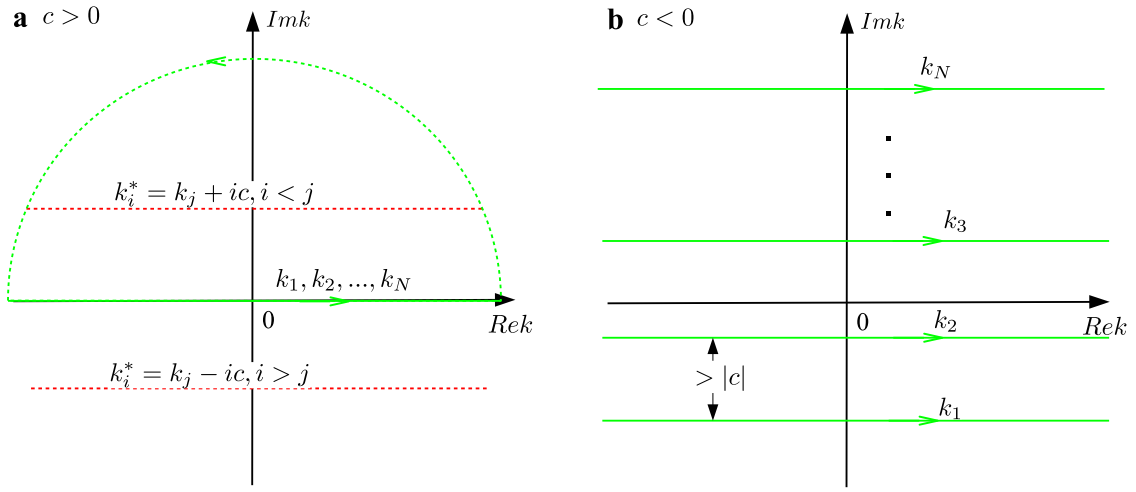

Figure 4.1: The integral contours for Lieb-Liniger model. (a) The repulsive case $c > 0$. The green solid lines denote the contour. The green dashed line denotes the typical way of closing the contours. The red dashed lines denote the position of the possible poles. (b) The attractive case $c < 0$. The spacing between the contours should be greater than $|c|$.

- If $y_N > x_N$, the contour of k_N can be closed by a big circle on the upper half plane. Since the possible poles of k_N are $k_N^* = k_j - ic$, for $j = 1, 2, \ldots, N-1$, the closed contour doesn't enclose any pole in it, so the integration over k_N gives zero. Thus the non-zero contribution of the integral comes from the region $y_N \leq x_N$. If $y_{N-1} > x_{N-1}$, the contour of k_{N-1} can be closed on the upper half plane. Because of the relation $y_{N-1} > x_{N-1} > x_N \geq y_N$, $\theta(y_N - y_{N-1}) = 0$, the pole of k_{N-1} at $k_{N-1}^* = k_N + ic$ doesn't exist. All the possible poles of k_{N-1} are at $k_{N-1}^* = k_j - ic$, for $j = 1, 2, \ldots, N-2$. Again, the closed contour of k_{N-1} doesn't enclose any pole, so the integration over k_{N-1} gives zero. Thus the non-zero contribution of the integral comes from the region $y_N \leq x_N \cap y_{N-1} \leq x_{N-1}$. Following this logic, we will finally get that the non-zero contribution of the integral comes from the region $y_N \leq x_N \cap y_{N-1} \leq x_{N-1} \cap \cdots \cap y_1 \leq x_1$.

- If $y_1 < x_1$, the contour of k_1 can be closed on the lower half plane. Since the possible poles of k_1 are $k_1^* = k_j + ic$, for $j = 2, 3, \ldots, N$, the closed contour doesn't enclose any pole in it,

so the integration over k_1 gives zero. Thus the non-zero contribution of the integral comes from the region $y_1 \geq x_1$. If $y_2 < x_2$, the contour of k_2 can be closed on the lower half plane. Because of the relation $y_2 < x_2 < x_1 \leq y_1$, $\theta(y_2 - y_1) = 0$, the pole of k_2 at $k_2^* = k_1 - ic$ doesn't exist. All the possible poles of k_2 are at $k_2^* = k_j + ic$, for $j = 3, 4, \ldots, N$. Again, the closed contour of k_2 doesn't enclose any pole, so the integration over k_2 gives zero. Thus the non-zero contribution of the integral comes from the region $y_1 \geq x_1 \cap y_2 \geq x_2$. Following this logic, we will finally get that the non-zero contribution of the integral comes from the region $y_1 \geq x_1 \cap y_2 \geq x_2 \cap \cdots \cap y_N \geq x_N$.

- Combining the conclusion above, the only region where the integral wouldn't vanish is $y_j = x_j$ for $j = 1, 2, \ldots, N$. However, in this region, because $x_1 > x_2 > \cdots > x_N$, we have $y_1 > y_2 > \cdots > y_N$, so all the θ functions give zero. To sum up, we proved the integral (4.11) is indeed zero, under all situations.

For the attractive case $c < 0$, we only need to spread out the contours with spacing greater than $|c|$, as shown in Fig. 4.1 (b). Then the arguments in repulsive case would completely apply here.

4.2 Proof of the Central Theorem in the XXZ Model

In this section I specify the contour γ and show the validity of the central theorem for the XXZ model. I work in the language of rapidity α. So in different regimes of Δ, the proof will take different forms but follow the same strategy.

Before the proof I give the argument that changing the sign of Δ doesn't affect the time evolution. It is observed in the numerical simulation [7]. A similar phenomenon is also observed for Hubbard model in experiment [121]. Here I follow the explanation in Ref. [66]. Let's denote the eigenstates and eigen energy of $H(\Delta)$ to be $|\alpha\rangle$ and E_α, where α is a set of quantum numbers. The eigenstates and eigen energy of $H(-\Delta)$ are denoted as $|\tilde{\alpha}\rangle$ and $\tilde{E}_\alpha$. Remember that $H(\Delta)$ and $H(-\Delta)$ are related by a unitary transformation

$$\mathcal{U} H(\Delta) \mathcal{U}^\dagger = -H(-\Delta). \tag{4.12}$$

The unitary operator $\mathcal{U}$ is defined in (3.4). It is easy to see that $|\tilde{\alpha}\rangle = \mathcal{U}|\alpha\rangle$ and $\tilde{E}_\alpha = -E_\alpha$. Then

the time evolution of an initial state $|\Psi_0\rangle$ under $H(\Delta)$ and $H(-\Delta)$ are respectively

$$\langle\hat{O}(t)\rangle_{H(\Delta)} = \sum_{\alpha,\alpha'}\langle\Psi_0|\alpha'\rangle\langle\alpha|\Psi_0\rangle\langle\alpha'|\hat{O}|\alpha\rangle e^{-i(E_\alpha - E_{\alpha'})t}, \tag{4.13}$$

$$\begin{aligned}\langle\hat{O}(t)\rangle_{H(-\Delta)} &= \sum_{\alpha,\alpha'}\langle\Psi_0|\tilde{\alpha'}\rangle\langle\tilde{\alpha}|\Psi_0\rangle\langle\tilde{\alpha'}|\hat{O}|\tilde{\alpha}\rangle e^{-i(\tilde{E}_\alpha - \tilde{E}_{\alpha'})t} \\ &= \sum_{\alpha,\alpha'}\langle\Psi_0|\mathcal{U}|\alpha'\rangle\langle\alpha|\mathcal{U}^\dagger|\Psi_0\rangle\langle\alpha'|\mathcal{U}^\dagger\hat{O}\mathcal{U}|\alpha\rangle e^{i(E_\alpha - E_{\alpha'})t}.\end{aligned} \tag{4.14}$$

For the initial state we are interested (4.17), the effect of operator $\mathcal{U}$ is just to give a possible minus sign $\mathcal{U}^\dagger|\Psi_0\rangle = \pm|\Psi_0\rangle$, which will be canceled as last since $|\Psi_0\rangle$ appears twice in (4.14). On the other hand, the operators of interest, such as the local magnetization, the staggered magnetization and the spin currents, are invariant under the transformation $\mathcal{U}$ (because they can be written in terms of σ_n^z and $\mathcal{U}\sigma_n^z\mathcal{U}^\dagger = \sigma_n^z$). So we have the evolution under $H(-\Delta)$,

$$\langle\hat{O}(t)\rangle_{H(-\Delta)} = \sum_{\alpha,\alpha'}\langle\Psi_0|\alpha'\rangle\langle\alpha|\Psi_0\rangle\langle\alpha'|\hat{O}|\alpha\rangle e^{i(E_\alpha - E_{\alpha'})t}, \tag{4.15}$$

is just the evolution under $H(\Delta)$ with reversal time. At last, under time reversal $t \to -t$, $\vec{\sigma} \to -\vec{\sigma}$, but $H(\Delta)$ is invariant. So we conclude that for the initial state and observables we are interested, the time evolution under $H(\Delta)$ and $H(-\Delta)$ are the same.

Thus it is general enough to prove the central theorem only in the regime $\Delta < 0$. I will show the explicit proof for the gapped regime $\Delta < -1$. For the other regimes, I will sketch the idea and identify the integral contours.

4.2.1 The Gapped Regime $\Delta < -1$

After the reparametrization in Table 3.1, the central theorem will be formally:

$$|\Psi_0\rangle = \int_\gamma d\vec{\alpha}|\vec{\alpha}\rangle(\vec{\alpha}|\Psi_0\rangle. \tag{4.16}$$

The initial state is chosen to be similar to (4.8):

$$|\Psi_0\rangle = \theta(\vec{n})\prod_j \sigma_{n_j}^-|\Uparrow\rangle, \tag{4.17}$$

where we define the notation $\theta(\vec{n}) = \theta(n_1 > n_2 > \cdots > n_M)$. A generic initial state can be expanded by this basis. The Yudson's auxiliary state takes the form

$$|\vec{\alpha}) = \sum_{\{m_j\}}\theta(\vec{m})\prod_j[\frac{\sin(\frac{i\lambda-\alpha_j}{2})}{\sin(\frac{i\lambda+\alpha_j}{2})}]^{m_j}\sigma_{m_j}^-|\Uparrow\rangle. \tag{4.18}$$

So it's easy to calculate the overlap

$$(\vec{\alpha}|\Psi_0\rangle = \prod_j[\frac{\sin(\frac{i\lambda-\alpha_j}{2})}{\sin(\frac{i\lambda+\alpha_j}{2})}]^{-n_j}. \tag{4.19}$$

The central theorem would be explicitly

$$|\Psi_0\rangle = \sum_{\{m_j\}} \int_{\gamma_j} \prod_j [\frac{d\alpha_j}{2\pi} \frac{\sinh\lambda}{2\sin\frac{\alpha_j+i\lambda}{2}\sin\frac{\alpha_j-i\lambda}{2}}] \prod_{i<j} [\theta(m_i-m_j) + \frac{\sin(\frac{\alpha_i-\alpha_j}{2}-i\lambda)}{\sin(\frac{\alpha_i-\alpha_j}{2}+i\lambda)}\theta(m_j-m_i)]$$
$$\times \prod_j [\frac{\sin(\frac{i\lambda-\alpha_j}{2})}{\sin(\frac{i\lambda+\alpha_j}{2})}]^{m_j-n_j} \sigma^-_{m_j} |\Uparrow\rangle. \tag{4.20}$$

Next we will specify the contour γ_j over which α_j is integrated, and prove this identity. For convenience, I define β to be a real varable that runs in $(-\infty, +\infty)$, and c is a real constant. So $\alpha = \beta + ic$ denotes the line parallel to the real axis. I claim the contours γ_j to be as in Fig. 4.2 (a): each γ_j has two parts: going forward from left to right on $\alpha_j = \beta$(real axis), and going backward from right to left on $\alpha_j = \beta + ic_j$, with

$$\lambda < c_j < 2\lambda. \tag{4.21}$$

Before proving this contour is valid, I need to point out some general properties of this set up:

1. Because all functions of α_j in (4.20) are periodic along the real axis, the value of α_j is actually defined modulo 2π, namely, α and $\alpha + 2n\pi$ are the same point. So we can choose the area between $-\pi$ and π to be the "first Brillouin zone" and finish our work in it.

2. We have two head-to-tail ways of closing the contour of α_j: "between" the contours as shown in Fig. 4.2 (c), and "beyond" the contours as shown in Fig. 4.2 (d). We first argue that the extra parts we add to the contours doesn't contribute to the integral: In either way, the vertical parts of the contours don't contribute because the part at $-\pi$ and π are running in the opposite direction and have the same value due to the periodicity of the integrand. For the second way, the horizontal parts at the top and the bottom are infinite far from the real axis. They don't contribute because the weight term, which control the convergence of the integrand, vanishes at $\pm i\infty$. Explicitly,

$$\text{weight term} = \frac{\sinh\lambda}{\cosh\lambda - \cos\alpha} \to \frac{2\sinh\lambda}{e^{|Im\alpha|}e^{\pm iRe\alpha}} \to 0 (Im\alpha \to \pm\infty). \tag{4.22}$$

   As a conclusion, the contour integral of (4.20) is equal to the residues of the poles in the enclosed area of Fig. 4.2 (c) or (d).

3. Let's define the notations (see Table 3.1 for the definitions of the functions)

$$I^j(\alpha) \equiv W(\alpha)P(\alpha)^{m_j-n_j} = -\frac{\sinh\lambda}{4\pi} \cdot \frac{(\sin\frac{i\lambda-\alpha}{2})^{m_j-n_j-1}}{(\sin\frac{i\lambda-\alpha}{2})^{m_j-n_j+1}}, \tag{4.23}$$

$$Z_{ij}(\alpha,\alpha') \equiv \theta(m_i-m_j) + S(\alpha,\alpha')\theta(m_j-m_i) = \theta(m_i-m_j) + \frac{\sin(\frac{\alpha-\alpha'}{2}-i\lambda)}{\sin(\frac{\alpha-\alpha'}{2}+i\lambda)}\theta(m_j-m_i). \tag{4.24}$$

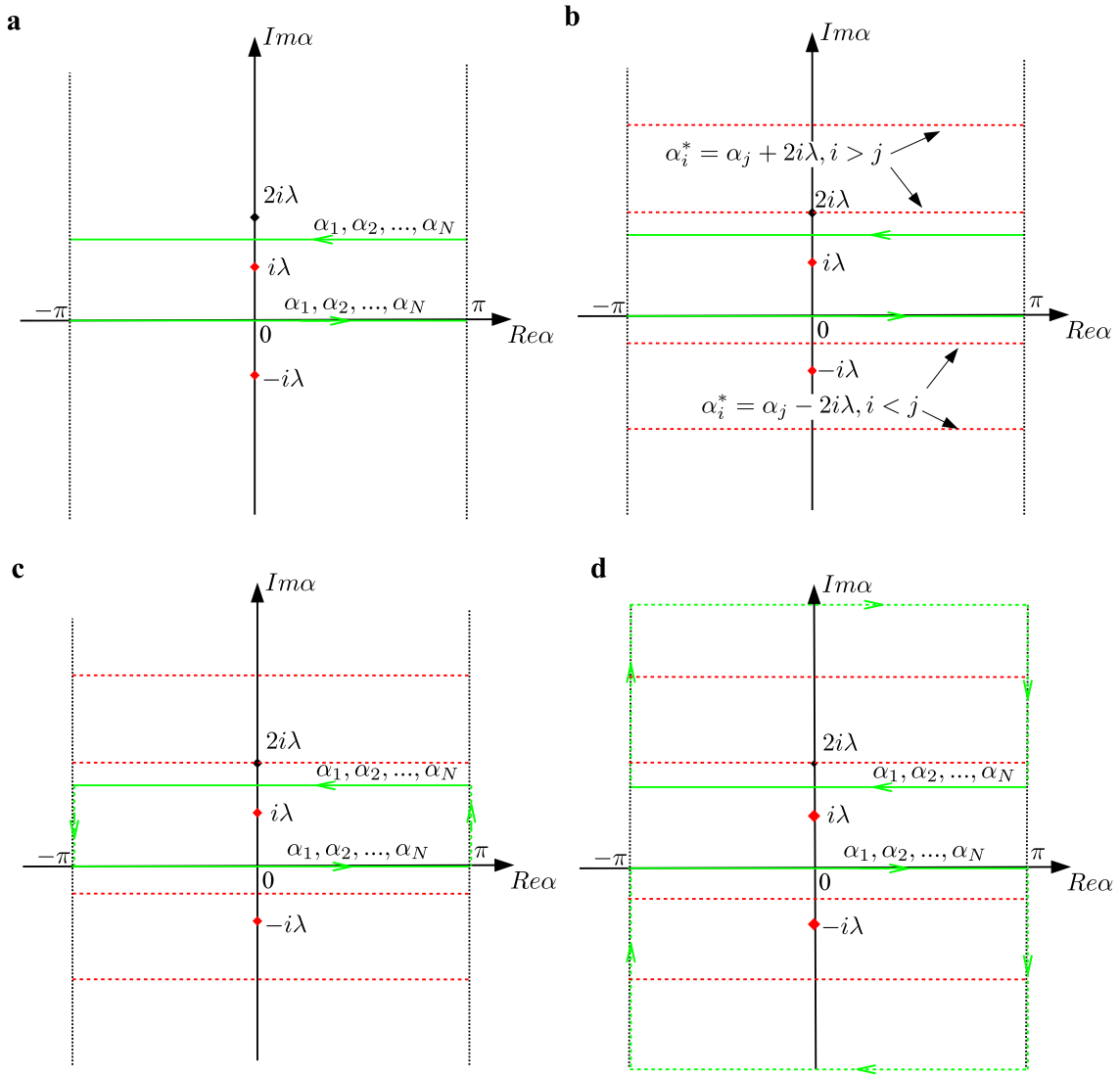

Figure 4.2: (a) The contours of integral on the α-plane for the region $\Delta < -1$. In the graph $\lambda = \cos^{-1}(-\Delta)$. (b) The position of all the possible poles of the integrand. The two red points, $\pm i\lambda$, are the poles of the planewave, depending on the order of m_j and n_j. The red lines are the poles of the S-matrix, depending on both the order of i and j, m_i and m_j. (c) The first way of closing the contours: "between" the contours. In this way, the poles of the S-matrix are never enclosed. (d) The second way of closing the contours: "beyond" the contours. In this way the poles of the S-matrix are always enclosed.

Then (4.20) can be written in a shorter and more meaningful way:

$$|\Psi_0\rangle = \sum_{\{m_j\}} \int_{\gamma_j} \prod_j [d\alpha_j I^j(\alpha_j)] \prod_{i<j} Z_{ij}(\alpha_i, \alpha_j) \prod_j \sigma^-_{m_j} |\Uparrow\rangle. \tag{4.25}$$

We define the (unsymmetrized) wave function in the coordinate basis to be

$$\Psi_0^{\{n_j\}}(\{m_j\}) \equiv \int_{\gamma_j} \prod_j [d\alpha_j I^j(\alpha_j)] \prod_{i<j} Z_{ij}(\alpha_i, \alpha_j). \tag{4.26}$$

Then what we need to prove is this wave function is equal to δ-function up to antisymmetric terms:

$$\Psi_0^{\{n_j\}}(\{m_j\}) = \prod_j \delta_{m_j,n_j} + A(\{m_j\}), \tag{4.27}$$

where $A(\{m_j\})$ is antisymmetric under the exchange of some pair of m_i and m_j. Because $\prod_j \sigma^-_{m_j} |\Uparrow\rangle$ is fully symmetric under the exchange of any pair of m_i and m_j, we have

$$\sum_{\{m_j\}} A(\{m_j\}) \prod_j \sigma^-_{m_j} |\Uparrow\rangle = 0. \tag{4.28}$$

So (4.27) is equivalent to (4.20). As a preparation of the proof of (4.27), we list the pole structure of $I^j(\alpha)$ and $Z_{ij}(\alpha, \alpha')$ here:

$$I^j(\alpha) \text{ has poles at } \begin{cases} \alpha^* = i\lambda & m_j \le n_j \\ \alpha^* = -i\lambda & m_j \ge n_j \end{cases}, \tag{4.29}$$

$$Z_{ij}(\alpha, \alpha') \text{ has poles at } \begin{cases} \alpha^* = \alpha' - 2i\lambda \\ \alpha'^* = \alpha + 2i\lambda \end{cases} \quad m_j > m_i. \tag{4.30}$$

The poles of $I^j(\alpha)$ are generally of high orders. While the poles of $Z_{ij}(\alpha, \alpha')$ are always first-order poles, with the residue

$$\text{Res}[Z_{ij}(\alpha, \alpha')]|_{\alpha^* = \alpha' - 2i\lambda} = 2i \sinh(2\lambda) \theta(m_j - m_i). \tag{4.31}$$

4. We are free to move the contours as long as they don't go over any possible poles. Later in the proof, we will use the slightly modified contours as in Fig. 4.3. This modification can change the intermediate calculation and avoid some bad definitions as will be shown later, but it doesn't affect the final result at all.

Now we are ready to prove the central theorem (4.27). The basic strategy of the proof is to argue in the case $m_j = n_j$ the integral gives 1, and in all the other cases the integral either vanishes or give an antisymmetric term.

- For the case $m_j > n_j$, all the possible poles for α_j are

$$\alpha_j^* = -i\lambda, \tag{4.32}$$

$$\alpha_j^* = \alpha_k + 2i\lambda, \text{ for } k < j, \tag{4.33}$$

$$\alpha_j^* = \alpha_k - 2i\lambda, \text{ for } k > j. \tag{4.34}$$

Note that $+i\lambda$ is not a pole. In this case, we can close the contours "between" the contours, and enclose none of the poles above. So the integral gives zero. So the only non-zero contribution of the integral comes from $m_j \leq n_j$.

- Now let's look at the case $m_1 < n_1$, and consider the integration over α_1. The poles of α_1 are

$$\alpha_1^* = +i\lambda, \tag{4.35}$$

$$\alpha_1^* = \alpha_j - 2i\lambda, \text{ for } j = 2, 3, \ldots, N. \tag{4.36}$$

We would close the contour of α_1 "beyond" the contours to avoid the high-order pole $\alpha_1^* = +i\lambda$ but enclose all the first-order poles $\alpha_1^* = \alpha_j - 2i\lambda$. Then the integral will be given by the summation of all the residues:

$$\begin{aligned}
\Psi_0^{\{n_j\}}(\{m_j\}) &= \int \prod_{j=2}^{N} d\alpha_j \int d\alpha_1 \text{Integrand} \\
&= \int \prod_{j=2}^{N} d\alpha_j 2\pi i \sum_{k=2}^{N} \text{Res}(\text{Integrand})|_{\alpha_1=\alpha_k-2i\lambda} \\
&= -4\pi \sin 2\lambda \sum_{k=2}^{N} \theta(m_k - m_1) \int \prod_{j=2}^{N} d\alpha_j \frac{\text{Integrand}}{Z_{1k}(\alpha_1, \alpha_k)}|_{\alpha_1=\alpha_k-2i\lambda}.
\end{aligned} \tag{4.37}$$

In the last line we used the residue of $Z_{ij}(\alpha, \alpha')(4.31)$. Here we defined

$$\text{Integrand} \equiv \prod_j [I^j(\alpha_j)] \prod_{i<j} Z_{ij}(\alpha_i, \alpha_j). \tag{4.38}$$

Now let's consider a term with particular k in the summation above, and integrate over α_k first

$$\begin{aligned}
T_k \equiv& \theta(m_k - m_1) \int \prod_{j=2}^{N} d\alpha_j \frac{\text{Integrand}}{Z_{1k}(\alpha_1, \alpha_k)}|_{\alpha_1=\alpha_k-2i\lambda} \\
=& \theta(m_k - m_1) \int \prod_{j=2, j\neq k}^{N} d\alpha_j \int d\alpha_k \frac{\text{Integrand}}{Z_{1k}(\alpha_1, \alpha_k)}|_{\alpha_1=\alpha_k-2i\lambda} \\
=& \theta(m_k - m_1) \int \prod_{j=2, j\neq k}^{N} d\alpha_j \\
& \times \int d\alpha_k I^1(\alpha_k - 2i\lambda) \prod_{l=2}^{N} I^l(\alpha_l) \prod_{l=2, l\neq k}^{N} Z_{1l}(\alpha_k - 2i\lambda, \alpha_l) \prod_{1<p<q} Z_{pq}(\alpha_p, \alpha_q).
\end{aligned} \tag{4.39}$$

Let's look at the integrand above term by term. The term $I^1(\alpha_k - 2i\lambda)\prod_{l=2}^{N} I^l(\alpha_l)$ as a function of α_k is given by

$$I^1(\alpha_k - 2i\lambda)I^k(\alpha_k) = \# \cdot \frac{(\sin\frac{i\lambda-\alpha_k}{2})^{m_k-n_k-1}}{(\sin\frac{i\lambda+\alpha_k}{2})^{m_k-n_k+1}} \frac{(\sin\frac{3i\lambda-\alpha_k}{2})^{m_1-n_1-1}}{(\sin\frac{i\lambda-\alpha_k}{2})^{m_1-n_1+1}}. \tag{4.40}$$

Since we have the relation $n_1 > n_k$, $m_k > m_1$, the power of $\sin\frac{i\lambda-\alpha_k}{2}$ is

$$m_k - n_k - m_1 + n_1 - 2 \geq 0. \tag{4.41}$$

So $\alpha_k^* = i\lambda$ is not a pole. For the term $\prod_{1<p<q} Z_{pq}(\alpha_p, \alpha_q)$, the poles of α_k are

$$\alpha_k^* = \begin{cases} \alpha_p - 2i\lambda & k < p \\ \alpha_p + 2i\lambda & k > p > 1 \end{cases}. \tag{4.42}$$

For either case, this pole is not in the area "beyond" the contours. Finally, the pole of $\prod_{l=2,l\neq k}^{N} Z_{1l}(\alpha_k - 2i\lambda, \alpha_l)$ are

$$\alpha_k^* = \alpha_l \text{ for } l > 1, l \neq k. \tag{4.43}$$

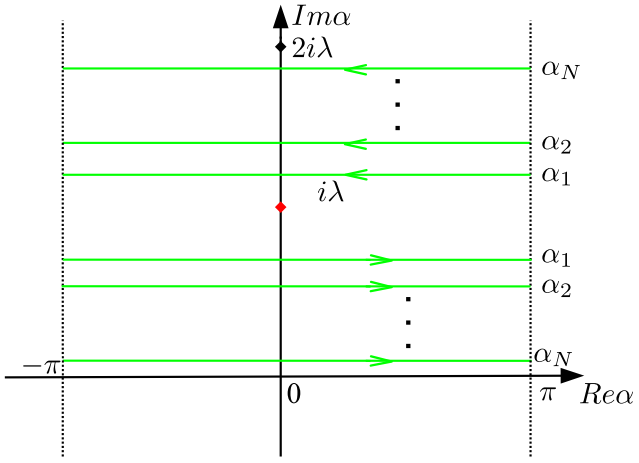

Figure 4.3: The contours of integral we use in the proof of central theorem. They are slightly different from the original ones, but this difference doesn't affect the final value of the integral.

So according to Figure 4.3, we have two possibility:

1. For those $l > k$, we can close the contour of α_k around $i\lambda$ and enclose no pole in it. The integral over α_k give 0. So $T_k = 0$.

2. For those $l < k$, we still close the contour of α_k around $i\lambda$, but we'll enclose the first-order poles $\alpha_k^* = \alpha_l$ in it, and we need to calculte the residues. For a particular l, this residue

is

$$\theta_{m_l,m_1}\cdot\frac{I^1(\alpha_k-2i\lambda)\prod_{p=2}^N I^p(\alpha_p)\prod_{p=2,p\neq k}^N Z_{1p}(\alpha_k-2i\lambda,\alpha_p)\prod_{1<p<q}Z_{pq}(\alpha_p,\alpha_q)}{Z_{1l}(\alpha_k-2i\lambda,\alpha_l)}|_{\alpha_k=\alpha_l}. \tag{4.44}$$

Note in the expression above, all the terms including m_k and m_l are

$$I^k(\alpha_l)I^l(\alpha_l)\prod_{\substack{1<p<k\\p\neq l}}Z_{pk}(\alpha_p,\alpha_l)\prod_{p>k}Z_{kp}(\alpha_l,\alpha_p)\prod_{p<l}Z_{pl}(\alpha_p,\alpha_l)\prod_{\substack{p>l\\p\neq k}}Z_{lp}(\alpha_l,\alpha_p)Z_{lk}(\alpha_l,\alpha_l). \tag{4.45}$$

We notice that $Z_{lk}(\alpha_l,\alpha_l)=\theta(m_l-m_k)-\theta(m_k-m_l)$ is antisymmetric under the exchange of m_l and m_k, and all the other terms are symmetric. So the whole term is antisymmetric and therefore vanishes when multiply with $\prod_j\sigma^-_{m_j}|\Uparrow\rangle$.

Based on the calculations above, any residue term in (4.39) vanishes given $m_1<n_1$. So the only non-zero contribution of the integral would require $m_1=n_1$.

- Since $m_1=n_1$, for any $j>1$, we have

$$m_1=n_1>n_j>m_j. \tag{4.46}$$

So $Z_{1j}(\alpha_1,\alpha_j)=1$. Therefore the integration over α_1 can be decoupled from the other α_j's:

$$\Psi_0^{\{n_j\}}(\{m_j\})=\int d\alpha_1 I^1(\alpha_1)|_{m_1=n_1}\int\prod_{j=2}^N[d\alpha_j I^j(\alpha_j)]\prod_{1<i<j}Z_{ij}(\alpha_i,\alpha_j)+A(\{m_j\}). \tag{4.47}$$

It's trivial to calculate

$$\int d\alpha_1 I^1(\alpha_1)|_{m_1=n_1}=\int d\alpha_1\frac{1}{2\pi}\frac{\sinh\lambda}{2\sin\frac{\alpha_1+i\lambda}{2}\sin\frac{\alpha_1-i\lambda}{2}}=1. \tag{4.48}$$

Thus,

$$\Psi_0^{\{n_j\}}(\{m_j\})=\delta_{m_1=n_1}\int\prod_{j=2}^N[d\alpha_j I^j(\alpha_j)]\prod_{1<i<j}Z_{ij}(\alpha_i,\alpha_j)+A(\{m_j\}). \tag{4.49}$$

So we reduced the numbers of flipped spins from N to $N-1$. Keep doing it, we can prove (4.27), namely the central theorem.

Up to here we proved the central theorem in the region $\Delta<-1$. The difference between my proof and Yudson's approach (see Section 4.1.1) is: Yudson is always able to completely avoid all the possible poles. I cannot do it for the XXZ model, but I calculate the residues of the S-matrix poles, and prove they always cancel out eventually. In this sense, I generalized Yudson's approach.

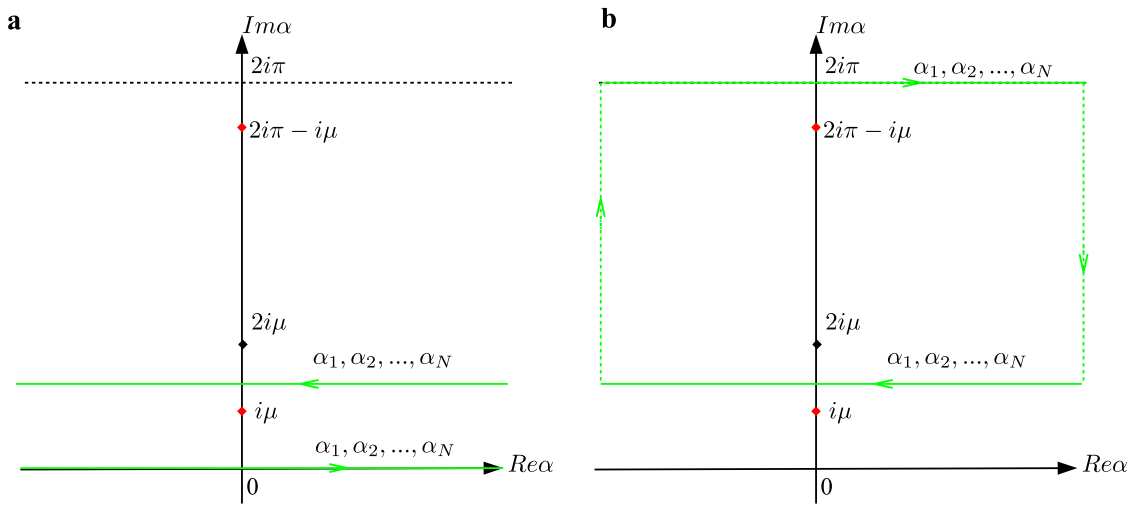

Figure 4.4: (a) The contours of integral for the region $-1 < \Delta < 0$. (b) The second way ("beyond") of closing the contours.

4.2.2 The Gapless Regime $-1 < \Delta < 0$

The central theorem in the gapless regime is very similar to the gapped regime, with a few differences. Following the reparametrization in Table 3.1, the central theorem takes the explicit form

$$|\Psi_0\rangle = \sum_{\{m_j\}} \int_{\gamma_j} \prod_j [\frac{d\alpha_j}{2\pi} \frac{\sin\mu}{2\sinh\frac{\alpha_j+i\mu}{2}\sinh\frac{\alpha_j-i\mu}{2}}] \prod_{i<j} [\theta(m_i-m_j) + \frac{\sinh(\frac{\alpha_i-\alpha_j}{2}-i\mu)}{\sinh(\frac{\alpha_i-\alpha_j}{2}+i\mu)}\theta(m_j-m_i)]$$
$$\times \prod_j [\frac{\sinh(\frac{i\mu-\alpha_j}{2})}{\sinh(\frac{i\mu+\alpha_j}{2})}]^{m_j-n_j} \sigma^-_{m_j} |\Uparrow\rangle. \tag{4.50}$$

This time the integrand is periodic along the imaginary axis with period $2i\pi$. We choose the "first Brillouin zone" to be between 0 and $2i\pi$. The contours of integration are chosen to be as in Fig. 4.4 (a): going forward along real axis from $-\infty$ to ∞, plus going backward from $+\infty + ic$ to $-\infty + ic$ with $\mu < c < 2\mu$. Note that the range of $-1 < \Delta < 0$ is corresponding to $0 < \mu < \pi/2$. We can still close the contour in the head-to-tail way, because the weight term that controls the convergence of the integrand along the vertical line at $\pm\infty$ goes to zero:

$$\text{weight term} = \frac{\sin\mu}{\cosh\alpha - \cos\mu} \to \frac{\sin\mu}{e^{|Re\alpha|}e^{\pm iIm\alpha}} \to 0 (Re\alpha \to \pm\infty). \tag{4.51}$$

Due to the periodicity of the integrand, the contour along the real axis is equivalent to along $\beta + 2i\pi$. So the second way of closing the contours in this case is as shown in Fig. 4.4 (b). With the different set up discussed above, the whole proof of central theorem in the gapped regime can be applied here.

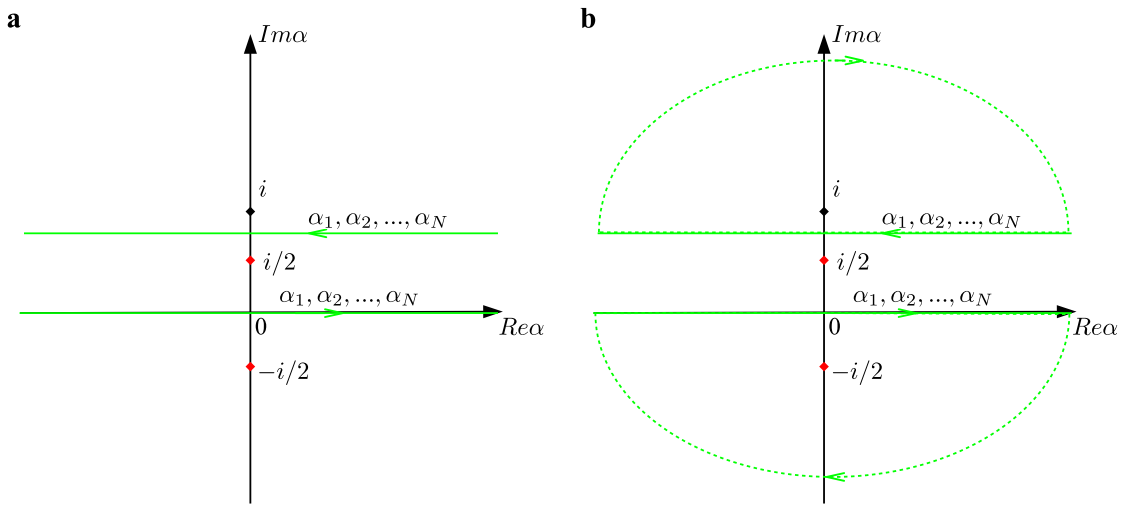

Figure 4.5: (a) The contours of integral for the critical point $\Delta = 1$ on the α-plane. (b) The second way ("beyond") of closing the contours.

4.2.3 Critical Point $\Delta = 1$

Following the reparametrization in Table 3.1, the central theorem for $\Delta = 1$ takes the explict form

$$|\Psi_0\rangle = \sum_{\{m_j\}} \int_{\gamma_j} \prod_j [\frac{d\alpha_j}{2\pi} \frac{1}{(\alpha_j - \frac{i}{2})(\alpha_j + \frac{i}{2})}] \prod_{i<j} [\theta(m_i - m_j) + \frac{\alpha_i - \alpha_j + i}{\alpha_i - \alpha_j - i}\theta(m_j - m_i)]$$
$$\times \prod_j \left(\frac{\alpha_j + \frac{i}{2}}{\alpha_j - \frac{i}{2}}\right)^{m_j - n_j} \sigma^-_{m_j} |\Uparrow\rangle. \tag{4.52}$$

The integrand is not periodic any more. But we can still choose the similar contours, as shown in Fig. 4.5 (a). The weight term still control the convergence of the integrand –it goes to zero as $|\alpha| \to \infty$. So we can always close the contours on the large circle. Fig. 4.5 (b) shows the second way of closing the contours. With this new set up, the proof of central theorem in the gapped regime can be applied here as well.

4.3 Exact Time-Dependent Wave functions in an Integral Form

In the previous section, we prove the central theorem

$$|\Psi_0\rangle = \int_\gamma d\vec{\alpha} |\vec{\alpha}\rangle\langle\vec{\alpha}|\Psi_0\rangle, \tag{4.53}$$

for all the values of Δ. They take the same form as above and follow the same logic, but with different definitions of the rapidity α, and different contours of integrals. With the central theorem, the time evolution of the initial state can be formally written as

$$|\Psi(t)\rangle = e^{-i\hat{H}t}|\Psi_0\rangle = \int_\gamma d\vec{\alpha} e^{-iE(\vec{\alpha})} |\vec{\alpha}\rangle\langle\vec{\alpha}|\Psi_0\rangle. \tag{4.54}$$

Explicitly, the time-dependent wave function in the coordinate basis is given by

$$\Psi^{\{n_j\}}(\{m_j\},t) = \mathcal{S}\int_\gamma \prod_j d\alpha_j W(\alpha_j) P(\alpha_j)^{m_j-n_j} e^{-i\epsilon(\alpha_j)t}$$
$$\times \prod_{i<j}[\theta(m_i-m_j)+S(\alpha_i,\alpha_j)\theta(m_j-m_i)]. \tag{4.55}$$

In different regions of Δ, the functions $W(\alpha)$, $P(\alpha)$, $\epsilon(\alpha)$ and $S(\alpha_1,\alpha_2)$ have different definitions as listed in Table 3.1, and the contours γ have different forms as discussed in the previous sections. The expression (4.55) is an exact result, and contains the full information of the dynamic evolution. Starting from it, I will calculate the time evolution of various observables in later chapters. But before that, I will explain some physical interpretations of the integral-formed wave function, especially the emergence of bound states of magnons.

Chapter 5
Physical Interpretation of the Integral Representation

In this chapter I discuss the physics interpretation of the exact time-dependent wave function (4.55) we obtained in the last chapter. By manipulating the contours properly, we will show the string solutions of the Bethe Ansatz equations, namely the bound states, emerge naturally from out approach. We will also show how the integral over strings can be obtained by taking the infinite-size limit from a finite size Yudson decomposition.

5.1 Contour Shift and Bound States

The parametrizations defined in Table 3.1 has a property: the real rapidities α are corresponding to real momenta k, or physically free propagating magnons. So the integral along the real lines (there's always a forwarding part along the real axis for all the three regimes of Δ) are interpreted as the summation of free magnons. On the other hand, the backward part of the integrals, corresponding to the magnons with complex momenta, are highly irregular in k-language. So I would like to manipulate this part of the contour and reveal its physical interpretation. I will show the derivation of two and three down spins in the gapped regime $-1 < \Delta < 0$ as examples, and discuss the other cases generally.

5.1.1 Two Down Spins for $\Delta < -1$

Let's extend the notation in (4.23) to

$$I^j(\alpha, t) = W(\alpha)P(\alpha)^{m_j - n_j} e^{-i\epsilon(\alpha)}. \tag{5.1}$$

This notation is physically meaningful because the single-down-spin evolution is given by the time-dependent wave function

$$\psi^{n_1}(m_1, t) = \int_\gamma d\alpha W(\alpha)P(\alpha)^{m_1 - n_1} e^{-i\epsilon(\alpha)t} = \int_\gamma d\alpha I^1(\alpha, t). \tag{5.2}$$

Using this notation with (4.24), the time-dependent wave function for two down spins is given by

$$\Psi^{n_1,n_2}(m_1, m_2, t) = \int_\gamma d\alpha_1 d\alpha_2 I(\alpha_1, t) I(\alpha_2, t) Z_{12}(\alpha_1, \alpha_2). \tag{5.3}$$

Let's consider shifting the backward part of the contours up to $+i\infty$, as shown in Fig. 5.1 (a). Note

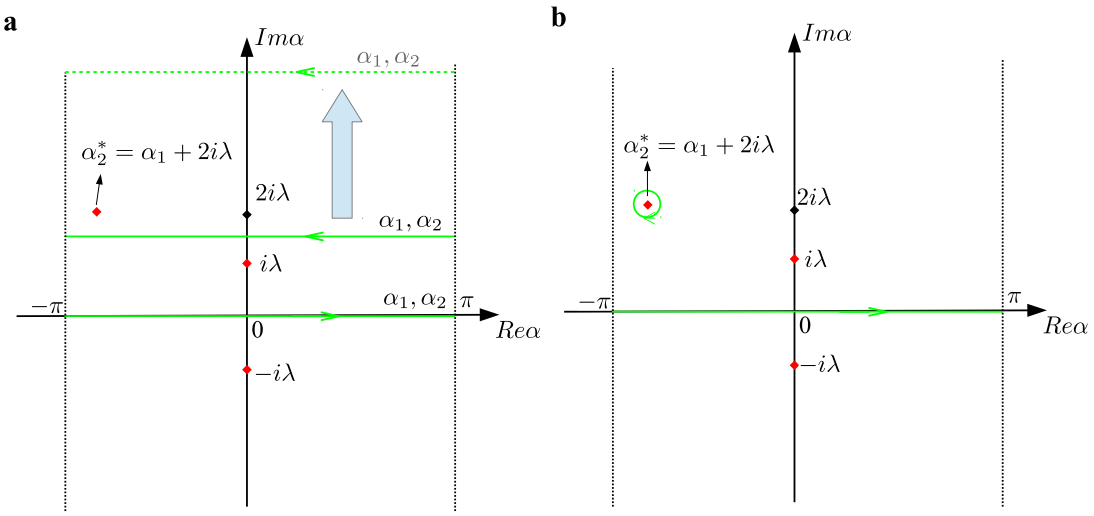

Figure 5.1: (a) We would like to move the backward part of the contours up to $+i\infty$. It will encounter a pole at $\alpha_2^* = \alpha_1 + 2i\lambda$ during this moving. (b) After the moving, the integral at $+i\infty$ vanishes, but the residue at the pole $\alpha_2^* = \alpha_1 + 2i\lambda$ need to be taken into account.

that the integrand vanishes at $+i\infty$ due to the weight term. But during this shifting, the contour of α_2 are moved over a pole from the S-matrix at $\alpha_2^* = \alpha_1 + 2i\lambda$ (the contour of α_1 doesn't encounter any pole). So after the shifting, the integral in (5.3) consists of two parts: the integral along the real axis, and the residue of the pole at $\alpha_2^* = \alpha_1 + 2i\lambda$, as shown in Fig. 5.1 (b). They can be calculated explicitly:

$$\begin{aligned}
\Psi^{n_1,n_2}(m_1,m_2,t) &= \int_\gamma d\alpha_1 I^1(\alpha_1,t) \int_\gamma d\alpha_2 I^2(\alpha_2) Z(\alpha_1,\alpha_2) \\
&= \int_\gamma d\alpha_1 I^1(\alpha_1,t) \{ \int_{-\pi}^{\pi} d\alpha_2 I^2(\alpha_2,t) Z(\alpha_1,\alpha_2) \\
&\quad - 2i\pi\theta(m_2-m_1) \mathrm{Res}\left[I^2(\alpha_2,t) Z(\alpha_1,\alpha_2) \right]_{\alpha_2=\alpha_1+2i\lambda} \} \\
&= \int_\gamma d\alpha_1 I^1(\alpha_1,t) \{ \int_{-\pi}^{\pi} d\alpha_2 I^2(\alpha_2,t) Z(\alpha_1,\alpha_2) \\
&\quad + 4i\pi \sinh(2\lambda) I^2(\alpha_1+2i\lambda) \theta(m_2-m_1) \} \\
&= \int_{-\pi}^{\pi} d\alpha_1 \int_{-\pi}^{\pi} d\alpha_2 I^1(\alpha_1,t) I^2(\alpha_2,t) Z_{12}(\alpha_1,\alpha_2) \\
&\quad + 4i\pi \sinh(2\lambda) \theta(m_2-m_1) \int_{-\pi}^{\pi} d\alpha_1 I^1(\alpha_1,t) I^2(\alpha_1+2i\lambda,t). \qquad (5.4)
\end{aligned}$$

Note that in the first term, the integrand is the same as in (5.3), but the integration contours are only along the real axis. This term is the freely propagating magnons, with the real momenta.

$$\Psi^{n_1,n_2}_{magn}(m_1,m_2,t) = \int_{-\pi}^{\pi} d\alpha_1 \int_{-\pi}^{\pi} d\alpha_2 I^1(\alpha_1,t) I^2(\alpha_2,t) Z_{12}(\alpha_1,\alpha_2). \qquad (5.5)$$

We will discuss its properties later. I claim the second term are the bound states

$$\Psi^{n_1,n_2}_{bound}(m_1,m_2,t) = 4i\pi \sinh(2\lambda)\theta(m_2-m_1)\int_{-\pi}^{\pi} d\alpha I^1(\alpha,t)I^2(\alpha+2i\lambda,t). \tag{5.6}$$

Its physical meaning will be explained in the next few lines. Let's look at the pole structure of its integrand

$$\begin{aligned} I^1(\alpha,t)I^2(\alpha+2i\lambda,t) =& W(\alpha)P(\alpha)^{m_1-n_1}e^{-i\epsilon(\alpha)t}W(\alpha+2i\lambda)P(\alpha+2i\lambda)^{m_2-n_2}e^{-i\epsilon(\alpha+2i\lambda)t} \\ =& \#\frac{(\sin\frac{i\lambda-\alpha}{2})^{m_1-n_1-1}}{(\sin\frac{i\lambda+\alpha}{2})^{m_1-n_1+1}}\frac{(\sin\frac{-i\lambda-\alpha}{2})^{m_2-n_2-1}}{(\sin\frac{3i\lambda+\alpha}{2})^{m_2-n_2+1}}\exp(\frac{-2iJt\sinh(2\lambda)\sinh\lambda}{\sin\frac{\alpha-i\lambda}{2}\sin\frac{\alpha+3i\lambda}{2}}). \end{aligned} \tag{5.7}$$

In the last line we used the definitions in Table 3.1. Because of the relations $n_1 > n_2$ and $m_2 > m_1$, the power of $\sin\frac{i\lambda+\alpha}{2}$ in the integrand is $m_2 - n_2 - m_1 + n_1 - 2 \geq 0$. So $\alpha = -i\lambda$ is not a pole, and we can move the integration contour down by $i\lambda$, or equivalently, change the integration variable $\alpha \to \alpha - i\lambda$. Thus,

$$\Psi^{n_1,n_2}_{bound}(m_1,m_2,t) = 4i\pi \sinh(2\lambda)\theta(m_2-m_1)\int_{-\pi}^{\pi} d\alpha I^1(\alpha-i\lambda,t)I^2(\alpha+i\lambda,t). \tag{5.8}$$

Compared with the string solution of the Bethe Ansatz equations Fig. 3.2, it is realized as the summation of all the possible 2-strings (see Section 3.4 for the string solutions of the Bethe ansatz equations). As a conclusion, the shifting of the contours (5.4) can be considered as a decomposition of the free magnons and the bound states. Note that this two components evolve independently with time.

It is easier to see the physical picture of both the free magnons and the bound states if we translate them back into k-language. It is helpful to look at the single-down-spin evolution first, which we have seen in (5.2).

$$\psi^n(m,t) = \int_{-\pi}^{\pi} dk e^{ik(m-n)-4iJt(\Delta-\cos k)} = ie^{-4iJt}J^B_{m-n}(4Jt). \tag{5.9}$$

The single-down-spin wave function only has the free-magnon component, so it doesn't matter whether we integrate over γ or just along the real axis. The integration can be done analytical, and given by the Bessel function of the first kind $J^B_n(x)$. For a fixed time t, when $m - n > 4Jt$, $J^B_{m-n}(4Jt)$ will decay exponentially, indicating the Lieb-Robinson bound [122], namely for a system with only short-range interaction, the propagation of correlations cannot exceed a certain velocity. It is characterized by a light-cone structure of the local magnetization, as will be shown in Chapter 6.

Now let's get back to the two-down-spin wave function. For the free magnons, everything is standard to be translated back to k-language

$$\Psi^{n_1,n_2}_{magn}(m_1,m_2,t) = \int_{-\pi}^{\pi} dk_1 dk_2 e^{ik_1(m_1-n_1)+ik_2(m_2-n_2)}e^{-4iJt(2\Delta-\cos k_1-\cos k_2)}Z_{12}(k_1,k_2). \tag{5.10}$$

The $Z_{12}(k_1,k_2)\equiv\theta(m_1-m_2)+s(k_1,k_2)\theta(m_2-m_1)$ is apparently the correspondence of (4.24) in k-language. When $m_1>m_2$, the integration over k_1 and k_2 can be decoupled

$$\begin{aligned}\Psi^{n_1,n_2}_{magn}(m_1,m_2,t)|_{m_1>m_2}=&\int_{-\pi}^{\pi}dk_1e^{ik_1(m_1-n_1)-4Jt(\Delta-\cos k_1)}\int_{-\pi}^{\pi}dk_2e^{ik_2(m_2-n_2)-4iJt(\Delta-\cos k_2)}\\ =&\psi^{n_1}(m_1,t)\psi^{n_2}(m_2,t).\end{aligned}\tag{5.11}$$

So the two-down-spin wave function is just the product of the single-down-spin wave functions. (Note here it doesn't mean there is no interaction. Because the "physical" wave function need to be symmetrized and therefore is the mixture of the two cases $m_1>m_2$ and $m_1<m_2$. The interaction will affect the $m_1<m_2$ part through the S-matrix.) For the region $m_1<m_2$, the integration cannot be decoupled any more due to the S-matrix

$$\Psi^{n_1,n_2}_{magn}(m_1,m_2,t)|_{m_1<m_2}=\int_{-\pi}^{\pi}dk_1dk_2e^{ik_1(m_1-n_1)+ik_2(m_2-n_2)}e^{-4iJt(2\Delta-\cos k_1-\cos k_2)}s(k_1,k_2).\tag{5.12}$$

This integration cannot be carried out analytically, but in the long time limit we can consider the saddle point approximation. Intuitively, when t is large, because of the fast oscillation of the exponential function, the integration like (5.9) will be determined by a few points where the derivative of the exponent vanishes

$$\frac{\partial}{\partial k^s}[4iJt\cos k^s+ik^s(m-n)]=0.\tag{5.13}$$

These points are called the saddle points. I will discuss this technique in detail in the next chapter. Here I just use some general conclusion. Since there is no large parameter in the S-matrix $s(k_1,k_2)$, the integral in (5.12) can be approximated by

$$\Psi^{n_1,n_2}_{magn}(m_1,m_2,t)|_{m_1<m_2}=\sum_{k_1^s,k_2^s}\psi^{n_1}(m_1,t)\psi^{n_2}(m_2,t)s(k_1^s,k_2^s).\tag{5.14}$$

Because the solution of (5.13) is determined by $m-n$, if the initial state is chosen as $n_1\approx n_2$ and when $m_1\approx m_2$, we would have $k_1^s\approx k_2^s$. Considering $s(k,k')\approx-1$ as $k\approx k'$, when $m_1\approx m_2$, the two-down-spin wave function in the cases $m_1>m_2$ and $m1<m_2$ will cancel each other during the symmetrization. As a result, the free-magnon component of the wave function would be roughly zero along the line $m_1\approx m_2$, as visualized in Fig. 5.2 (c).

The bound-state component of the wave function is trickier. One need to make use of the

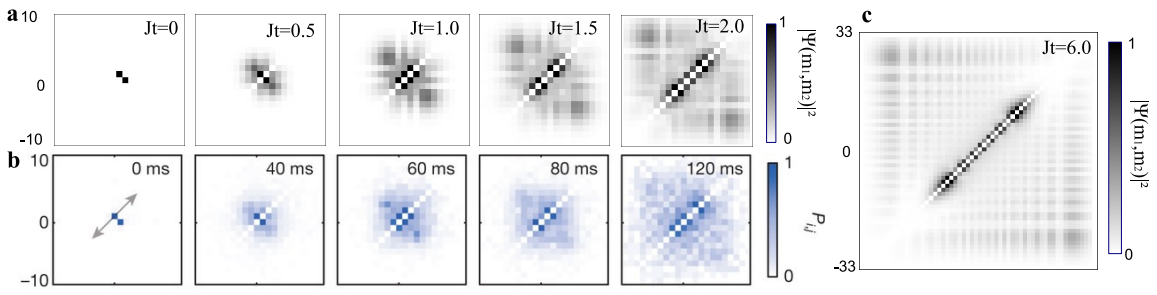

Figure 5.2: Visualization of the time-dependent wave functions from the initial state $|\Psi_0\rangle = \sigma_1^-\sigma_0^-|\Uparrow\rangle$, for $\Delta = 1.2$. (a) Norm square of the wave function $|\Psi^{1,0}(m_1, m_2, t)|^2$ evaluated by numerical integration. (b) Joint probabilities of having the two down spins at site i and j, measured experimentally in Ref. [5]. (c) Norm square of the wave function $|\Psi^{1,0}(m_1, m_2, t)|^2$ at a large time $Jt = 6$. It shows the features derived by saddle point approximation. The dark part along the diagonal is the bound state component. The gray part that vanishes on the diagonal is the free-magnon component.

following identities

$$e^{iK} = P(\alpha - i\lambda)P(\alpha + i\lambda) = \frac{\sin\frac{\alpha-2i\lambda}{2}}{\sin\frac{\alpha+2i\lambda}{2}}, \tag{5.15}$$

$$E = \epsilon(\alpha - i\lambda) + \epsilon(\alpha + i\lambda) = \frac{4J\sinh\lambda\sinh(2\lambda)}{\cos\alpha - \cosh(2\lambda)}, \tag{5.16}$$

$$W(\alpha - i\lambda)W(\alpha + i\lambda) = \frac{1}{4\pi^2}\frac{\sinh(2\lambda)}{2\sin\frac{\alpha-2i\lambda}{2}\sin\frac{\alpha+2i\lambda}{2}}\frac{\sinh\lambda}{2\cosh\lambda(1-\cos\alpha)}, \tag{5.17}$$

$$\frac{P(\alpha + i\lambda)}{P(\alpha - i\lambda)} = \frac{1-\cos\alpha}{\cosh(2\lambda) - \cos\alpha}. \tag{5.18}$$

In (5.15) and (5.16), K and E are the total momentum and total energy of the 2-string. They have the spectrum relation

$$E = \frac{4J\sinh\lambda}{\sinh(2\lambda)}[\cos K - \cosh(2\lambda)]. \tag{5.19}$$

The more general version of these identities for n-string can be found in Ref. [95]. Our purpose is to write the integration in (5.8) in terms of the integral over the total momentum K. To do that, we first notice that the weight of K

$$\frac{dK}{d\alpha} = \frac{\sinh(2\lambda)}{2\sin\frac{\alpha-2i\lambda}{2}\sin\frac{\alpha+2i\lambda}{2}} \tag{5.20}$$

is very similar to (5.17). Second, we define the center of the two down spins M and the distance between the two down spins N to be

$$M = \frac{m_1 - n_1 + m_2 - n_2}{2}, \tag{5.21}$$

$$N = \frac{m_2 - n_2 - m_1 + n_1}{2} > 0. \tag{5.22}$$

then the planewave terms in (5.8) can be written as

$$P(\alpha - i\lambda)^{m_1-n_1}P(\alpha + i\lambda)^{m_2-n_2} = [P(\alpha - i\lambda)P(\alpha + i\lambda)]^M[\frac{P(\alpha + i\lambda)}{P(\alpha - i\lambda)}]^N. \tag{5.23}$$

Combine the identities above, we can rewrite (5.8) as

$$\Psi_{bound}^{n_1,n_2}(m_1,m_2,t)=\theta(m_2-m_1)(-1)^M e^{2iJt(\frac{\cosh(2\lambda)}{\cosh\lambda}-1)}\int_{-\pi}^{\pi}\frac{dK}{2\pi}e^{iKM-i4Jt\frac{\sinh\lambda}{\sinh(2\lambda)}(\Delta-\cos K)}g(K), \tag{5.24}$$

where

$$g(K)=\frac{\cos K+\cosh(2\lambda)}{1-\cos K}(\frac{1-\cos K}{2\cosh^2\lambda})^N. \tag{5.25}$$

Since it contains no large parameter, in large time it will be approximately determined by the values at saddle points $g(K^s)$. Further more, the term $\frac{1-\cos K}{2\cosh^2\lambda}$ in $g(K)$ only takes real values between 0 and 1, so $g(K)$ will decay exponentially as N increases. In a 2-D visualization of the wave function as in Fig. 5.2, N denotes the distance in the off-diagonal direction. Thus the wave function decays fast in the off-diagonal direction. One the other hand, without $g(K)$, the integral in (5.24) is the same as in single-down-spin propagation (5.9), with a change of parameter $t\to t\cdot\frac{\sinh\lambda}{\sinh(2\lambda)}$. As a result, in the bound state, the center of the two down spins propagates similarly as a single down spin, with the rescaled time $\frac{\sinh\lambda}{\sinh(2\lambda)}t$; while the two down spins are a part, the wave function decays exponentially –that's why it is called bound state. All these features of a bound state are shown clearly in Fig. 5.2 (c), although it is obtained by numerical integration.

The norm square of the wave functions we calculated can actually be measured in experiments –they are the the joint probabilities of having the two down spins at particular sites. I reproduce the experimental data from Ref. [5] in Fig. 5.2 (b). It shows a good agreement with Fig 5.2 (a), which is obtained by numerical evaluation of the integrals in (5.5) and (5.8). Note that we express time in a dimensionless unit Jt. Under the condition of Ref. [5], the coupling constant $J/\hbar=54$ Hz. Thus the dimensionless time unit Jt = 1 in our convention corresponds to t = 74 ms in their experiment. It provides the criteria of the comparison in Fig. 5.2.

5.1.2 Three Down Spins for $\Delta<-1$

In the last section, we showed the two-down-spin wave function can be decomposed into the free-magnon component and the boundstate component, in Eq. (5.4). In this section we will do a similar calculation for three down spins, and show that higher-order strings will also emerge from the contour approach. A general decomposition for arbitrary number of down spins is expected, but will not be derived.

The three-down-spin wave function is explicitly written as

$$\Psi^{\vec{n}}(\vec{m},t)=\int_\gamma d\alpha_1 d\alpha_2 d\alpha_3 I^1(\alpha_1,t)I^2(\alpha_2,t)I^3(\alpha_3,t)Z_{12}(\alpha_1,\alpha_2)Z_{23}(\alpha_2,\alpha_3)Z_{13}(\alpha_1,\alpha_3). \tag{5.26}$$

As in two-down-spin case, we want to shift the backward part of the three contours up to $+i\infty$, where the integrand vanishes. In this more complicated case, one need to be careful of the order of shifting. In particular, shifting the backward part of α_1 doesn't encounter any pole, thus leads to no extra term

$$\Psi^{\vec{n}}(\vec{m},t)=\int_{-\pi}^{\pi}d\alpha_1\int_{\gamma}d\alpha_2\int_{\gamma}d\alpha_3 I^1(\alpha_1,t)I^2(\alpha_2,t)I^3(\alpha_3,t)Z_{12}(\alpha_1,\alpha_2)Z_{23}(\alpha_2,\alpha_3)Z_{13}(\alpha_1,\alpha_3). \tag{5.27}$$

When shifting the contour of α_2, it goes over the only pole from $Z_{12}(\alpha_1,\alpha_2)$ at $\alpha_2^*=\alpha_1+2i\lambda$. So one need to consider its residue

$$\begin{aligned}
&\Psi^{\vec{n}}(\vec{m},t)=\int_{-\pi}^{\pi}d\alpha_1\int_{\gamma}d\alpha_3 I^1(\alpha_1,t)I^3(\alpha_3,t)Z_{13}(\alpha_1,\alpha_3)\\
&\times[\int_{-\pi}^{\pi}I^2(\alpha_2)Z_{12}(\alpha_1,\alpha_2)Z_{23}(\alpha_2,\alpha_3)+4i\pi\theta_{21}\sinh(2\lambda)I^2(\alpha_1+2i\lambda)Z_{23}(\alpha_1+2i\lambda,\alpha_3)]\\
=&\int_{-\pi}^{\pi}d\alpha_1\int_{-\pi}^{\pi}d\alpha_2\int_{\gamma}d\alpha_3 I^1(\alpha_1,t)I^2(\alpha_2,t)I^3(\alpha_3,t)Z_{12}(\alpha_1,\alpha_2)Z_{23}(\alpha_2,\alpha_3)Z_{13}(\alpha_1,\alpha_3)\\
&+4i\pi\sinh(2\lambda)\theta_{21}\int_{-\pi}^{\pi}d\alpha_1\int_{\gamma}d\alpha_3 I^1(\alpha_1,t)I^3(\alpha_3,t)Z_{13}(\alpha_1,\alpha_3)I^2(\alpha_1+2i\lambda,t)Z_{23}(\alpha_1+2i\lambda,\alpha_3).
\end{aligned} \tag{5.28}$$

Here we make use of the pole of $Z_{ij}(\alpha,\alpha')$ (4.30), just like in the two-down-spin case (5.4). Sometimes we use the short notation θ_{21} for $\theta(m_2-m_1)$. Then we want to shift the contour of α_3. For the first term in (5.28), the contour of α_3 is moved over two poles at $\alpha_3^*=\alpha_1+2i\lambda$ and $\alpha_3^*=\alpha_2+2i\lambda$. We can calculate their residues just like above. But for the second term in (5.28), because

$$Z_{23}(\alpha_1+2i\lambda,\alpha_3)=\theta(m_2-m_3)+\frac{\sin(\frac{\alpha_1-\alpha_3}{2})}{\sin(\frac{\alpha_1-\alpha_3}{2}+2i\lambda)}\theta(m_3-m_2), \tag{5.29}$$

the contour of α_3 is moved over the pole from $Z_{13}(\alpha_1,\alpha_3)$ at $\alpha_3^*=\alpha_1+2i\lambda$, and the pole from $Z_{23}(\alpha_1+2i\lambda,\alpha_3)$ at $\alpha_3^*=\alpha_1+4i\lambda$. Taking into account all the poles, we have

$$\begin{aligned}
\Psi^{\vec{n}}(\vec{m},t)=&\int_{-\pi}^{\pi}d\alpha_1\int_{-\pi}^{\pi}d\alpha_2\int_{-\pi}^{\pi}d\alpha_3 I^1(\alpha_1,t)I^2(\alpha_2,t)I^3(\alpha_3,t)Z_{12}(\alpha_1,\alpha_2)Z_{23}(\alpha_2,\alpha_3)Z_{13}(\alpha_1,\alpha_3)\\
&+4i\pi\sinh(2\lambda)\theta_{31}\int_{-\pi}^{\pi}d\alpha_1\int_{-\pi}^{\pi}d\alpha_2 I^1(\alpha_1,t)I^2(\alpha_2,t)I^3(\alpha_1+2i\lambda,t)Z_{12}(\alpha_1,\alpha_2)Z_{23}(\alpha_2,\alpha_1+2i\lambda)\\
&+4i\pi\sinh(2\lambda)\theta_{32}\int_{-\pi}^{\pi}d\alpha_1\int_{-\pi}^{\pi}d\alpha_2 I^1(\alpha_1,t)I^2(\alpha_2,t)I^3(\alpha_2+2i\lambda,t)Z_{12}(\alpha_1,\alpha_2)Z_{13}(\alpha_1,\alpha_2+2i\lambda)\\
&+4i\pi\sinh(2\lambda)\theta_{21}\int_{-\pi}^{\pi}d\alpha_1\int_{-\pi}^{\pi}d\alpha_3 I^1(\alpha_1,t)I^2(\alpha_1+2i\lambda,t)I^3(\alpha_3,t)Z_{13}(\alpha_1,\alpha_3)Z_{23}(\alpha_1+2i\lambda,\alpha_3)\\
&+[4i\pi\sinh(2\lambda)]^2\frac{\sinh(3\lambda)}{\sinh\lambda}\theta_{321}\int_{-\pi}^{\pi}d\alpha_1 I^1(\alpha_1,t)I^2(\alpha_1+2i\lambda,t)I^3(\alpha_1+4i\lambda,t).
\end{aligned} \tag{5.30}$$

Here θ_{321} is apparently a short notation for $\theta(m_3>m_2>m_1)$. Note that actually the second term of (5.28) generates a term like

$$\theta_{31}\theta_{21}\int_{-\pi}^{\pi}d\alpha_1 I^1(\alpha_1,t)I^2(\alpha_1+2i\lambda,t)I^3(\alpha_1+2i\lambda,t)Z_{23}(\alpha_1+2i\lambda,\alpha_1+2i\lambda). \tag{5.31}$$

But since $Z_{23}(\alpha_1+2i\lambda,\alpha_1+2i\lambda)=\theta_{23}-\theta_{32}$ is antisymmetric under the exchange of m_2 and m_3, and all the other terms in (5.31) are symmetric, so the whole term (5.31) will be canceled by $\sigma^-_{m_2}\sigma^-_{m_3}$. Finally, with a similar argument as in two-down-spin case, we can move the contour of integral in (5.30) properly so it becomes

$$\begin{aligned}
\Psi^{\vec{n}}(\vec{m},t) =& \int_{-\pi}^{\pi} d\alpha_1 \int_{-\pi}^{\pi} d\alpha_2 \int_{-\pi}^{\pi} d\alpha_3 I^1(\alpha_1,t)I^2(\alpha_2,t)I^3(\alpha_3,t)Z_{12}(\alpha_1,\alpha_2)Z_{23}(\alpha_2,\alpha_3)Z_{13}(\alpha_1,\alpha_3)\\
&+ 4i\pi\sinh(2\lambda)\theta_{31}\int_{-\pi}^{\pi} d\alpha \int_{-\pi}^{\pi} d\alpha_2 I^1(\alpha-i\lambda,t)I^2(\alpha_2,t)I^3(\alpha+i\lambda,t)Z_{12}(\alpha_1-i\lambda,\alpha_2)Z_{23}(\alpha_2,\alpha_1+i\lambda)\\
&+ 4i\pi\sinh(2\lambda)\theta_{32}\int_{-\pi}^{\pi} d\alpha_1 \int_{-\pi}^{\pi} d\alpha I^1(\alpha_1,t)I^2(\alpha-i\lambda,t)I^3(\alpha+i\lambda,t)Z_{12}(\alpha_1,\alpha-i\lambda)Z_{13}(\alpha_1,\alpha+i\lambda)\\
&+ 4i\pi\sinh(2\lambda)\theta_{21}\int_{-\pi}^{\pi} d\alpha \int_{-\pi}^{\pi} d\alpha_3 I^1(\alpha-i\lambda,t)I^2(\alpha+i\lambda,t)I^3(\alpha_3,t)Z_{13}(\alpha-i\lambda,\alpha_3)Z_{23}(\alpha+i\lambda,\alpha_3)\\
&+ [4i\pi\sinh(2\lambda)]^2\frac{\sinh(3\lambda)}{\sinh\lambda}\theta_{321}\int_{-\pi}^{\pi} d\alpha I^1(\alpha-2i\lambda,t)I^2(\alpha,t)I^3(\alpha+2i\lambda,t). \qquad (5.32)
\end{aligned}$$

This is the decomposition of the three-down-spin wave function into free magnons and different boundstates. It clearly takes the form as the summation over the free magnons and all the possible strings: the first term is the free magnons; the next three terms are consist of the 2-strings and one free magnon, i.e. in this state two down spins are bounded but the third one is free; the last term is the 3-string, i.e. all the three down spins are bounded together. The position of the strings agrees with Fig. 3.2.

5.1.3 Multiple Down Spins and $-1<\Delta<0$

For arbitrary number of down spins, one expects a decomposition similar as (5.32). Since it doesn't have a concise form, and is not very useful for further calculation, we don't give the general form.

For the other region $-1<\Delta<0$, the decomposition work in the similar way, but with two main differences in details: (1) The order of the strings is restrained by the value of Δ. As shown in Fig. 5.3, the backward part of the contours are moved to $i\pi$ instead of $+i\infty$. If one follow the way of shifting contours as in the gapped regime, the pole at $\alpha^*_N=\alpha_1+2ni\mu$ will not be encountered if $2n\mu>\pi$. As a result, the order of a string cannot be arbitrary large, but has to be smaller than π/μ, which agrees with the thermodynamic Bethe ansatz [95]. (2) The momentum of the bound state is also restrained by the value of Δ. Let's illustrate it with the bound state of two down spins. Following the same contour shift as in ferromagnetic region, the bound-state component of the wave function is given by

$$\Psi^{n_1,n_2}_{bound}(m_1,m_2,t) = 4i\pi\sin(2\mu)\theta(m_2-m_1)\int_{-\infty}^{\infty} d\alpha I^1(\alpha-i\mu,t)I^2(\alpha+i\mu,t). \qquad (5.33)$$

Not surprisingly, it takes the same form as (5.8). But the function $I^j(\alpha)$ is defined according to the parametrization in the region $-1<\Delta<0$, as shown in Table 3.1. Correspondingly, the α is

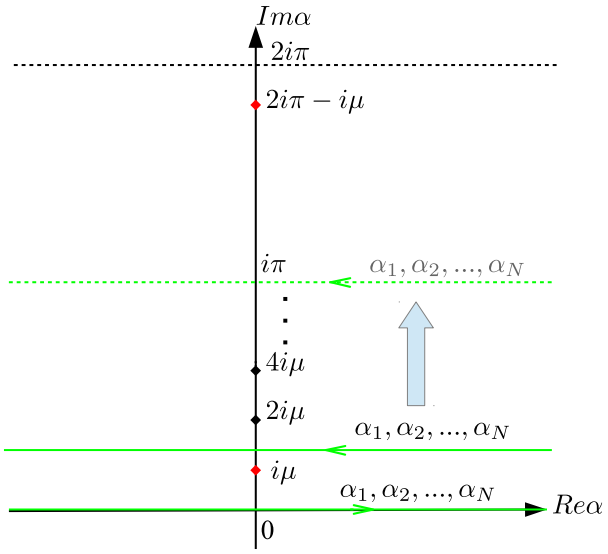

Figure 5.3: For $-1 < \Delta < 0$, the length of the string is restrained by the value of Δ through μ.

integrated over $(-\infty, \infty)$ instead of $[\pi, \pi]$. However, if translated back into k-language, the range of $\alpha \in (-\infty, \infty)$ represents $k \in [-\pi + \mu, \pi - \mu]$. Thus the bound state in terms of the total momentum K will be given by

$$\Psi^{n_1,n_2}_{bound}(m_1, m_2, t) = \# \cdot \theta(m_2 - m_1) \int_{-\pi+2\mu}^{\pi-2\mu} \frac{dK}{2\pi} e^{iKM - i4Jt\frac{\sin\mu}{\sin(2\mu)}(\Delta - \cos K)} g(K). \tag{5.34}$$

As a conclusion, the total momentum of the bound state of two down spins is restricted in the range $[-\pi + 2\mu, \pi - 2\mu]$. It also agrees with the result of the thermodynamic Bethe ansatz [95]. Applying the same saddle point approximation in long time limit, we find that one of the saddle point $K^s = \pi - \sin^{-1}(\frac{M}{4Jt})$ may fall off this range, severely diminishing the contribution of the bound state. We will discuss it more when we show the results of observables in Chapter 6.

5.2 Relation to Goldstein-Yudson Decomposition in the Finite System

In this section, I introduce the Yudson representation in the finite system, called the Goldstein-Yudson decomposition. It has been applied to study the equilibration of the Lieb-Liniger gas [123]. I will show that by properly taking the infinite-size limit, it leads to the same results of the contour approach introduced in the last chapter. I will derive this method in the context of the XXZ model, but the derivation can be easily generalized to other integrable models.

5.2.1 Goldstein-Yudson Decomposition

Let's begin with the Bethe eigenstate of the XXZ model under the other convention (3.18)

$$|\vec{k}\rangle = \sum_{m_1>m_2>\cdots>m_M} \sum_P A_P(\vec{k}) \prod_j e^{ik_{P_j} m_j} \sigma^-_{m_j} |\Uparrow\rangle, \tag{5.35}$$

where

$$A_P(\vec{k}) = \prod_{\substack{i<j \\ P_i>P_j}} s(k_i, k_j). \tag{5.36}$$

This is just another way of writing the Bethe eigenstate we have been using (3.11) (see Section 3.2.2 for the equivalence of the two conventions). On a finite line with periodic boundary condition, the momentum $\vec{k} = \{k_1, k_2, \ldots, k_M\}$ need to satisfy the Bethe Ansatz equations (BAE)

$$k_j = \frac{2\pi n_j}{L} - \frac{i}{L} \sum_l \ln[s(k_l, k_j)] \text{ for } j = 1, 2, \ldots, M. \tag{5.37}$$

as discussed in Chapter 3. For all possible sets of solutions $\{k_j\}$, the eigenstates (5.35) form a complete basis of the Hilbert space. So for any initial state $|\Psi_0\rangle$, we have

$$|\Psi_0\rangle = \sum_{\{k_j\}} \frac{|\vec{k}\rangle\langle\vec{k}|\Psi_0\rangle}{N(\vec{k})}, \tag{5.38}$$

where $N(\vec{k}) = \langle\vec{k}|\vec{k}\rangle$ is the norm square of the eigenstate (5.35), which is not normalized. We want to emphasize here any permutation $\{k_{P_1}, k_{P_2}, \ldots, k_{P_M}\}$ of a solution set $\{k_1, k_2, \ldots, k_M\}$ is still considered to be the same solution set, and was taken into account only once in the summation above. Note that by permuting the $\{k_j\}$ in the eigenstate (5.35), one gets the same state with a different normalizing factor, for example

$$|k_2, k_1\rangle = s^{-1}(k_1, k_2)|k_1, k_2\rangle. \tag{5.39}$$

It is not hard to find its general form

$$|k_{P_1}, k_{P_2}, \ldots, k_{P_M}\rangle = A_P^{-1}(k_1, k_2, \ldots, k_M)|k_1, k_2, \ldots, k_M\rangle. \tag{5.40}$$

Since the order of the k_j's becomes important, in this section we will write out $\vec{k}$ explicitly. Let's define Yudson's auxiliary state as

$$|k_1, k_2, \ldots, k_M) = \sum_{m_1>m_2>\cdots>m_M} \prod_j e^{ik_j m_j} \sigma^-_{m_j} |\Uparrow\rangle. \tag{5.41}$$

It has the same form as (4.18), but with quantized k_j's. With this definition, the eigenstate (5.35) can be written as

$$|k_1, k_2, \ldots, k_M\rangle = \sum_P A_P(k_1, k_2, \ldots, k_M)|k_{P_1}, k_{P_2}, \ldots, k_{P_M}). \tag{5.42}$$

From (5.40) we know

$$\begin{aligned} N(k_1,k_2,\ldots,k_M) =& \langle k_1,k_2,\ldots,k_M|k_1,k_2,\ldots,k_M\rangle \\ =& \langle k_{P_1},k_{P_2},\ldots,k_{P_M}|A_P^*(k_1,k_2,\ldots,k_M)A_P(k_1,k_2,\ldots,k_M)|k_{P_1},k_{P_2},\ldots,k_{P_M}\rangle \\ =& |A_P(k_1,k_2,\ldots,k_M)|^2 N(k_{P_1},k_{P_2},\ldots,k_{P_M}). \end{aligned} \tag{5.43}$$

Making use of these identities, we can write the expansion (5.38) in a form similar to Yudson's approach

$$\begin{aligned} |\Psi_0\rangle =& \sum_{\{k_j\}} \frac{|k_1,k_2,\ldots,k_M\rangle}{N(k_1,k_2,\ldots,k_M)} \sum_P A_P^*(k_1,k_2,\ldots,k_M)(k_{P_1},k_{P_2},\ldots,k_{P_M}|\Psi_0\rangle \\ =& \sum_{\{k_j\}}\sum_P \frac{A_P^*(k_1,k_2,\ldots,k_M)}{|A_P(k_1,k_2,\ldots,k_M)|^2 N(k_{P_1},k_{P_2},\ldots,k_{P_M})}|k_1,k_2,\ldots,k_M\rangle(k_{P_1},k_{P_2},\ldots,k_{P_M}|\Psi_0\rangle \\ =& \sum_{\{k_j\}}\sum_P \frac{A_P^{-1}(k_1,k_2,\ldots,k_M)|k_1,k_2,\ldots,k_M\rangle(k_{P_1},k_{P_2},\ldots,k_{P_M}|\Psi_0\rangle}{N(k_{P_1},k_{P_2},\ldots,k_{P_M})} \\ =& \sum_{\{k_j\}}\sum_P \frac{|k_{P_1},k_{P_2},\ldots,k_{P_M}\rangle(k_{P_1},k_{P_2},\ldots,k_{P_M}|\Psi_0\rangle}{N(k_{P_1},k_{P_2},\ldots,k_{P_M})} \\ =& \sum_{k_1,k_2,\ldots,k_M} \frac{|k_1,k_2,\ldots,k_M\rangle(k_1,k_2,\ldots,k_M|\Psi_0\rangle}{N(k_1,k_2,\ldots,k_M)}. \end{aligned} \tag{5.44}$$

In the last line, the summation runs over all sets of solutions $k_1,k_2,\ldots,k_M$, with all possible permutations of a set $\{k_j\}$ being considered different sets of solutions. Eq. 5.44 is the Goldstein-Yudson decomposition, or the finite-size version of the Yudson representation. The overlap $(k_1,k_2,\ldots,k_M|\Psi_0\rangle$ is still trivial to calculate. While the summation over k_j's is only simplified in special cases or with approximation. For example, for repulsive Lieb-Liniger model all solutions of momenta are real, and the summation in (5.44) can be simplified in the large-interaction limit [123]. In the next subsection I will show, in the large-size limit, the summation in (5.44) becomes integrals, and lead to the same results from the contour approach.

5.2.2 Connection to the Contour Approach

Next let's consider the limit: the size of the system $L\to\infty$, with the number of down spins M fixed. This is the same setup as I introduce Yudson's contour approach in the last chapter. I will first demonstrate here for the two-down-spin case, this limit leads to the same decomposition (5.4) as we obtained from the contour approach. Then I explain how it can be generalized to multi-down-spin cases.

To be specific, I only consider the regime $\Delta<-1$ here. I will sometimes use the rapidity language, since the string structure is regular with it. The decomposition (5.44) is easily translated

into α-language according to Table. 3.1. In particular, for two-down-spin case, it takes the form

$$|\Psi_0\rangle = \sum_{\alpha_1,\alpha_2} \frac{|\alpha_1,\alpha_2\rangle(\alpha_1,\alpha_2|\Psi_0\rangle}{N(\alpha_1,\alpha_2)}. \tag{5.45}$$

Here the summation is taken over all possible solutions of the Bethe ansatz equations, and over all permutations. According to the string hypothesis, all the possible solutions can be categorized as (1) Both α_1 and α_2 are real. (2) The two rapidities form a 2-string, i.e. $\alpha_1 = \beta + i\lambda$, $\alpha_2 = \beta - i\lambda$, where β is real, called the center of the 2-string, and λ is the reparametrized Δ following $\Delta = -\cosh\lambda$. (3) $\alpha_1 = \beta - i\lambda$, $\alpha_2 = \beta + i\lambda$. The third category is actually the permutation of the second, but it is still considered to be a new set of solution, as explained in the last section. Let's use the short notation $\alpha^{\pm} = \beta \pm i\lambda$. Then (5.45) is written as

$$|\Psi_0\rangle = \sum_{\text{real } \alpha_1,\alpha_2} \frac{|\alpha_1,\alpha_2\rangle(\alpha_1,\alpha_2|\Psi_0\rangle}{N(\alpha_1,\alpha_2)} + \sum_{\beta} \frac{|\alpha^+,\alpha^-\rangle(\alpha^+,\alpha^-|\Psi_0\rangle}{N(\alpha^+,\alpha^-)} + \sum_{\beta} \frac{|\alpha^-,\alpha^+\rangle(\alpha^-,\alpha^+|\Psi_0\rangle}{N(\alpha^-,\alpha^+)}. \tag{5.46}$$

The first term represents the free magnons, and last two are the bound states. Let's calculate them explicitly.

The free-magnon term is easier to calculate back in k-language

$$I_{\text{magn}} = \sum_{\text{real } k_1,k_2} \frac{|k_1,k_2\rangle(k_1,k_2|\Psi_0\rangle}{N(k_1,k_2)}, \tag{5.47}$$

where k_1, k_2 satisfy the BAE

$$\begin{aligned} e^{ik_1L} &= s(k_1,k_2), \\ e^{ik_2L} &= s(k_2,k_1). \end{aligned} \tag{5.48}$$

Or,

$$\begin{aligned} k_1 &= \frac{2\pi n_{k_1}}{L} - \frac{i}{L}\sum_l \ln[s(k_1,k_2)] \\ k_2 &= \frac{2\pi n_{k_2}}{L} - \frac{i}{L}\sum_l \ln[s(k_2,k_1)], \end{aligned} \tag{5.49}$$

where the integers n_{k_1} and n_{k_2} are the quantum numbers. When $L \to \infty$, the effect of the S-matrices are negligible, and k_1, k_2 are quantized as free momenta, so

$$\sum_{k_j} \to \frac{L}{2\pi}\int_{-\pi}^{\pi} dk_j \text{ for } j = 1,2. \tag{5.50}$$

So the free-magnon term becomes

$$I_{\text{magn}} = L^2 \int_{-\pi}^{\pi} \frac{dk_1}{2\pi}\int_{-\pi}^{\pi} \frac{dk_2}{2\pi} \frac{|k_1,k_2\rangle(k_1,k_2|\Psi_0\rangle}{N(k_1,k_2)}. \tag{5.51}$$

It is not hard to show that as $L \to \infty$ the leading contribution of $N(k_1, k_2) = \langle k_1, k_2 | k_1, k_2 \rangle \to L^2$. So

$$I_{\text{magn}} = \int_{-\pi}^{\pi} \frac{dk_1}{2\pi} \int_{-\pi}^{\pi} \frac{dk_2}{2\pi} |k_1, k_2\rangle (k_1, k_2 | \Psi_0 \rangle. \tag{5.52}$$

It is identical to (5.10), which is obtained from the contour approach, at $t = 0$.

The bound state terms need to be treated more carefully, because the S-matrix between two complex momenta may diverge. Let's first roughly determine the diverging scale of various terms. Let's denote the 2-string solution of the momenta to be $k^{\pm} = k \pm ic$, where k and c are the real and imaginary part of the momenta, and c is in principle a function of k. Then investigating the BAE (5.48), one can see, as $L \to \infty$, the S-matrices between the 2-string diverge (or go to 0) as

$$\begin{aligned} s(k^+, k^-) &\sim e^{-cL} \\ s(k^-, k^+) &\sim e^{cL}. \end{aligned} \tag{5.53}$$

Following the notation of the last section, the two-particle Bethe state is written as a summation over auxiliary states as

$$|k^+, k^-\rangle = |k^+, k^-) + s(k^+, k^-)|k^-, k^+). \tag{5.54}$$

It is not hard to estimate the overlaps of the auxiliary states

$$\begin{aligned} (k^+, k^- | k^+, k^-) &\sim L \\ (k^-, k^+ | k^-, k^+) &\sim e^{2cL} \\ (k^+, k^- | k^-, k^+) &\sim L^2. \end{aligned} \tag{5.55}$$

Combining (5.53) and (5.55), one can see in the Bethe state (5.54), the second term is negligible compared with the first term as $L \to \infty$, and

$$N(k^+, k^-) = \langle k^+, k^- | k^+, k^- \rangle \approx (k^+, k^- | k^+, k^-) \sim L. \tag{5.56}$$

On the other hand, because $|k^+, k^-\rangle = s(k^+, k^-)|k^-, k^+\rangle$, we have

$$N(k^+, k^-) = |s(k^+, k^-)|^2 N(k^-, k^+) \sim e^{-2cL} N(k^-, k^+). \tag{5.57}$$

So,

$$\frac{|k^+, k^-\rangle}{N(k^+, k^-)} \sim e^{cL} \frac{|k^-, k^+\rangle}{N(k^-, k^+)} \tag{5.58}$$

As a result, in (5.46), the second bound state term is negligible compared to the first bound state term. (Note that both $(k^+, k^- | \Psi_0\rangle$ and $(k^-, k^+ | \Psi_0\rangle$ are of order $O(1)$, because initially the two

down spins are at finite positions n_1 and n_2.) Summing up all the scaling analysis above, the only term from the bound state we need to consider is

$$I_{\text{bound}} = \sum_{\beta} \frac{|\alpha^+, \alpha^-)(\alpha^+, \alpha^-|\Psi_0\rangle}{N(\alpha^+, \alpha^-)} \tag{5.59}$$

Let's see how to write it as an integral in the limit $L \to \infty$. First, one need to calculate explicitly the normalization factor (5.56). To do that, one can write out the auxiliary state explicitly and separate the real and imaginary part of the momenta,

$$\begin{aligned} |\alpha^+, \alpha^-) &= \sum_{m_1 > m_2} P^{m_1}(\beta + i\lambda) P^{m_2}(\beta - i\lambda) \sigma^-_{m_1} \sigma^-_{m_2} |\Uparrow\rangle \\ &= \sum_{m_1 > m_2} \left(\frac{\sin \frac{\beta - 2i\lambda}{2}}{\sin \frac{\beta + 2i\lambda}{2}} \right)^{\frac{m_1+m_2}{2}} \left(\frac{1 - \cos\beta}{\cosh(2\lambda) - \cos\beta} \right)^{\frac{m_1-m_2}{2}} \sigma^-_{m_1} \sigma^-_{m_2} |\Uparrow\rangle. \end{aligned} \tag{5.60}$$

Then it is easy to get

$$N(\alpha^+, \alpha^-) \approx (\alpha^+, \alpha^-|\alpha^+, \alpha^-) = \sum_{m_1 > m_2} \left(\frac{1 - \cos\beta}{\cosh(2\lambda) - \cos\beta} \right)^{m_1 - m_2} = \frac{1 - \cos\beta}{2 \sinh^2 \lambda} L. \tag{5.61}$$

Second, one also need to quantize the center of the string β, and change the summation in (5.59) to an integral. Starting with the BAE in α-language,

$$\begin{aligned} \left(\frac{\sin \frac{i\lambda - \alpha^+}{2}}{\sin \frac{i\lambda + \alpha^+}{2}} \right)^L &= \frac{\sin(\frac{\alpha^+ - \alpha^-}{2} - i\lambda)}{\sin(\frac{\alpha^+ - \alpha^-}{2} + i\lambda)} \\ \left(\frac{\sin \frac{i\lambda - \alpha^-}{2}}{\sin \frac{i\lambda + \alpha^-}{2}} \right)^L &= \frac{\sin(\frac{\alpha^- - \alpha^+}{2} - i\lambda)}{\sin(\frac{\alpha^- - \alpha^+}{2} + i\lambda)}, \end{aligned} \tag{5.62}$$

one can remove the divergence in the equations by multiply them together (a common trick in thermodynamic Bethe ansatz), and get

$$\left(\frac{\sin \frac{\beta - 2i\lambda}{2}}{\sin \frac{\beta + 2i\lambda}{2}} \right)^L = 1. \tag{5.63}$$

If we define

$$e^{iK} = \frac{\sin \frac{\beta - 2i\lambda}{2}}{\sin \frac{\beta + 2i\lambda}{2}} \text{ (the total momentum of the 2-string)}, \tag{5.64}$$

then K is quantized as $K = \frac{2\pi}{L} \cdot \text{integer}$, and it's easy to get

$$\frac{dK}{d\beta} = \frac{\sinh 2\lambda}{\cosh 2\lambda - \cos\beta}. \tag{5.65}$$

So the summation over β is transformed to

$$\sum_{\beta} = \sum_{K} = \frac{L}{2\pi} \int dK = \frac{L}{2\pi} \int d\beta \cdot \frac{dK}{d\beta}. \tag{5.66}$$

Putting (5.61), (5.65) and (5.66) into (5.59), one gets

$$I_{\text{bound}} = 4\pi \sinh 2\lambda \sum_{m_1 > m_2} \int_{-\pi}^{\pi} d\beta W(\beta + i\lambda) W(\beta - i\lambda) P^{m_1 - n_1}(\beta + i\lambda) P^{m_2 - n_2}(\beta - i\lambda) \sigma_{m_1}^{-} \sigma_{m_2}^{-} | \Uparrow \rangle, \tag{5.67}$$

which is the same as the result of the contour approach (5.8). During the calculation, the identity (5.17) is useful.

Let me sum up this subsection. I explicitly showed for two-down-spin case, after carefully taking the limit $L \to \infty$, the Goldstein-Yudson decomposition leads to the same results of the contour approach. For multi-down-spin situation, a general argument can be made: for any real momentum, its S-matrix with any other momentum is finite, and in the limit $L \to \infty$ has ignorable effect on quantizing the momentum. So real momenta are quantized like free momenta. The complex momenta in general will cause divergent S-matrices, but the divergence can be removed by multiplying a whole string together. Then the total momentum of the string can be quantized as free. As a result, the representation of the initial state as a summation over integrals of strings is expected, such as (5.4) and (5.32). This can be considered as a double check between the contour representation and the completeness of the string hypothesis. However, the integrals over all possible strings have a tedious form, so I didn't give the general form explicitly. Why it can be organized concisely in the form of the central theorem (4.20) is to be studied.

Chapter 6
Results – Observables Calculated by Numerical Methods

With the time-dependent wave function obtained in Chapter 4, the evolution of any observable can be calculated in the standard way $\langle O(t)\rangle = \langle\Psi(t)|\hat{O}|\Psi(t)\rangle$. The integration in (4.55) in general is difficult to carry out analytically. In this chapter I discuss the methods to evaluate the integral numerically: numerical integration and saddle point approximation. The I show the results including the evolution of local magnetization, staggered magnetization and induced spin currents.

6.1 Numerical Methods

6.1.1 Numerical Integration

There are two difficulties to numerically evaluate the integral in (4.55): (1) The dimension of the integral increases with the number of down spins. High dimensional numerical integration is generically a difficult problem. (2) At large time, the integrand becomes highly oscillatory due to the energy term $e^{-it\epsilon(k)}$. It severely damages the efficiency of most numerical integration methods.

Due to these difficulties, I apply different methods in different cases: For two down spins and moderate time $Jt < 10$, I evaluate the integral numerically by the Gauss-Kronrod Rule, a global adaptive method for a generic integrand [124], implemented by Mathematica. The same method can be applied to three-down-spin case with very short time $Jt < 2$. For the integral of the 3-string from three down spins (it is still a one-dimensional integral) and moderate time $Jt < 12$, I make use of the cubature rules implemented in a C library called Cuba [125, 126]. The cubature rule is also a globally adaptive subdivision scheme for subregion estimation. It is one of the few deterministic, not a Monte Carlo method for high dimensional numerical integration. It is usually the only viable method to obtain high precision, say relative accuracies smaller than 0.01. For the free-magnon states and 2-strings of three down spins, any known numerical integration method is too slow. But for long time (in practice, for $Jt > 3$ I can already get reasonable precision) I use the saddle point approximation, as discussed later.

Generally speaking, numerical integration works for short time while saddle point approximation works for long time. For two down spins, the applicable regions of these two methods overlap, so

one can verify the two methods with each other. For three down spins, their applicable regions have a gap. I will only show the long time part of the results later in this chapter. For larger number of down spins, both of these two method becomes inefficient. So more analytical work is required for arbitrary numbers of down spins. I will discuss it in the outlook part of Chapter 7.

6.1.2 Saddle Point Approximation

At large time, the highly oscillatory factor $e^{-it\epsilon(k)}$ tends to cancel out the integral, leaving only a few saddle points of the exponent important. This picture leads to a method to approximately evaluate the integrals in (4.55). I briefly introduce this useful mathematical tool in this subsection. I will focus on the integral

$$I(m,t) = \int_{-\pi}^{\pi} dk e^{imk+it\cos k} s(k), \tag{6.1}$$

where t is a large parameter, m can take integer values comparable to t, and $s(k)$ has no large parameter in it. We use the symbol $s(k)$ because it usually consists of S-matrices. (See Chapter 5 for the origin of this form.) Our problem is formally defined as to expand the integral (6.1) with respect to $1/t$ as $t \to \infty$. This problem is called the *asymptotic expansion of integrals*, and is generally a broad topic in mathematics. I will focus only on the techniques related to our problem, and usually only consider the leading order term. Most of the discussion here comes from the book by Bleistein and Handelsman [127]. Many of the derivation below will be not very rigorous, but I will try to give the intuition of this approximation approach. The book [127] provides complete and rigorous proof of all the arguments below.

Let's first consider a different integral as it is the building block of the method

$$I(t) = \int_a^b dx e^{tf(x)} s(x), \tag{6.2}$$

for which a is the only saddle point in $[a,b]$, namely $f'(a) = 0$ and $f''(a) < 0$, but $f'(x) \neq 0$ for any $x \in (a,b]$. When $t \to \infty$, only the neighborhood of a is important for the integral

$$\begin{aligned} I(t) \approx & \int_a^{a+\epsilon} dx e^{tf(x)} s(x) \\ = & e^{tf(a)} s(a) \int_a^{a+\epsilon} dx e^{t[f(x)-f(a)]}, \end{aligned} \tag{6.3}$$

where ϵ is a fixed, small number. In the neighborhood of a, we can expand $f(x)-f(a) = \frac{1}{2}|f''(a)|(x-$

$a)^2$. By changing the variable $\xi = \sqrt{\frac{t}{2}f''(a)}(x-a)$, we have

$$\begin{aligned} I(t) \approx & e^{tf(a)}s(a)\int_a^{a+\epsilon} dx e^{\frac{t}{2}f''(a)(x-a)^2} \\ = & e^{tf(a)}s(a)\sqrt{\frac{2}{t|f''(a)|}}\int_0^{\sqrt{\frac{t}{2}|f''(a)|}\epsilon} e^{-\xi^2} \\ \approx & e^{tf(a)}s(a)\sqrt{\frac{\pi}{2t|f''(a)|}}. \end{aligned} \tag{6.4}$$

In the last line we make use of the fact $t \to \infty$ and the result of the Gaussian integral. The formula (6.4) is roughly the *Laplace method* for asymptotic expansions. Our derivation above is not rigorous but intuitive. I need to point out: (1) Formula (6.4) gives the leading order of $I(t) \sim \sqrt{1/t}$. Actually, the end point b will give corrections of order $1/t$. They are not important in our problem, because our end points are $-\pi$ and π, due to the periodicity of our integrand, the contribution of the two end points will cancel each other. (2) When the saddle point is not at one of the end points, one can simply break the integration range into two. (3) In our case a is called the first order saddle point. If $f'(a) = f''(a) = 0$ and $f'''(a) \neq 0$, a is called the second order saddle point. In that case, similar approach will result in

$$I(t) \approx \frac{e^{tf(a)}s(a)}{2}(\frac{3}{t|f'''(a)|})^{\frac{1}{3}}\Gamma(\frac{4}{3}). \tag{6.5}$$

Note that $I(t) \sim t^{-1/3}$ in this case.

Let's come back to the integral (6.1). Since m can be comparable to t, we rewrite it as

$$I(m,t) = \int_{-\frac{\pi}{2}}^{\frac{3\pi}{2}} dz e^{t(iz+i\beta\cos z)}s(z), \tag{6.6}$$

where $\beta = m/t$, and now t is the only large parameter. We change the integration variable to z to emphasize it is a complex integral. For a reason that will be clear later, we also changed the range of integration to $[-\pi/2, 3\pi/2]$. It doesn't change the integral due to periodicity of the integrand (note that m takes integer values). It's easy to see that $I(-m,t) = I(m,t)$ by redefine the variable $z \to -z$. Thus we only consider the case $\beta > 0$. Let's consider the saddle points of the exponent function $w(z) = iz + ia\cos z$ for different values of β.

- $0 < \beta < 1$. $w'(z) = 0$ gives two solutions

$$\begin{aligned} z_+ &= \sin^{-1}\beta, \\ z_- &= \pi - \sin^{-1}\beta. \end{aligned} \tag{6.7}$$

  Like in most asymptotic expansion problems, our $w(x+iy) = u(x,y)+iv(x,y)$ is a holomorphic function. From the Cauchy-Riemann equations, it's easy to get

$$(\frac{\partial u}{\partial x}\vec{e}_x + \frac{\partial u}{\partial y}\vec{e}_y)\cdot(\frac{\partial v}{\partial x}\vec{e}_x + \frac{\partial v}{\partial y}\vec{e}_y) = 0. \tag{6.8}$$

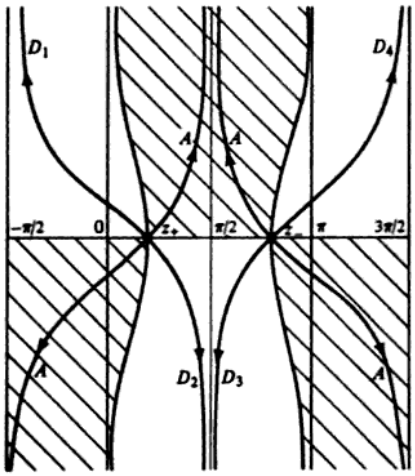

Figure 6.1: The steepest paths through the saddle points for function $w(k)$ when $0 < \beta < 1$. The shaded parts are the "hills", where the real part of $w(k)$ goes to infinity. The arrow on "A"/"D" paths labels the steepest ascent/descent directions.

It means the fastest ascending direction of u and v are perpendicular to each other. In another word, the paths on which the imaginary part v is a constant, are also the paths along which the real part u ascends or descends the fastest. These paths are called the *steepest ascent/descent paths*. In Fig. 6.1, the steepest paths through the two saddle points (6.7) are plotted, and the arrow labels the steepest descent directions. We see that we can replace our integration contours by some combination of these steepest paths. In particular,

$$I(m,t) = (\int_{-\frac{\pi}{2}}^{-\frac{\pi}{2}+i\infty} - \int_{D_1} + \int_{D_2} - \int_{D_3} + \int_{D_4} + \int_{\frac{3\pi}{2}+i\infty}^{\frac{3\pi}{2}})dz e^{tw(z)} s(z). \tag{6.9}$$

The first and last terms will cancel each other due to periodicity. Note that these contours reach infinity, but never go to the shaded "hills". It guarantees the integrand along these contours never diverges. The purpose of these new contours is to transform the integral (6.1) to Laplace type integrals

$$\begin{aligned} I(m,t) =& (-\int_{D_1} + \int_{D_2})dz e^{tu(z)+itv(z_+)} s(z) + (-\int_{D_3} + \int_{D_4})dk e^{tu(z)+itv(z_-)} s(z) \\ =& e^{itv(z_+)}(-\int_{D_1} + \int_{D_2})dk e^{tu(z)} s(z) + e^{itv(z_-)}(-\int_{D_3} + \int_{D_4})dz e^{tu(z)} s(z). \end{aligned} \tag{6.10}$$

Here we make use of the fact that along the D-paths the imaginary part $v(z)$ is a constant. Let's define the distance along the D-path to be x, then the integral along one of the D-paths in (6.10) takes the same form as the Laplace method (6.4)

$$\int_{D_j} dx \frac{dz}{dx} e^{tu(z(x))} s(z(x)). \tag{6.11}$$

Generally, the path D_j and the function $z(x)$ are both hard to quantify. However, the integral of the form (6.4) is determined only by the behavior at the saddle point. In particular,

we only need to find $w(z_\pm)$, $u''(x)|_{z=z_\pm}$ and $\frac{dz}{dx}|_{z=z_\pm}$. Specifically, $w(z_\pm)$ can be calculated straightforwardly

$$w(z_\pm) = \pm i[\sqrt{1-\beta^2} - \beta\cos^{-1}\beta]. \tag{6.12}$$

For the holomorphic function $w(z)$, its derivative in any direction is the same, so

$$u''(x)|_{z=z_\pm} = w''(z_\pm) = \mp i\sqrt{1-\beta^2}. \tag{6.13}$$

As for $\frac{dz}{dx}|_{z=z_\pm}$, it is actually the direction of the D-path at $z_\pm$. The steepest descent directions at a saddle point are not hard to find, given by the Theorem 7.1 of Ref. [127]. In our particular case,

$$\begin{aligned}\frac{dz}{dx}|_{z=z_+} &= e^{\frac{3\pi}{4}} \text{ for } D_1,\ e^{-\frac{\pi}{4}} \text{ for } D_2,\\ \frac{dz}{dx}|_{z=z_-} &= e^{-\frac{3\pi}{4}} \text{ for } D_3,\ e^{\frac{\pi}{4}} \text{ for } D_4,\end{aligned} \tag{6.14}$$

which are easily visualized in Fig. 6.1. Combine the conclusions above, we find

$$\begin{aligned}I(m,t) \approx &\sqrt{\frac{2}{\pi t}}\frac{\exp[it(\sqrt{1-\beta^2} - \beta\cos^{-1}\beta) - \frac{i\pi}{4}]}{(1-\beta^2)^{1/4}}s(z_+)\\ &+ \sqrt{\frac{2}{\pi t}}\frac{\exp[-it(\sqrt{1-\beta^2} - \beta\cos^{-1}\beta) + \frac{i\pi}{4}]}{(1-\beta^2)^{1/4}}s(z_-).\end{aligned} \tag{6.15}$$

Note it decays as $\sqrt{1/t}$ and oscillates with respect to β (or equivalently with respect to m).

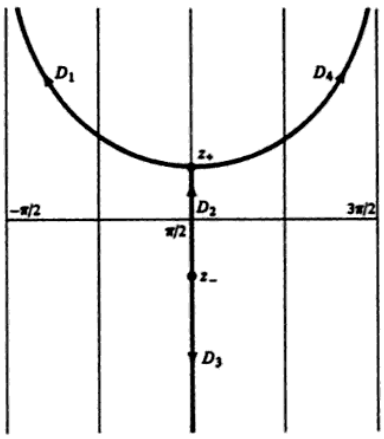

Figure 6.2: The steepest paths through the saddle points for function $w(k)$ when $\beta > 1$. The arrows label the steepest descent directions.

- $\beta > 1$. The saddle points becomes

$$z_\pm = \frac{\pi}{2} \pm i\cosh^{-1}\beta. \tag{6.16}$$

The steepest paths through these saddle points are depicted in Fig. 6.2. Note that D_2 descends from z_- to z_+, indicating that z_+ is "lower", and therefore contributes exponentially smaller, than z_-. However, our original contour can be replaced by just $-D_1 + D_4$, so z_- doesn't contribute at all and z_+ still gives the leading order. After similar calculation as $0 < \beta < 1$, we have

$$I(m,t) = \sqrt{\frac{2}{\pi t}} \frac{\exp[-t(\beta \cosh^{-1}\beta - \sqrt{\beta^2-1})]}{(\beta^2-1)^{1/4}} s(z_+). \tag{6.17}$$

It still decays as $\sqrt{1/t}$ with respect to t. But as β gets large ($m >> t$), it becomes exponentially small, implying the Lieb-Robinson bound.

- $\beta = 1$. This case is special because $w'(z) = 0$ gives only one solution, which is a second order saddle point

$$z_o = \frac{\pi}{2} \text{ where } w''(z_o) = 0,\ w'''(z_o) = i. \tag{6.18}$$

The steepest descent paths are shown in Fig. 6.3. This time the integral contour can be

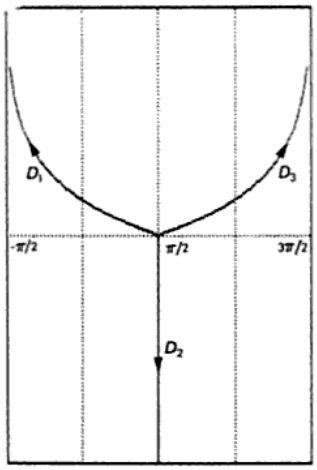

Figure 6.3: The steepest paths through the saddle point $z_o = \frac{\pi}{2}$ when $\beta = 1$. The arrows label the steepest descent directions.

replaced by $-D_1 + D_3$. And the steepest directions at $z_o = \frac{\pi}{2}$ are

$$\frac{dz}{dx}|_{z=z_o} = \frac{5\pi}{6} \text{ for } D_1,\ \frac{\pi}{6} \text{ for } D_3. \tag{6.19}$$

Making use of (6.5), we get

$$I(m,t) \approx \frac{\Gamma(\frac{1}{3})}{\pi t^{1/3}} (\frac{4}{3})^{1/6} s(z_o). \tag{6.20}$$

In this case $I(m,t)$ decays as $t^{-1/3}$.

Up to here, it seems that we have obtained the saddle point approximation of (6.1) for any value of m. But in practice, there is actually still a problem: when $\beta \to 1^{\pm}$, the approximated form (6.15) and (6.17) doesn't smoothly go to (6.20). On the contrary, they diverge as $\beta \to 1$, on both sides. It happens because when $\beta \to 1$, two first order saddle points merges into one second order saddle point, causing that $I(m,t)$ decays as different power of $1/t$ for $\beta = 1$ and $\beta \neq 1$. To connect these two different behavior, their amplitudes must diverge. As a result, if one calculates the wave function at a certain m that leads to $\beta \approx 1$, one gets very bad precision. To overcome this problem, we need an approach that can give a uniform, non-diverging approximation of (6.1) for $\beta \in [0, +\infty)$. This approach is called *uniform asymptotic expansion*, which I discuss in Appendix B. In the end, I implement (B.25), (B.40) and (B.41) in a C++ code to calculate the numerical values of the time-dependent wave functions.

6.2 Local Magnetizations

Starting from a certain initial state, at a later time t, the expected local magnetization at site n is given by

$$m(n,t) = \langle \Psi(t) | \sigma_n^z | \Psi(t) \rangle. \tag{6.21}$$

In experiments, the measurement of σ^z on any site can only yield two values 1 or -1. Taking the average over an ensemble will give the expectation value above [5]. In our approach, the expectation value of the local magnetization can be calculated in a standard way as follow. In Chapter 4, we write the evolved state in the form

$$|\Psi(t)\rangle = \sum_{\{m_j\}} \Psi^{\{n_j\}}(\{m_j\}, t) \prod_j \sigma_{m_j}^- | \Uparrow \rangle, \tag{6.22}$$

where the exact time-dependent wave function $\Psi^{\{n_j\}}(\{m_j\}, t)$ is given by (4.55). Note that it has been symmetrized, namely any permutation among the coordinates $\{m_j\}$ are equivalent

$$\Psi^{\{n_j\}}(\{m_{P_j}\}, t) = \Psi^{\{n_j\}}(\{m_j\}, t). \tag{6.23}$$

In practice, I evaluate the integrals in (4.55) by the methods discussed in the last section and then numerically symmetrized it. Then we can calculate the local magnetization

$$m(n,t) = \sum_{\{m_j\}} \sum_{\{m'_j\}} \Psi^*(\{m'_j\}, t) \Psi(\{m_j\}, t) \langle \Uparrow | (\prod_j \sigma_{m'_j}^+) \sigma_n^z (\prod_j \sigma_{m_j}^-) | \Uparrow \rangle. \tag{6.24}$$

where we omit the initial coordinates $\{n_j\}$, since they are constant and doesn't play any role in this calculation. From the commutation relations

$$[\sigma_n^z, \sigma_m^-] = -2\sigma_m^-\delta_{nm}, \tag{6.25}$$

$$[\sigma_n^-, \sigma_m^+] = -\sigma_n^z\delta_{nm}, \tag{6.26}$$

it is easy to derive

$$\begin{aligned}\langle \Uparrow |(\prod_j \sigma^+_{m'_j})\sigma^z_n(\prod_j \sigma^-_{m_j})| \Uparrow\rangle =&(-2\sum_j \delta_{nm_j}+1)\langle \Uparrow (\prod_j \sigma^+_{m'_j})(\prod_j \sigma^-_{m_j})| \Uparrow\rangle \\ =&(-2\sum_j \delta_{nm_j}+1)\sum_P\prod_j \delta_{m_j m'_{P_j}}.\end{aligned} \tag{6.27}$$

Making use of it, we get

$$\begin{aligned}m(n,t) =& \sum_{\{m_j\}}\sum_P(-2\sum_j \delta_{nm_j}+1)\Psi^*(\{m_{P_j}\},t)\Psi(\{m_j\},t) \\ =&M!\sum_{\{m_j\}}(-2\sum_j \delta_{nm_j}+1)\Psi^*(\{m_j\},t)\Psi(\{m_j\},t) \\ =&-2M!\sum_{m_2,\ldots,m_M}|\Psi(n,m_2,m_3,\ldots,m_M,t)|^2+1.\end{aligned} \tag{6.28}$$

Here M is the total number of the down spins. In both lines we make use of (6.23). In the last line we also make use of the fact the time evolution is a unitary operation, so $\langle\Psi(t)|\Psi(t)\rangle = \langle\Psi_0|\Psi_0\rangle = 1$. From (6.28), we calculate the numerical values of the local magnetization from the time-dependent wave function.

We show here the evolution of the local magnetizations from the initial states with consecutive down spins, because these initial states overlap with the bound states maximumly. The evolutions from the initial state $\Psi_0 = \sigma_1^-\sigma_0^-|\Uparrow\rangle$ for various values of the anisotropy Δ are shown in Fig. 6.4. The non-interacting case $\Delta = 0$ is calculated as the product of the single-down-spin evolutions (5.2). It has a closed form

$$m(n,t)|_{\Delta=0} = -2J^B_{n-1}(4Jt)^2 - 2J^B_n(4Jt)^2 + 1, \tag{6.29}$$

where $J^B_n(x)$ is the Bessel function of order n. For all the other values of Δ, the local magnetizations are calculated numerically from (6.28).

For the non-interacting case $\Delta = 0$, the frontier of the local magnetization shows a light-cone structure, indicating the Lieb-Robinson bound. The slope of the light cone represents the velocity of the free magnon propagation. From the single-particle spectrum relation $\epsilon(k) = 4J(\Delta - \cos k)$, one gets the propagating velocity

$$|v| = \left|\frac{d\epsilon}{dk}\right| = 4J\sin k. \tag{6.30}$$

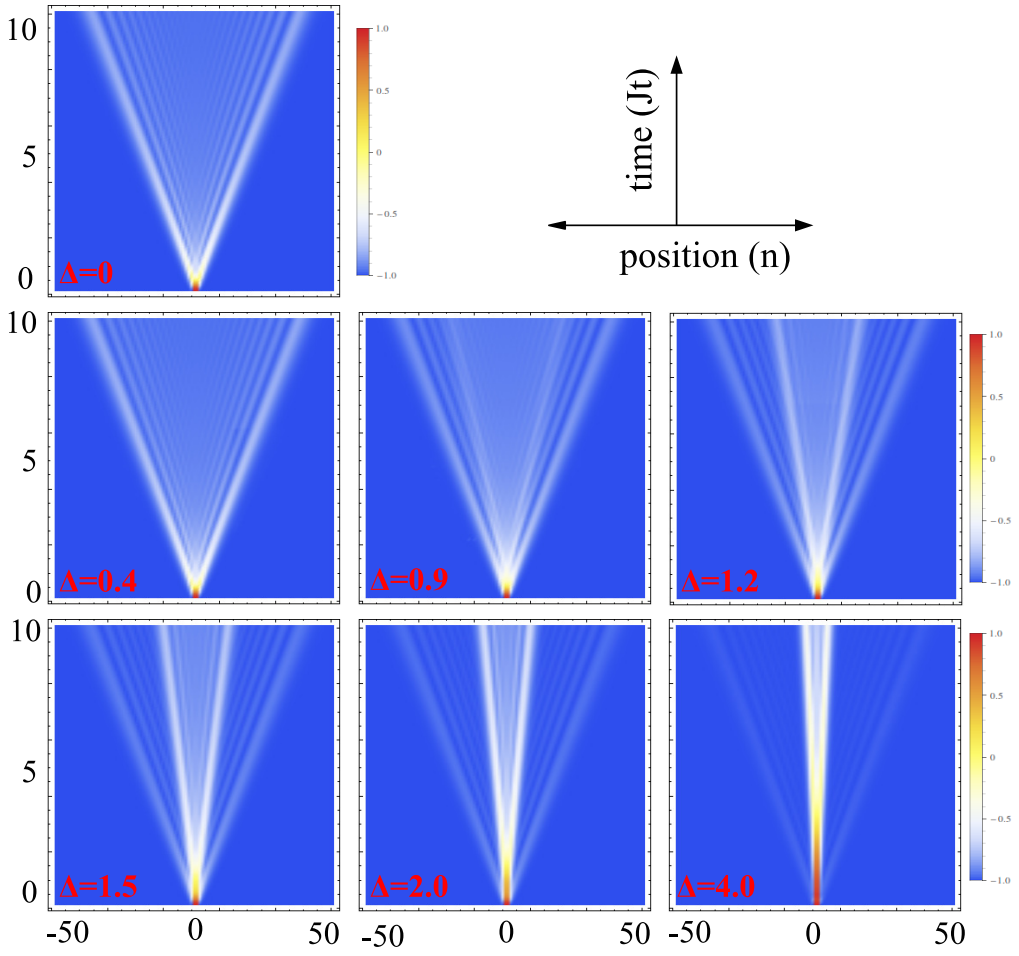

Figure 6.4: Evolution of local magnetization for various values of Δ, starting from the initial state $|\Psi_0\rangle = \sigma_1^- \sigma_0^- |\Uparrow\rangle$. For a reasonable legend, the color in the graphs actually represents $-m(n,t)$.

At $k = \pi/2$, the velocity reaches the maximum $|v|_{\max} = 4J$, and the density of states also reaches the maximum. Thus one can see the sharp wave front in Fig. 6.4. With the dimensionless time unite Jt, the slope of the light cone is supposed to be $1/4$, which agrees with the graph. Besides the wave front, one can also see the patten from interference between the two spins.

For the interacting case $\Delta \neq 0$, the obvious feature is the emergence of the second light-cone inside the wave front of the free mangons. Both the slope and the strength of the second light-cone are functions of Δ. We claim it belongs to the bound state of the two down spins. It can be explained through the analysis of the time-dependent wave function in Chapter 5. We showed in (5.4) that the two-down-spin wave function can be separated into the free-magnon component and the bound-state component, with proportions depending on Δ. The free-magnon component is almost the same as the non-interacting case, with the only difference that the integral is tuned by the S-matrix. Thus for any $\Delta \neq 0$ in Fig. 6.4, one can still see the outer light-cone very similar to $\Delta = 0$ case, with a lower intensity. As for the bound-state component, when $|\Delta| > 1$, it takes the form of a single-down-spin propagation, with a rescaled time, as shown in (5.24). The rescaling factor $\frac{\sinh\lambda}{\sinh(2\lambda)}$ is thus also the ratio of the propagating velocities of the bound over that of the free magnons. This dependence on Δ (as a reminder, $\Delta = -\cosh\lambda$) of the slope of inner light-cone is well visualized in Fig. 6.4. The proportion of the bound state in the initial state is represented by the factor $4\pi\sinh\lambda$ in (5.4). So as Δ gets large, the bound state gets dominant, as shown in the $\Delta = 4$ graph. On the other hand, when $|\Delta| < 1$, the total momentum of the bound state is restrained in the range $[-\pi + 2\mu, \pi - 2\mu]$. Investigating (5.34) in the long time limit, we see that the integral is determined mostly by the two saddle points

$$K_1^s = \sin^{-1}(\frac{M}{4Jt}), K_2^s = \pi - \sin^{-1}(\frac{M}{4Jt}). \tag{6.31}$$

For a small μ ($|\Delta| < 1$ but $|\Delta| \approx 1$), only the saddle point K_2^s will be prohibited for some coordinate M. It leads to a diffuse wave front as shown in the $\Delta = 0.9$ graph. When $\mu > \pi/4$ ($|\Delta| < \sqrt{2}/2$), both the saddle point K_1^s and K_2^s are prohibited for any M, causing the bound state component severely suppressed. That's why the magnetization for $\Delta = 0.4$ looks almost identical to the non-interacting case.

For the initial state with three down spins, numerical integration is only feasible for very short time ($Jt < 0.5$). I show here the results calculate by saddle point approximation. In principle, the saddle point approximation is justified only for long time limit. In practice, I use the norm of the wave function as a test of the precision of my calculation. I found that $|\frac{\langle\Psi(t)|\Psi(t)\rangle}{\langle\Psi_0|\Psi_0\rangle} - 1| < 0.05$ for $Jt > 3$, indicating an acceptable precision. I show in Fig. 6.5 the evolution of the local magnetization from the initial state $|\Psi_0\rangle = \sigma_1^-\sigma_0^-\sigma_{-1}^-|\Uparrow\rangle$, calculated by saddle point approximation for $Jt > 3$.

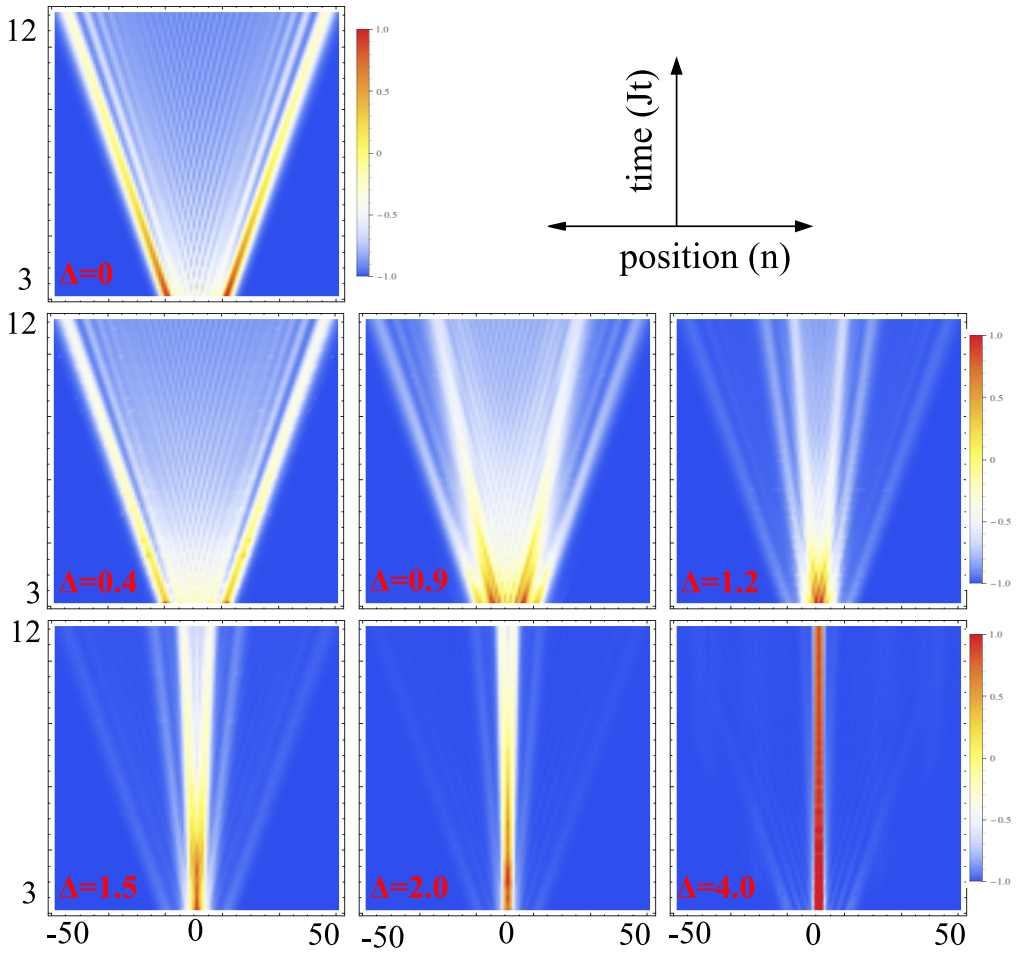

Figure 6.5: Evolution of local magnetization for various values of Δ, starting from the initial state $|\Psi_0\rangle = \sigma_1^- \sigma_0^- \sigma_{-1}^- | \Uparrow \rangle$. For a reasonable legend, the color in the graphs actually represents $-m(n,t)$.

Again, for the non-interacting case $\Delta = 0$, we only see the wave front of the free magnons, and the interference pattern. For the interacting case $\Delta \neq 0$, we typically see three wave fronts: the outermost one comes from the free-magnon component; the middle one belongs to the wave function component with two down spins bounded together, but the third one free; the innermost one comes from the component with all three down spins bounded together. We showed this decomposition of the wave function in Eq. (5.32) of Chapter 5. For $\Delta = 4$, the three-spin bound state dominates, causing that the three down spins almost never depart. It is a good interpretation of the infinite Δ limit of the anisotropic Heisenberg model –it goes to the Ising model, with the initial state to be its eigenstate. Again, for $|\Delta| < 1$, the wave fronts of the bound states get diffuse, and almost disappear for $\Delta = 0.4$.

To sum up this section, through the numerically evaluated wave function, we calculated the evolution of the local magnetization as functions of both site position and time. The local magnetization clearly shows the propagation of the bound states predicted by the Bethe ansatz.

6.3 Staggered Magnetization –the Antiferromagnetic Order-Parameter

As discussed in the Introduction, the quantum quench through a critical point is especially interesting. For the anisotropic Heisenberg model, one can prepare the initial state in the antiferromagnetic ordered Néel state

$$|\Psi_0\rangle = \prod_j \sigma_{2j}^- |\Uparrow\rangle, \tag{6.32}$$

and evolve it with the Hamiltonian $\Delta < 1$. It is equivalent to a quench from $\Delta = \infty$ to $\Delta < 1$, through the critical point $\Delta = 1$. The staggered magnetization defined as

$$m_s(t) = \sum_n (-1)^n \langle \Psi(t) | \sigma_n^z | \Psi(t) \rangle \tag{6.33}$$

is the antiferromagnetic order parameter –it takes the value 1 for anti-ferromagnetic phase and 0 for ferromagnetic phase. Its behavior after a quench is of great interest, as discussed in Section 2.6.2.

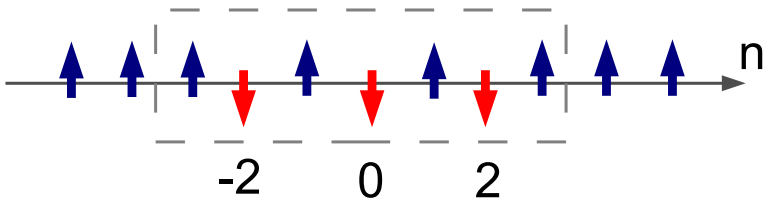

Figure 6.6: The initial state we choose to investigate the evolution of antiferromagnetic order parameter. It can be considered "locally" antiferromagnetic in the gray box.

With our contour approach, only the few-down-spin case is feasible. So I prepare the initial state as $\Psi_0\rangle = \sigma_2^-\sigma_0^-\sigma_{-2}^-|\Uparrow\rangle$. As shown in Fig. 6.6, within a small box consisting of 7 sites, it can be considered to have antiferromagnetic order. I measure the evolution of the staggered magnetization in this box as well.

The results calculated by saddle point approximation for $Jt \in [5, 12]$ are shown in Fig. 6.7. Note that all the three graphs have the same scale on both axes, therefore can be compared directly. Numerical simulations by Barmettler *et al.* [7] by the infinite-size matrix product method (iMPS) show oscillation and decay to be the basic features of the the staggered magnetization. Because our set-up is quite different from theirs, as explained in Section 2.6.2, the comparison with their results is very qualitative.

First let's notice I show results on different time regimes from Barmettler *et al.* Due to the different definitions of Eq. (1.15) (theirs) and Eq. (3.2) (mine), their exchange coupling J is four times as large as mine. So the "intermediate" time regime $Jt < 16$ they claimed actually corresponds to $Jt < 4$ in my convention. In another word, I can show the "large" time regime, compared to theirs. (In my approach, the saddle point approximation does not give high enough accuracy for the time regime $Jt < 4$.) Our work is supplementary to each other in this sense.

Generally speaking, the decay rate depending on Δ qualitatively agrees with the numerical work, but the oscillation behavior does not. The largest difference happens in the regime $\Delta > 1$. My results show oscillation, while the numerical work only shows decay. It is possibly because I only consider a small box and ignore the magnons that propagates away. However, the period of Rabi oscillation (see Section 2.6.2 for details) agrees with expectation. By theory it is

$$T_{\text{theo}} = \frac{2\pi}{\omega} = \frac{2\pi}{8} = 0.79(\text{in unit of } Jt). \tag{6.34}$$

From Fig. 6.7, we can read $T_{\text{calc}} \approx 0.79$, and doesn't show distinguishable dependence on Δ. So the oscillation frequency agree with the numerical work and non-interacting case. On the other hand, let's look at the decay rate. In the numerical work, they claim all the decay are exponential except for the non-interacting case $\Delta = 0$. But it is only from the observation of data. And in the regime $0 < \Delta < 1$, even the authors of Ref. [7] admit exponential function does not give a good fit. In my results, from Fig. 6.7, it is hard to identify the decaying behavior with a simple function, and it doesn't make sense to do so because of the "finte box". But we can still see qualitative agreement with the numerical work. In particular, they found the relaxation time scales diverge when $\Delta \to 0$ or $\Delta \to \infty$, and vanish when $\Delta \to 1$ from both sides. From Fig. 6.7, we can clearly see $m_s(t)$ decays faster as Δ is close to 1, while decays slower when Δ is away from 1, showing this qualitative agreement. I expect in future work the precise relaxation time scales and their dependence on the

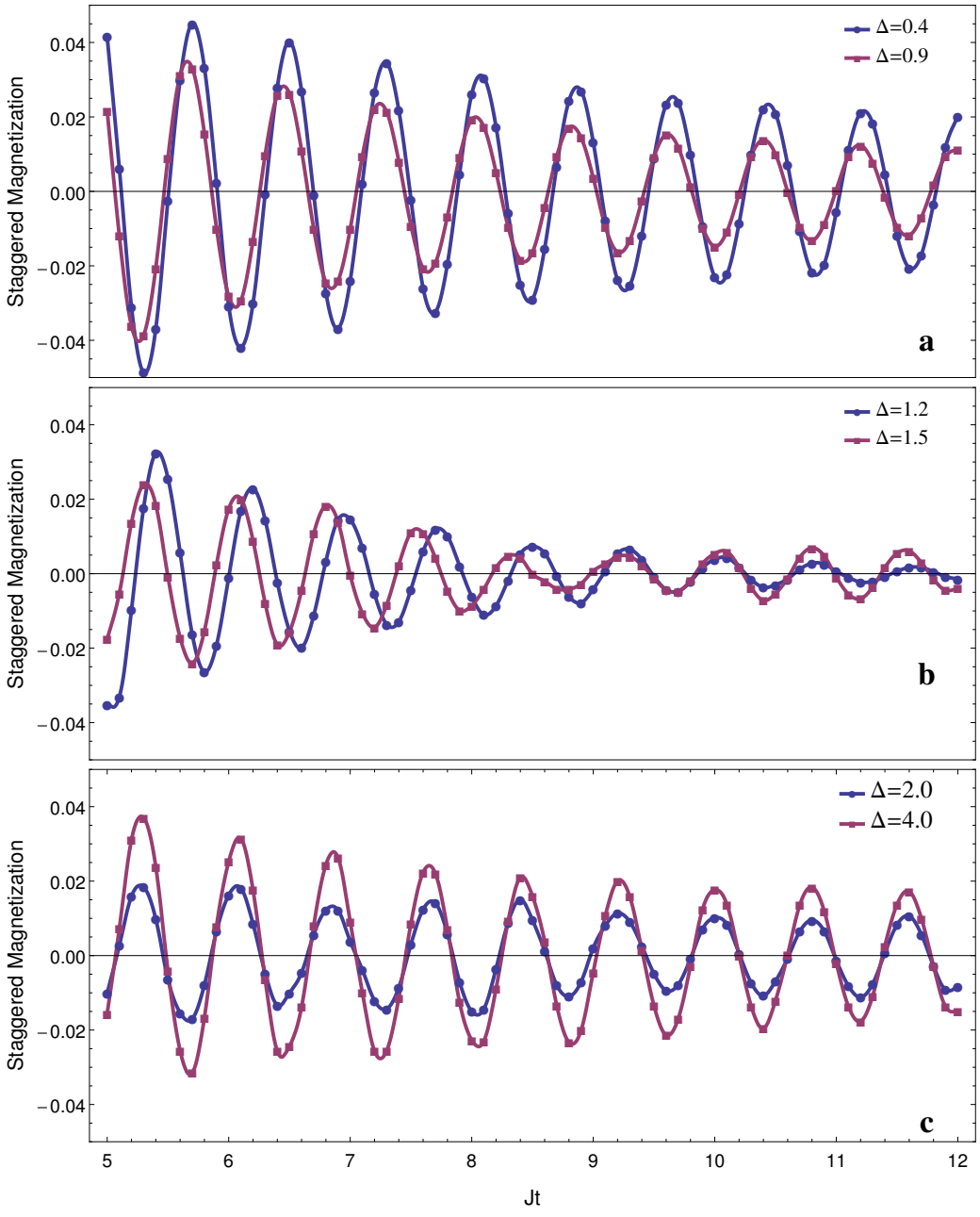

Figure 6.7: The time evolution of the staggered magnetization $m_s(t)$ from the initial state $|\Psi_0\rangle = \sigma_2^- \sigma_0^- \sigma_{-2}^- | \Uparrow\rangle$, and within a box from site $n = -3$ to $n = 3$. The curves connecting data points are quadratic spline interpolation.

Hamiltonian parameters can be obtained by cunning reformulation of the integral (4.55).

6.4 Induced Spin Currents

The quantum quench will induce spin currents, which is defined as the magnetization going through a particular site n per unit time. If we define the total magnetization to the "right" of a particular site n as

$$\hat{N}(n) \equiv \sum_{m=n+1}^{\infty} \sigma_m^z. \tag{6.35}$$

The spin current through this site is given by

$$\hat{J}(n,t) = \frac{d\hat{N}(n)}{dt} = i[\hat{N}(n), \hat{H}]. \tag{6.36}$$

It is easy to derive

$$\hat{J}(n,t) = 2iJ(\sigma_n^+\sigma_{n+1}^- - \sigma_n^-\sigma_{n+1}^+). \tag{6.37}$$

As discussed in the Introduction, the anisotropic Heisenberg model can be mapped to fermions on a lattice with nearest-neighbor interaction, through a Jordan-Wigner transformation. In the fermionic language, the spins current we define above becomes the usual particle current. I expect the measurement of the currents in the fermionic system to be an easier way to probe the bound states in experiments.

I calculate the expectation of the spin currents $J(n,t) = \langle\Psi(t)|\hat{J}(n,t)|\Psi(t)\rangle$ from the initial state $\Psi_0\rangle = \sigma_1^-\sigma_0^-\sigma_{-1}^-|\Uparrow\rangle$, which maximizes the bound states. In Fig. 6.8, I show the spin currents through the site $n = 9$ and $n = 15$ for various values of Δ. For a particular choice of site n, one can identify certain bound states from the currents. In Fig. 6.8 (a), where the currents are calculated at site $n = 15$, the first bump of the currents comes simultaneously for different Δ. It is due to the free magnons whose propagating speeds are independent of Δ. Meanwhile, the second bump corresponding to the two-magnon bound state comes in the order of increasing Δ, since the speed of bound states decreases with Δ. For $\Delta = 2$, time is not long enough to see the two-magnon bound state arrives. In Fig. 6.8 (b) I show the current at site $n = 9$, closer to the origin. The free state has already passed for all the Δ's, while the two-magnon bound states can be seen clearly coming in order of increasing Δ. For $\Delta = 0.9$, the three-magnon bound state has too small a weight to show in the current, while for $\Delta = 1.2$ one can see the three-magnon bound state arriving.

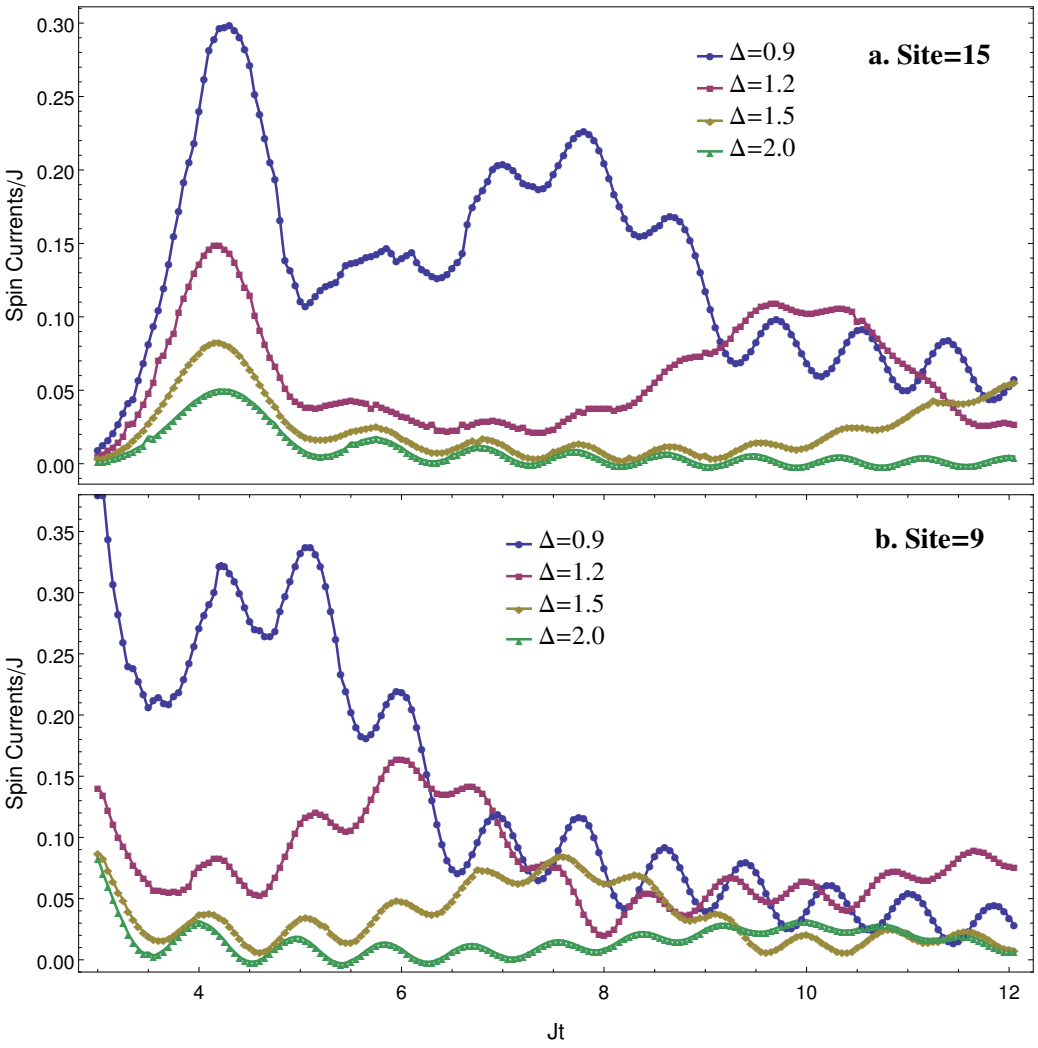

Figure 6.8: The spin currents measured at (a) site $n = 15$ and (b) site $n = 9$, from the initial state $|\Psi_0\rangle = \sigma_1^- \sigma_0^- \sigma_{-1}^- |\Uparrow\rangle$. One can see bumps caused by different bound states.

Chapter 7
Conclusion and Outlook

7.1 Conclusion

In this thesis I presented an exact approach to obtain the full time evolution of the XXZ Heisenberg spin chain, for generic initial states and any values of parameters. Based on it, I studied various aspects of the quench dynamics of the XXZ model.

I proposed the contour representation of a generic initial state in Eq. (4.3) and proved it mathematically. From it I obtained in Eq. (4.55) the exact time-dependent wave function in an integral form, and used it to compute the time evolution of several physical quantities: the joint probability function, local magnetization, staggered magnetization, and local spin currents, for various values of the anisotropy Δ and from different initial states. Some of the physical quantities can be analytically studied from the time-dependent wave function, others need evaluations by approximation or numerics, for which I provided explicit methods.

In particular situations, I applied the new approach to two specific quantum quenches of the XXZ spin chain: from a local quench I calculated the propagation of magnons and their bound states; from a global quench I calculated the decay and oscillating behavior of the antiferromagnetic order parameter. All the results were compared to either experimental works by ultracold atoms in optical lattice, or recently developed numerical methods, or both. I further made predictions on the spin currents after a quench.

I expect the real time evolution of the XXZ model would contribute to the understanding of many open questions on the non-equilibrium dynamics of isolated many-body systems.

7.2 Future work

From the methodology aspect, the future work includes extending the contour representation to thermodynamics limit and efficient calculation of observables. These can be achieved possibly by incorporating the algebraic Bethe ansatz with the contour representation. Specifically, the new approach proposed by this thesis provides an efficient representation of the wave function Eq. (4.55),

compactly written as

$$|\Psi(t)\rangle = \int_\gamma d\vec{k} e^{-iE(\vec{k})t} |\vec{k}\rangle (\vec{k}|\Psi_0\rangle. \tag{7.1}$$

It is efficient because $(\vec{k}|\Psi_0\rangle$ is simple to calculate and one doesn't have to solve the Bethe ansatz equations since k's takes continuous values (as thoroughly explained in Chapter 4). But in the thermodynamic limit, the number of particles goes to infinity, so one has to deal with infinite dimensional integrals. (High dimensional integrable as a numerical problem is already unachievable.) Furthermore, what people are ultimately interested of is the expectation of observables

$$O(t) = \langle \Psi(t)|\hat{O}|\Psi(t)\rangle \tag{7.2}$$

From the representation above, it can be calculated as

$$O(t) = \int_\gamma d\vec{k} \int_{\gamma^*} d\vec{p} e^{-i[E(\vec{k})-E(\vec{p})]t} (\vec{k}|\Psi_0\rangle\langle\Psi_0|\vec{p})\langle\vec{p}|\hat{O}|\vec{k}\rangle \tag{7.3}$$

Taking fully advantage of the contour representation, the only difficult part in (7.3) is $\langle\vec{p}|\hat{O}|\vec{k}\rangle$, the matrix element of an observable in between two Bethe eigenstates, which is called *form factor* in algebraic Bethe ansatz. There has been systematic work on calculation of form factors both for generic integrable models [98] and for the XXZ model specifically [128]. Even in thermodynamic limit, for some special cases, the form factor can be represented in terms of Fredholm determinant. Unfortunately, when k's and p's are arbitrary, i.e. they don't have to satisfy Bethe ansatz equations as we require, the form factor takes a very complicated form [98]. To incorporate the results of algebraic Bethe ansatz into Eq. (7.3) and get an analytical result is a possible future direction. It could be difficult, but it will give the full answer to the global quench problem for thermodynamic limit.

Another possible way to get the thermodynamic limit is through the finite-size Yudson representation. In Chapter 5, I introduce the Goldstein-Yudson decomposition (5.44), which follows the same idea as the Yudson contour representation, but works for finite-size situation:

$$|\Psi(t)\rangle = \sum_{\vec{k}} \frac{e^{-iE(\vec{k})t}|\vec{k}\rangle(\vec{k}|\Psi_0\rangle}{N(\vec{k})}, \tag{7.4}$$

where $N(\vec{k}) = \langle\vec{k}|\vec{k}\rangle$ is the norm of the Bethe eigenstate. In this decomposition, the k's are the solutions of the Bethe ansatz equations, and the summation over $\vec{k}$ means summing over all possible solutions, with any permutation of a solution set $\{k_j\}$ being considered a new set of solutions. This unconventional definition of summation comes from the manipulation to simplify the overlap $(\vec{k}|\Psi_0\rangle$ (see Chapter 5 for details). The solutions of the Bethe ansatz equations in the thermodynamic limit are well studied. They can be represented by the distribution functions on strings [95]. Then

physical quantities in thermodynamic limit can be calculated through integral over these distribution functions on strings. Methods following this way are summarized as the Thermodynamic Behte ansatz (TBA). I expect the summation in (7.4) can be transformed to integrals in a similarly way as TBA. In fact, in some very recent works, the distribution functions of the TBA has been used to study the asymptotic states of integrable models and show the failure of GGE [129, 108, 109]. So it seems promising to combine the TBA with the finite-size Yudson decomposition to give the full time evolution in thermodynamic limit.

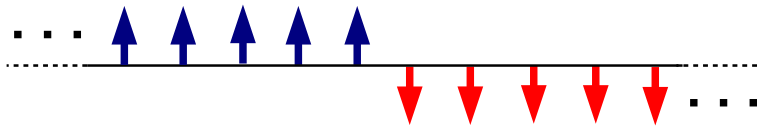

Figure 7.1: The "domain wall" initial state of the XXZ model.

From the physics aspect, future works include the study of other interesting initial states. For example, the initial state can be prepared to be a "domain wall", shown in Fig. 7.1. In the long time limit, a steady spin current is expected. This setup provides a good analogy to the quench problem with the quantum dot, discussed in Section 1.2. It is also expected to test the applicability of the classic Drude's law in quantum systems. But solution of this problem requires progress in methodology mentioned above.

References

[1] W. Liu and N. Andrei, "Quench dynamics of the anisotropic heisenberg model," *Phys. Rev. Lett.*, vol. 112, p. 257204, Jun 2014.

[2] W. Liu and N. Andrei, "to be submitted,"

[3] I. Bloch, J. Dalibard, and W. Zwerger, "Many-body physics with ultracold gases," *Rev. Mod. Phys.*, vol. 80, pp. 885–964, Jul 2008.

[4] M. Rigol, V. Dunjko, and M. Olshanii, "Thermalization and its mechanism for generic isolated quantum systems," *Nature*, vol. 452, no. 7189, pp. 854–858, 2008.

[5] T. Fukuhara, P. Schauß, M. Endres, S. Hild, M. Cheneau, I. Bloch, and C. Gross, "Microscopic observation of magnon bound states and their dynamics," *Nature*, vol. 502, pp. 76–79, 2013.

[6] P. Barmettler, M. Punk, V. Gritsev, E. Demler, and E. Altman, "Relaxation of antiferromagnetic order in spin-1/2 chains following a quantum quench," *Phys. Rev. Lett.*, vol. 102, p. 130603, Apr 2009.

[7] P. Barmettler, M. Punk, V. Gritsev, E. Demler, and E. Altman, "Quantum quenches in the anisotropic spin-1/2 Heisenberg chain: different approaches to many-body dynamics far from equilibrium," *New Journal of Physics*, vol. 12, no. 5, p. 055017, 2010.

[8] E. Farhi, J. Goldstone, S. Gutmann, J. Lapan, A. Lundgren, and D. Preda, "A quantum adiabatic evolution algorithm applied to random instances of an np-complete problem," *Science*, vol. 292, no. 5516, pp. 472–475, 2001.

[9] J. Berges, "Introduction to nonequilibrium quantum field theory," in *AIP Conference Proceedings*, vol. 739, 2004.

[10] A. Altland and B. D. Simons, *Condensed matter field theory*. Cambridge University Press, 2010.

[11] A. Mitra, S. Takei, Y. B. Kim, and A. J. Millis, "Nonequilibrium quantum criticality in open electronic systems," *Phys. Rev. Lett.*, vol. 97, p. 236808, Dec 2006.

[12] A. Mitra and T. Giamarchi, "Mode-coupling-induced dissipative and thermal effects at long times after a quantum quench," *Phys. Rev. Lett.*, vol. 107, p. 150602, Oct 2011.

[13] S. Diehl, A. Tomadin, A. Micheli, R. Fazio, and P. Zoller, "Dynamical phase transitions and instabilities in open atomic many-body systems," *Phys. Rev. Lett.*, vol. 105, p. 015702, Jul 2010.

[14] M. H. Anderson, J. R. Ensher, M. R. Matthews, C. E. Wieman, and E. A. Cornell, "Observation of bose-einstein condensation in a dilute atomic vapor," *Science*, vol. 269, no. 5221, pp. 198–201, 1995.

[15] K. B. Davis, M. O. Mewes, M. R. Andrews, N. J. van Druten, D. S. Durfee, D. M. Kurn, and W. Ketterle, "Bose-einstein condensation in a gas of sodium atoms," *Phys. Rev. Lett.*, vol. 75, pp. 3969–3973, Nov 1995.

[16] C. C. Bradley, C. A. Sackett, J. J. Tollett, and R. G. Hulet, "Evidence of bose-einstein condensation in an atomic gas with attractive interactions," *Phys. Rev. Lett.*, vol. 75, pp. 1687–1690, Aug 1995.

[17] S. Inouye, M. Andrews, J. Stenger, H.-J. Miesner, D. Stamper-Kurn, and W. Ketterle, "Observation of feshbach resonances in a bose–einstein condensate," *Nature*, vol. 392, no. 6672, pp. 151–154, 1998.

[18] P. Courteille, R. S. Freeland, D. J. Heinzen, F. A. van Abeelen, and B. J. Verhaar, "Observation of a feshbach resonance in cold atom scattering," *Phys. Rev. Lett.*, vol. 81, pp. 69–72, Jul 1998.

[19] C. Chin, R. Grimm, P. Julienne, and E. Tiesinga, "Feshbach resonances in ultracold gases," *Rev. Mod. Phys.*, vol. 82, pp. 1225–1286, Apr 2010.

[20] N. Navon, S. Nascimbne, F. Chevy, and C. Salomon, "The equation of state of a low-temperature fermi gas with tunable interactions," *Science*, vol. 328, no. 5979, pp. 729–732, 2010.

[21] M. Greiner, O. Mandel, T. Esslinger, T. W. Hänsch, and I. Bloch, "Quantum phase transition from a superfluid to a mott insulator in a gas of ultracold atoms," *Nature*, vol. 415, no. 6867, pp. 39–44, 2002.

[22] M. P. A. Fisher, P. B. Weichman, G. Grinstein, and D. S. Fisher, "Boson localization and the superfluid-insulator transition," *Phys. Rev. B*, vol. 40, pp. 546–570, Jul 1989.

[23] L.-M. Duan, E. Demler, and M. D. Lukin, "Controlling spin exchange interactions of ultracold atoms in optical lattices," *Phys. Rev. Lett.*, vol. 91, p. 090402, Aug 2003.

[24] O. Mandel, M. Greiner, A. Widera, T. Rom, T. W. Hänsch, and I. Bloch, "Coherent transport of neutral atoms in spin-dependent optical lattice potentials," *Phys. Rev. Lett.*, vol. 91, p. 010407, Jul 2003.

[25] D. Jaksch, H.-J. Briegel, J. I. Cirac, C. W. Gardiner, and P. Zoller, "Entanglement of atoms via cold controlled collisions," *Phys. Rev. Lett.*, vol. 82, pp. 1975–1978, Mar 1999.

[26] P. W. Anderson, "New approach to the theory of superexchange interactions," *Phys. Rev.*, vol. 115, pp. 2–13, Jul 1959.

[27] J. R. Schrieffer and P. A. Wolff, "Relation between the anderson and kondo hamiltonians," *Phys. Rev.*, vol. 149, pp. 491–492, Sep 1966.

[28] S. Trotzky, P. Cheinet, S. Fölling, M. Feld, U. Schnorrberger, A. M. Rey, A. Polkovnikov, E. Demler, M. Lukin, and I. Bloch, "Time-resolved observation and control of superexchange interactions with ultracold atoms in optical lattices," *Science*, vol. 319, no. 5861, pp. 295–299, 2008.

[29] T. Fukuhara, A. Kantian, M. Endres, M. Cheneau, P. Schauß, S. Hild, D. Bellem, U. Schollwöck, T. Giamarchi, C. Gross, *et al.*, "Quantum dynamics of a mobile spin impurity," *Nature Physics*, vol. 9, no. 4, pp. 235–241, 2013.

[30] J. F. Sherson, C. Weitenberg, M. Endres, M. Cheneau, I. Bloch, and S. Kuhr, "Single-atom-resolved fluorescence imaging of an atomic mott insulator," *Nature*, vol. 467, no. 7311, pp. 68–72, 2010.

[31] W. S. Bakr, A. Peng, M. E. Tai, R. Ma, J. Simon, J. I. Gillen, S. Flling, L. Pollet, and M. Greiner, "Probing the superfluidtomott insulator transition at the single-atom level," *Science*, vol. 329, no. 5991, pp. 547–550, 2010.

[32] C. Weitenberg, M. Endres, J. F. Sherson, M. Cheneau, P. Schauß, T. Fukuhara, I. Bloch, and S. Kuhr, "Single-spin addressing in an atomic mott insulator," *Nature*, vol. 471, no. 7338, pp. 319–324, 2011.

[33] I. Bloch, J. Dalibard, and S. Nascimbène, "Quantum simulations with ultracold quantum gases," *Nature Physics*, vol. 8, no. 4, pp. 267–276, 2012.

[34] R. P. Feynman, "Simulating physics with computers," *International journal of theoretical physics*, vol. 21, no. 6, pp. 467–488, 1982.

[35] A. Polkovnikov and V. Gritsev, "Breakdown of the adiabatic limit in low-dimensional gapless systems," *Nature Physics*, vol. 4, no. 6, pp. 477–481, 2008.

[36] A. Polkovnikov, "Universal adiabatic dynamics in the vicinity of a quantum critical point," *Phys. Rev. B*, vol. 72, p. 161201, Oct 2005.

[37] A. Polkovnikov, K. Sengupta, A. Silva, and M. Vengalattore, "Colloquium: Nonequilibrium dynamics of closed interacting quantum systems," *Rev. Mod. Phys.*, vol. 83, pp. 863–883, Aug 2011.

[38] M. Greiner, O. Mandel, T. W. Hänsch, and I. Bloch, "Collapse and revival of the matter wave field of a bose–einstein condensate," *Nature*, vol. 419, no. 6902, pp. 51–54, 2002.

[39] S. Hofferberth, I. Lesanovsky, B. Fischer, T. Schumm, and J. Schmiedmayer, "Non-equilibrium coherence dynamics in one-dimensional bose gases," *Nature*, vol. 449, no. 7160, pp. 324–327, 2007.

[40] L. Sadler, J. Higbie, S. Leslie, M. Vengalattore, and D. Stamper-Kurn, "Spontaneous symmetry breaking in a quenched ferromagnetic spinor bose–einstein condensate," *Nature*, vol. 443, no. 7109, pp. 312–315, 2006.

[41] B. Doyon and N. Andrei, "Universal aspects of nonequilibrium currents in a quantum dot," *Phys. Rev. B*, vol. 73, p. 245326, Jun 2006.

[42] C. Kollath, A. M. Läuchli, and E. Altman, "Quench dynamics and nonequilibrium phase diagram of the bose-hubbard model," *Phys. Rev. Lett.*, vol. 98, p. 180601, Apr 2007.

[43] F. Iglói and H. Rieger, "Long-range correlations in the nonequilibrium quantum relaxation of a spin chain," *Phys. Rev. Lett.*, vol. 85, pp. 3233–3236, Oct 2000.

[44] R. W. Cherng and L. S. Levitov, "Entropy and correlation functions of a driven quantum spin chain," *Phys. Rev. A*, vol. 73, p. 043614, Apr 2006.

[45] S. R. Manmana, S. Wessel, R. M. Noack, and A. Muramatsu, "Strongly correlated fermions after a quantum quench," *Phys. Rev. Lett.*, vol. 98, p. 210405, May 2007.

[46] K. Sengupta, S. Powell, and S. Sachdev, "Quench dynamics across quantum critical points," *Phys. Rev. A*, vol. 69, p. 053616, May 2004.

[47] M. Kollar and M. Eckstein, "Relaxation of a one-dimensional mott insulator after an interaction quench," *Phys. Rev. A*, vol. 78, p. 013626, Jul 2008.

[48] M. A. Cazalilla, "Effect of suddenly turning on interactions in the luttinger model," *Phys. Rev. Lett.*, vol. 97, p. 156403, Oct 2006.

[49] J. Berges, S. Borsányi, and C. Wetterich, "Prethermalization," *Phys. Rev. Lett.*, vol. 93, p. 142002, Sep 2004.

[50] E. Bettelheim, A. G. Abanov, and P. Wiegmann, "Orthogonality catastrophe and shock waves in a nonequilibrium fermi gas," *Phys. Rev. Lett.*, vol. 97, p. 246402, Dec 2006.

[51] A. A. Burkov, M. D. Lukin, and E. Demler, "Decoherence dynamics in low-dimensional cold atom interferometers," *Phys. Rev. Lett.*, vol. 98, p. 200404, May 2007.

[52] V. Gritsev, E. Demler, M. Lukin, and A. Polkovnikov, "Spectroscopy of collective excitations in interacting low-dimensional many-body systems using quench dynamics," *Phys. Rev. Lett.*, vol. 99, p. 200404, Nov 2007.

[53] A. Iucci and M. Cazalilla, "Quantum quench dynamics of some exactly solvable models in one dimension," *arXiv preprint arXiv:0903.1205*, 2009.

[54] J. Sabio and S. Kehrein, "Sudden interaction quench in the quantum sine-gordon model," *New Journal of Physics*, vol. 12, no. 5, p. 055008, 2010.

[55] P. Calabrese and J. Cardy, "Time dependence of correlation functions following a quantum quench," *Phys. Rev. Lett.*, vol. 96, p. 136801, Apr 2006.

[56] P. Calabrese and J. Cardy, "Quantum quenches in extended systems," *Journal of Statistical Mechanics: Theory and Experiment*, vol. 2007, no. 06, p. P06008, 2007.

[57] A. J. Daley, C. Kollath, U. Schollwöck, and G. Vidal, "Time-dependent density-matrix renormalization-group using adaptive effective hilbert spaces," *Journal of Statistical Mechanics: Theory and Experiment*, vol. 2004, no. 04, p. P04005, 2004.

[58] S. R. White and A. E. Feiguin, "Real-time evolution using the density matrix renormalization group," *Phys. Rev. Lett.*, vol. 93, p. 076401, Aug 2004.

[59] M. A. Cazalilla and J. B. Marston, "Time-dependent density-matrix renormalization group: A systematic method for the study of quantum many-body out-of-equilibrium systems," *Phys. Rev. Lett.*, vol. 88, p. 256403, Jun 2002.

[60] G. Vidal, "Classical simulation of infinite-size quantum lattice systems in one spatial dimension," *Phys. Rev. Lett.*, vol. 98, p. 070201, Feb 2007.

[61] B. Derrida, M. Evans, V. Hakim, and V. Pasquier, "Exact solution of a 1d asymmetric exclusion model using a matrix formulation," *Journal of Physics A: Mathematical and General*, vol. 26, no. 7, p. 1493, 1993.

[62] M. Fannes, B. Nachtergaele, and R. F. Werner, "Finitely correlated states on quantum spin chains," *Communications in Mathematical Physics*, vol. 144, no. 3, pp. 443–490, 1992.

[63] M. Eckstein, M. Kollar, and P. Werner, "Thermalization after an interaction quench in the hubbard model," *Phys. Rev. Lett.*, vol. 103, p. 056403, Jul 2009.

[64] B. Sutherland, *Beautiful models: 70 years of exactly solved quantum many-body problems.* World Scientific Publishing Company, 2004.

[65] D. Iyer and N. Andrei, "Quench dynamics of the interacting bose gas in one dimension," *Phys. Rev. Lett.*, vol. 109, p. 115304, Sep 2012.

[66] D. Iyer, H. Guan, and N. Andrei, "Exact formalism for the quench dynamics of integrable models," *Phys. Rev. A*, vol. 87, p. 053628, May 2013.

[67] J.-S. Caux and F. H. L. Essler, "Time evolution of local observables after quenching to an integrable model," *Phys. Rev. Lett.*, vol. 110, p. 257203, Jun 2013.

[68] B. Pozsgay, M. Mestyán, M. A. Werner, M. Kormos, G. Zaránd, and G. Takács, "Correlations after quantum quenches in the XXZ spin chain: Failure of the Generalized Gibbs Ensemble," *ArXiv e-prints*, May 2014.

[69] J. v. Neumann, "Beweis des ergodensatzes und desh-theorems in der neuen mechanik," *Zeitschrift für Physik*, vol. 57, no. 1-2, pp. 30–70, 1929.

[70] S. Goldstein, J. L. Lebowitz, R. Tumulka, and N. Zanghi, "Long-time behavior of macroscopic quantum systems," *The European Physical Journal H*, vol. 35, no. 2, pp. 173–200, 2010.

[71] G. Berman and F. Izrailev, "The fermi–pasta–ulam problem: fifty years of progress," *Chaos: An Interdisciplinary Journal of Nonlinear Science*, vol. 15, no. 1, p. 015104, 2005.

[72] T. Kinoshita, T. Wenger, and D. S. Weiss, "A quantum newton's cradle," *Nature*, vol. 440, no. 7086, pp. 900–903, 2006.

[73] M. Rigol, V. Dunjko, V. Yurovsky, and M. Olshanii, "Relaxation in a completely integrable many-body quantum system: An *Ab Initio* study of the dynamics of the highly excited states of 1d lattice hard-core bosons," *Phys. Rev. Lett.*, vol. 98, p. 050405, Feb 2007.

[74] M. Rigol, "Breakdown of thermalization in finite one-dimensional systems," *Phys. Rev. Lett.*, vol. 103, p. 100403, Sep 2009.

[75] J. M. Deutsch, "Quantum statistical mechanics in a closed system," *Phys. Rev. A*, vol. 43, pp. 2046–2049, Feb 1991.

[76] M. Srednicki, "Chaos and quantum thermalization," *Phys. Rev. E*, vol. 50, pp. 888–901, Aug 1994.

[77] M. Horoi, V. Zelevinsky, and B. A. Brown, "Chaos vs thermalization in the nuclear shell model," *Phys. Rev. Lett.*, vol. 74, pp. 5194–5197, Jun 1995.

[78] S. Zelditch *et al.*, "Uniform distribution of eigenfunctions on compact hyperbolic surfaces," *Duke mathematical journal*, vol. 55, no. 4, pp. 919–941, 1987.

[79] M. Rigol and L. F. Santos, "Quantum chaos and thermalization in gapped systems," *Phys. Rev. A*, vol. 82, p. 011604, Jul 2010.

[80] C. Neuenhahn and F. Marquardt, "Thermalization of interacting fermions and delocalization in fock space," *Phys. Rev. E*, vol. 85, p. 060101, Jun 2012.

[81] V. Oganesyan and D. A. Huse, "Localization of interacting fermions at high temperature," *Phys. Rev. B*, vol. 75, p. 155111, Apr 2007.

[82] D. A. Huse, R. Nandkishore, V. Oganesyan, A. Pal, and S. L. Sondhi, "Localization-protected quantum order," *Phys. Rev. B*, vol. 88, p. 014206, Jul 2013.

[83] H. A. Bethe, "Zur theorie der metalle. i. eigenwerte und eigenfunktionen der linearen atomkette," *Z. Phys.*, vol. 71, p. 205, 1931.

[84] W. Heisenberg, "Zur theorie des ferromagnetismus," *Zeitschrift für Physik*, vol. 49, no. 9-10, pp. 619–636, 1928.

[85] E. H. Lieb and W. Liniger, "Exact analysis of an interacting bose gas. i. the general solution and the ground state," *Phys. Rev.*, vol. 130, pp. 1605–1616, May 1963.

[86] N. Andrei, K. Furuya, and J. H. Lowenstein, "Solution of the kondo problem," *Rev. Mod. Phys.*, vol. 55, pp. 331–402, Apr 1983.

[87] A. Tsvelick and P. Wiegmann, "Exact results in the theory of magnetic alloys," *Advances in Physics*, vol. 32, no. 4, pp. 453–713, 1983.

[88] H. B. Thacker, "Exact integrability in quantum field theory and statistical systems," *Rev. Mod. Phys.*, vol. 53, pp. 253–285, Apr 1981.

[89] E. H. Lieb and F. Y. Wu, "Absence of mott transition in an exact solution of the short-range, one-band model in one dimension," *Phys. Rev. Lett.*, vol. 20, pp. 1445–1448, Jun 1968.

[90] R. J. Baxter, *Exactly solved models in statistical mechanics*. Courier Dover Publications, 2007.

[91] C. N. Yang and C. P. Yang, "One-dimensional chain of anisotropic spin-spin interactions. i. proof of bethe's hypothesis for ground state in a finite system," *Phys. Rev.*, vol. 150, pp. 321–327, Oct 1966.

[92] C. N. Yang, "Some exact results for the many-body problem in one dimension with repulsive delta-function interaction," *Phys. Rev. Lett.*, vol. 19, pp. 1312–1315, Dec 1967.

[93] C. N. Yang, "s," *Phys. Rev.*, vol. 168, pp. 1920–1923, Apr 1968.

[94] C.-N. Yang and C. Yang, "Thermodynamics of a one-dimensional system of bosons with repulsive delta-function interaction," *Journal of Mathematical Physics*, vol. 10, no. 7, pp. 1115–1122, 1969.

[95] M. Takahashi, *Thermodynamics of one-dimensional solvable models*. Cambridge University Press, 2005.

[96] E. K. Sklyanin, L. A. Takhtadzhyan, and L. D. Faddeev, "Quantum inverse problem method. i," *Theoretical and Mathematical Physics*, vol. 40, no. 2, pp. 688–706, 1979.

[97] L. D. Faddeev and L. A. Takhtajan, *Hamiltonian methods in the theory of solitons*. Springer, 2007.

[98] V. E. Korepin, *Quantum inverse scattering method and correlation functions*. Cambridge university press, 1997.

[99] E. T. Jaynes, "Information theory and statistical mechanics," *Phys. Rev.*, vol. 106, pp. 620–630, May 1957.

[100] M. Cramer, C. M. Dawson, J. Eisert, and T. J. Osborne, "Exact relaxation in a class of nonequilibrium quantum lattice systems," *Phys. Rev. Lett.*, vol. 100, p. 030602, Jan 2008.

[101] D. Fioretto and G. Mussardo, "Quantum quenches in integrable field theories," *New Journal of Physics*, vol. 12, no. 5, p. 055015, 2010.

[102] A. C. Cassidy, C. W. Clark, and M. Rigol, "Generalized thermalization in an integrable lattice system," *Phys. Rev. Lett.*, vol. 106, p. 140405, Apr 2011.

[103] T. Barthel and U. Schollwöck, "Dephasing and the steady state in quantum many-particle systems," *Phys. Rev. Lett.*, vol. 100, p. 100601, Mar 2008.

[104] M. A. Cazalilla, A. Iucci, and M.-C. Chung, "Thermalization and quantum correlations in exactly solvable models," *Phys. Rev. E*, vol. 85, p. 011133, Jan 2012.

[105] P. Calabrese, F. H. Essler, and M. Fagotti, "Quantum quench in the transverse field ising chain: I. time evolution of order parameter correlators," *Journal of Statistical Mechanics: Theory and Experiment*, vol. 2012, no. 07, p. P07016, 2012.

[106] P. Calabrese, F. H. Essler, and M. Fagotti, "Quantum quenches in the transverse field ising chain: Ii. stationary state properties," *Journal of Statistical Mechanics: Theory and Experiment*, vol. 2012, no. 07, p. P07022, 2012.

[107] B. Wouters, M. Brockmann, J. De Nardis, D. Fioretto, M. Rigol, and J.-S. Caux, "Quenching the Anisotropic Heisenberg Chain: Exact Solution and Generalized Gibbs Ensemble," *ArXiv e-prints*, May 2014.

[108] G. Goldstein and N. Andrei, "Failure of the GGE hypothesis for integrable models with bound states," *ArXiv e-prints*, May 2014.

[109] B. Pozsgay, "Failure of the generalized eigenstate thermalization hypothesis in integrable models with multiple particle species," *arXiv preprint arXiv:1406.4613*, 2014.

[110] G. Roux, "Quenches in quantum many-body systems: One-dimensional bose-hubbard model reexamined," *Phys. Rev. A*, vol. 79, p. 021608, Feb 2009.

[111] C. Gogolin, M. P. Müller, and J. Eisert, "Absence of thermalization in nonintegrable systems," *Phys. Rev. Lett.*, vol. 106, p. 040401, Jan 2011.

[112] D. Rossini, A. Silva, G. Mussardo, and G. E. Santoro, "Effective thermal dynamics following a quantum quench in a spin chain," *Phys. Rev. Lett.*, vol. 102, p. 127204, Mar 2009.

[113] M. Moeckel and S. Kehrein, "Interaction quench in the hubbard model," *Phys. Rev. Lett.*, vol. 100, p. 175702, May 2008.

[114] T. Giamarchi, *Quantum Physics in One Dimension*. International Series of Monographs on Physics, Clarendon Press, 2004.

[115] M. Ganahl, E. Rabel, F. H. L. Essler, and H. G. Evertz, "Observation of complex bound states in the spin-1/2 heisenberg xxz chain using local quantum quenches," *Phys. Rev. Lett.*, vol. 108, p. 077206, Feb 2012.

[116] B. Pozsgay, "The dynamical free energy and the loschmidt echo for a class of quantum quenches in the heisenberg spin chain," *Journal of Statistical Mechanics: Theory and Experiment*, vol. 2013, no. 10, p. P10028, 2013.

[117] M. Fagotti and F. H. Essler, "Stationary behaviour of observables after a quantum quench in the spin-1/2 heisenberg xxz chain," *Journal of Statistical Mechanics: Theory and Experiment*, vol. 2013, no. 07, p. P07012, 2013.

[118] M. Fagotti, "Dynamical phase transitions as properties of the stationary state: Analytic results after quantum quenches in the spin-1/2 xxz chain," *arXiv preprint arXiv:1308.0277*, 2013.

[119] B. Pozsgay, "The generalized gibbs ensemble for heisenberg spin chains," *Journal of Statistical Mechanics: Theory and Experiment*, vol. 2013, no. 07, p. P07003, 2013.

[120] V. Yudson, "Dynamics of the integrable one-dimensional system photons+ two-level atoms," *Physics Letters A*, vol. 129, no. 1, pp. 17–20, 1988.

[121] U. Schneider, L. Hackermüller, J. P. Ronzheimer, S. Will, S. Braun, T. Best, I. Bloch, E. Demler, S. Mandt, D. Rasch, *et al.*, "Fermionic transport and out-of-equilibrium dynamics in a homogeneous hubbard model with ultracold atoms," *Nature Physics*, vol. 8, no. 3, pp. 213–218, 2012.

[122] E. Lieb and D. Robinson, "The finite group velocity of quantum spin systems," *Communications in Mathematical Physics*, vol. 28, no. 3, pp. 251–257, 1972.

[123] G. Goldstein and N. Andrei, "Equilibration and generalized GGE in the Lieb-Liniger gas," *arXiv preprint arXiv:1309.3471*, 2013.

[124] "http://reference.wolfram.com/mathematica/tutorial/nintegrateoverview.html."

[125] "http://www.feynarts.de/cuba/."

[126] T. Hahn, "Cubaa library for multidimensional numerical integration," *Computer Physics Communications*, vol. 168, no. 2, pp. 78 – 95, 2005.

[127] N. Bleistein and R. A. Handerlsman, *Asymptotic Expansions of Integrals*. Holt, Rinehart and Winston, 1975.

[128] N. Kitanine, J. Maillet, and V. Terras, "Correlation functions of the xxz heisenberg spin-12 chain in a magnetic field," *Nuclear Physics B*, vol. 567, no. 3, pp. 554–582, 2000.

[129] J. Mossel and J.-S. Caux, "Generalized tba and generalized gibbs," *Journal of Physics A: Mathematical and Theoretical*, vol. 45, no. 25, p. 255001, 2012.

Appendix A
Derivation of S-matrix

The exact form of the S-matrix (3.10) is critical for the proof of the contour representation, but it depends on the convention of writing eigenstate. Further more, the detailed derivation is usually absent in books and references, causing a lot of confusion. So here I derive the S-matrix explicitly in this appendix. Without loss of generality, I choose $J = \frac{1}{2}$ in this derivation.

I do it under Sutherland's convention [64], since it simplifies the summation. Suppose the length of the chain is L. I consider the $L+1$th site to be equivalent to the first site. In later calculation, I'll do many change of variables like $m_1 \to m_1 + 1$, where I use $\sum_{m_1}$ to denote "summing over all possible m_1", without caring too much about the boundary at $m_1 = 1, L$. However, we do need to concern the boundary between m_1 and m_2: I use $\sum_{m_2=m_1+1}$ to denote summing over m_2 from $m_2 = m_1 + 1$ and up. With these notations, the two-particle Bethe Ansatz state is

$$\begin{aligned}
|k_1, k_2\rangle &= \sum_{m_1} \sum_{m_2=m_1+1} [s e^{ik_1 m_1 + ik_2 m_2} + e^{ik_1 m_2 + ik_2 m_1}] \sigma^-_{m_1} \sigma^-_{m_2} |\Uparrow\rangle \\
&= \sum_{m_1} \sum_{m_2=m_1+2} [s e^{ik_1 m_1 + ik_2 m_2} + e^{ik_1 m_2 + ik_2 m_1}] \sigma^-_{m_1} \sigma^-_{m_2} |\Uparrow\rangle \\
&+ \sum_{m_1} [s e^{ik_1 m_1 + ik_2 m_1 + ik_2} + e^{ik_1 m_1 + ik_2 m_1 + ik_1}] \sigma^-_{m_1} \sigma^-_{m_1+1} |\Uparrow\rangle
\end{aligned} \tag{A.1}$$

I separate some terms that behaves differently under operation by the Hamiltonian. We are looking for the s here, from the Schrodinger's equation $H|k_1, k_2\rangle = E|k_1, k_2\rangle$. From the single particle eigen energy, we know $E = 2(\Delta - \cos k_1) + 2(\Delta - \cos k_2)$. Applying Hamiltonian on the state, we have

$$\begin{aligned}
H|k_1, k_2\rangle = &-\frac{1}{2} \sum_{m_1} \sum_{m_2=m_1+2} [s e^{ik_1 m_1 + ik_2 m_2} + e^{ik_1 m_2 + ik_2 m_1}] \\
&\times [2(\sigma^-_{m_1-1}\sigma^-_{m_2} + \sigma^-_{m_1+1}\sigma^-_{m_2} + \sigma^-_{m_1}\sigma^-_{m_2-1} + \sigma^-_{m_1}\sigma^-_{m_2+1}) - 8\Delta\sigma^-_{m_1}\sigma^-_{m_2}] |\Uparrow\rangle \\
&- \frac{1}{2} \sum_{m_1} (s e^{ik_2} + e^{ik_1}) e^{i(k_1+k_2)m_1} [2(\sigma^-_{m_1-1}\sigma^-_{m_1+1} + \sigma^-_{m_1}\sigma^-_{m_1+2}) - 4\Delta\sigma^-_{m_1}\sigma^-_{m_1+1}] |\Uparrow\rangle
\end{aligned} \tag{A.2}$$

Then we change varables to make every term multiply by $\sigma^-_{m_1}\sigma^-_{m_2}|\Uparrow\rangle$:

$$
\begin{aligned}
H|k_1,k_2\rangle = 4\Delta \sum_{m_1}\sum_{m_2=m_1+2}&[se^{ik_1m_1+ik_2m_2}+e^{ik_1m_2+ik_2m_1}]\sigma^-_{m_1}\sigma^-_{m_2}|\Uparrow\rangle\\
-\sum_{m_1}\sum_{m_2=m_1+3}&[se^{ik_1m_1+ik_2m_2}e^{ik_1}+e^{ik_1m_2+ik_2m_1}e^{ik_2}]\sigma^-_{m_1}\sigma^-_{m_2}|\Uparrow\rangle\\
-\sum_{m_1}\sum_{m_2=m_1+1}&[se^{ik_1m_1+ik_2m_2}e^{-ik_1}+e^{ik_1m_2+ik_2m_1}e^{-ik_2}]\sigma^-_{m_1}\sigma^-_{m_2}|\Uparrow\rangle\\
-\sum_{m_1}\sum_{m_2=m_1+1}&[se^{ik_1m_1+ik_2m_2}e^{ik_2}+e^{ik_1m_2+ik_2m_1}e^{ik_1}]\sigma^-_{m_1}\sigma^-_{m_2}|\Uparrow\rangle\\
-\sum_{m_1}\sum_{m_2=m_1+3}&[se^{ik_1m_1+ik_2m_2}e^{-ik_2}+e^{ik_1m_2+ik_2m_1}e^{-ik_1}]\sigma^-_{m_1}\sigma^-_{m_2}|\Uparrow\rangle\\
+2\Delta\sum_{m_1}&(se^{ik_2}+e^{ik_1})e^{i(k_1+k_2)m_1}\sigma^-_{m_1}\sigma^-_{m_1+1}]|\Uparrow\rangle\\
-\sum_{m_1}&(se^{2ik_2+ik_1}+e^{2ik_1+ik_2})e^{i(k_1+k_2)m_1}\sigma^-_{m_1}\sigma^-_{m_1+2}]|\Uparrow\rangle\\
-\sum_{m_1}&(se^{ik_2}+e^{ik_1})e^{i(k_1+k_2)m_1}\sigma^-_{m_1}\sigma^-_{m_1+2}]|\Uparrow\rangle
\end{aligned}
\tag{A.3}
$$

Notice we have changed the range over which m_2 is summed correspondingly. Next, we want to

unify the range of summation, and then make up the terms when we overcounted or undercounted:

$$
\begin{aligned}
H|k_1,k_2\rangle = 4\Delta &\sum_{m_1}\sum_{m_2=m_1+2}[se^{ik_1m_1+ik_2m_2}+e^{ik_1m_2+ik_2m_1}]\sigma^-_{m_1}\sigma^-_{m_2}|\Uparrow\rangle\\
&-\sum_{m_1}\sum_{m_2=m_1+2}[se^{ik_1m_1+ik_2m_2}e^{ik_1}+e^{ik_1m_2+ik_2m_1}e^{ik_2}]\sigma^-_{m_1}\sigma^-_{m_2}|\Uparrow\rangle\\
&+\sum_{m_1}[se^{ik_1m_1+ik_2m_2}e^{ik_1+2ik_2}+e^{ik_1m_2+ik_2m_1}e^{2ik_1+ik_2}]\sigma^-_{m_1}\sigma^-_{m_1+2}|\Uparrow\rangle\\
&-\sum_{m_1}\sum_{m_2=m_1+2}[se^{ik_1m_1+ik_2m_2}e^{-ik_1}+e^{ik_1m_2+ik_2m_1}e^{-ik_2}]\sigma^-_{m_1}\sigma^-_{m_2}|\Uparrow\rangle\\
&-\sum_{m_1}[se^{ik_1m_1+ik_2m_2}e^{ik_2-ik_1}+e^{ik_1m_2+ik_2m_1}e^{ik_1-ik_2}]\sigma^-_{m_1}\sigma^-_{m_1+1}|\Uparrow\rangle\\
&-\sum_{m_1}\sum_{m_2=m_1+2}[se^{ik_1m_1+ik_2m_2}e^{ik_2}+e^{ik_1m_2+ik_2m_1}e^{ik_1}]\sigma^-_{m_1}\sigma^-_{m_2}|\Uparrow\rangle\\
&-\sum_{m_1}[se^{ik_1m_1+ik_2m_2}e^{2ik_2}+e^{ik_1m_2+ik_2m_1}e^{2ik_1}]\sigma^-_{m_1}\sigma^-_{m_1+1}|\Uparrow\rangle\\
&-\sum_{m_1}\sum_{m_2=m_1+2}[se^{ik_1m_1+ik_2m_2}e^{-ik_2}+e^{ik_1m_2+ik_2m_1}e^{-ik_1}]\sigma^-_{m_1}\sigma^-_{m_2}|\Uparrow\rangle\\
&+\sum_{m_1}[se^{ik_1m_1+ik_2m_2}e^{ik_2}+e^{ik_1m_2+ik_2m_1}e^{ik_1}]\sigma^-_{m_1}\sigma^-_{m_1+2}|\Uparrow\rangle\\
&+2\Delta\sum_{m_1}(se^{ik_2}+e^{ik_1})e^{i(k_1+k_2)m_1}\sigma^-_{m_1}\sigma^-_{m_1+1}]|\Uparrow\rangle\\
&-\sum_{m_1}(se^{2ik_2+ik_1}+e^{2ik_1+ik_2})e^{i(k_1+k_2)m_1}\sigma^-_{m_1}\sigma^-_{m_1+2}]|\Uparrow\rangle\\
&-\sum_{m_1}(se^{ik_2}+e^{ik_1})e^{i(k_1+k_2)m_1}\sigma^-_{m_1}\sigma^-_{m_1+2}]|\Uparrow\rangle
\end{aligned}
\tag{A.4}
$$

Then we combine the terms of the same category. It turns out the terms with $\sigma^-_{m_1}\sigma^-_{m_1+2}|\Uparrow\rangle$ cancel out. We get

$$
\begin{aligned}
H|k_1,k_2\rangle = (4\Delta-2\cos k_1-2\cos k_2)&\sum_{m_1}\sum_{m_2=m_1+2}[se^{ik_1m_1+ik_2m_2}+e^{ik_1m_2+ik_2m_1}]\sigma^-_{m_1}\sigma^-_{m_2}|\Uparrow\rangle\\
&+\sum_{m_1}[se^{ik_2}(2\Delta-e^{ik_2}-e^{-ik_1})+e^{ik_1}(2\Delta-e^{ik_1}-e^{-ik_2})]e^{i(k_1+k_2)m_1}\sigma^-_{m_1}\sigma^-_{m_1+1}]|\Uparrow\rangle
\end{aligned}
\tag{A.5}
$$

We know from Schrodinger's equation

$$
\begin{aligned}
H|k_1,k_2\rangle &= E|k_1,k_2\rangle\\
&= (4\Delta-2\cos k_1-2\cos k_2)\sum_{m_1}\sum_{m_2=m_1+1}[se^{ik_1m_1+ik_2m_2}+e^{ik_1m_2+ik_2m_1}]\sigma^-_{m_1}\sigma^-_{m_2}|\Uparrow\rangle
\end{aligned}
\tag{A.6}
$$

Make them equal, we get

$$
(4\Delta-2\cos k_1-2\cos k_2)(se^{ik_2}+e^{ik_1}) = se^{ik_2}(2\Delta-e^{ik_2}-e^{-ik_1})+e^{ik_1}(2\Delta-e^{ik_1}-e^{-ik_2}) \tag{A.7}
$$

Finally, we get the S-matrix

$$s(k_1, k_2) = -\frac{1 + e^{ik_1+ik_2} - 2\Delta e^{ik_1}}{1 + e^{ik_1+ik_2} - 2\Delta e^{ik_2}} \tag{A.8}$$

Appendix B
Uniform Asymptotic Expansion

In Chapter 6, the asymptotic expansions we obtained for (6.1)

$$I(\beta,t)=\int_{-\pi/2}^{3\pi/2}\frac{dz}{2\pi}e^{tw(z;\beta)}s(z) \tag{B.1}$$

diverge as $\beta\to 1$. Here we use the notation $w(z;\beta)\equiv i\cos z+i\beta z$ to emphasize β is the special parameter that causes problem at certain values. In this appendix, we introduce the uniform asymptotic expansion, the technique that gives well-defined expansion of (B.1) for any value of β.

The basic idea of uniform asymptotic expansion is to find a conformal transformation mapping the exponent function $w(z;\beta)$ to some other function with the same saddle point structure, which we know how to deal with. Our problem comes from the phenomenon that as $\beta\to 1$ (from either side), two first order saddle points $z_\pm$ of $w(z;\beta)$ collapse into one second order saddle point z_o. A simple function that has the same pole structure is

$$\phi(x;\gamma,\rho)=-(\frac{x^3}{3}-\gamma^2x)+\rho \tag{B.2}$$

which has two first order saddle points $x_\pm=\pm\gamma$, but they collapse into one second order saddle point $x_o=0$ when $\gamma\to 0$. We want to establish a conformal mapping

$$w(z;\beta)=\phi(x;\gamma,\rho) \tag{B.3}$$

and choose the parameters γ and ρ in a way that the saddle points of these two functions always have a one-to-one correspondence. With this mapping, the integral (B.1) can be written as

$$I(\beta,t)=\int_D\frac{dz}{dx}s(z(x))e^{t[-(\frac{x^3}{3}-\gamma^2x)+\rho]}\frac{dx}{2\pi} \tag{B.4}$$

where the integral contour D is the image of the integral contour of z in (B.1). We want to write the leading order of the integral (B.4) in terms of the Airy function of the first kind, which has the integral representation

$$\mathrm{Ai}(x)=\frac{1}{2\pi}\int_{\gamma_1}e^{zx-z^3/3}dz \tag{B.5}$$

where the contour γ_1 is shown in Fig. B.1. For this to work: (1) the integral contours D and γ_1 should be asymptotic equivalent –they should come from and go to the same "valleys", and can

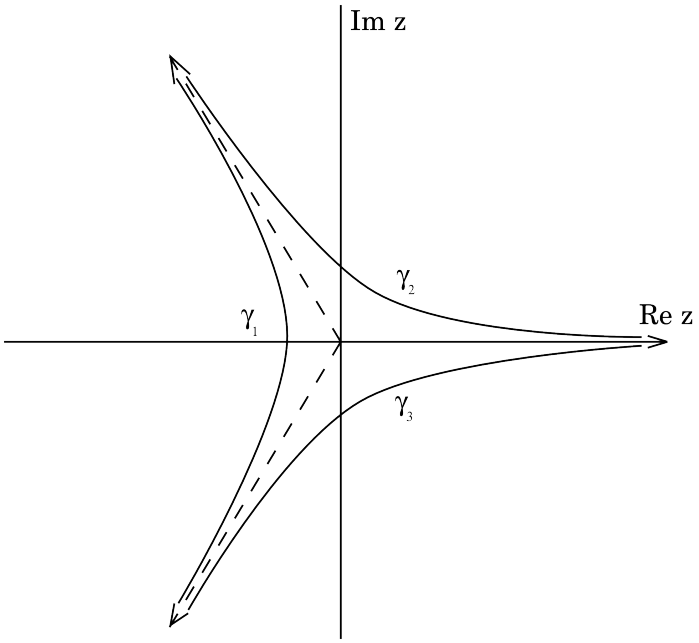

Figure B.1: Contours for integral representation of Airy functions.

be deformed into each other without getting over any poles. It can be achieved by choosing the proper square roots of some parameters, as explained later. (2) We need to properly deal with the non-exponential-function part of the integrand in (B.4).

Now let's be specific. First we need to find the parameters γ and ρ. Let the saddle points $z_\pm$ correspond to $x_\pm = \pm\gamma$ respectively. Then from (B.3), we get

$$\rho = \frac{1}{2}[w(z_+;\beta) + w(z_-;\beta)] \tag{B.6}$$

$$\frac{4\gamma^3}{3} = w(z_+;\beta) - w(z_-;\beta) \tag{B.7}$$

Note that ρ can be uniquely identified as a function of β. But due to the ambiguity of the cube root, the value of γ need to be determined by the structure of the contour. Generally we want to choose the proper argument (phase) of γ so that some part of the integral contour in (B.1) is mapped to γ_1 in (B.5). The detail will vary from case to case, as we will discuss later. Secondly, from the intuition of the saddle point approximation, we deduce that only the values of $\frac{dz}{dx}s(z(x))$ at the saddle points $x_\pm = \pm\gamma$ are important. More rigorously, let's write this term in the following way

$$G(x) \equiv \frac{1}{2\pi}\frac{dz}{dx}s(z(x)) = a_0 + a_1 x + (x^2 - \gamma^2)H(x) \tag{B.8}$$

The constant term just gives the Airy function, and the linear term can be easily written in terms of the derivative of the Airy function. More importantly, the last term is 0 at the two saddle points $x_\pm = \pm\gamma$. As long as the function $H(x)$ doesn't diverge at $x_\pm$, the contribution of the last term to

the asymptotic expansion is diminished. We will show it is indeed the case. The parameters a_0 and a_1 can be found by

$$a_0 = \frac{G(\gamma) + G(-\gamma)}{2} \tag{B.9}$$

$$a_1 = \frac{G(\gamma) - G(-\gamma)}{2\gamma} \tag{B.10}$$

To get $G(\pm\gamma)$, we need to find $\frac{dz}{dx}|_{z=z_\pm}$. By differentiating (B.3), we get

$$\frac{dz}{dx} = \frac{\gamma^2 - x^2}{\partial_z w(z;\beta)} \tag{B.11}$$

Its value at the saddle points can be obtained by L'Hospital's rule

$$\left(\frac{dz}{dx}\right)^2\Bigg|_{\substack{x=\pm\gamma \\ z=z_\pm}} = \frac{\mp 2\gamma}{\partial_{zz} w(z_\pm;\beta)} \tag{B.12}$$

Again, when taking the square root, the phase will be determined through the mapping of the contours. With a_0 and a_1 determined as above,

$$H(x) = \frac{G(x) - a_0 - a_1 x}{x^2 - \gamma^2} \tag{B.13}$$

It has removable singularity at the saddle points $\pm\gamma$, since by L'Hospital's rule

$$\lim_{x\to\pm\gamma} H(x) = \pm\frac{G'(\pm\gamma) - G'(0)}{2\gamma} \tag{B.14}$$

So the contribution of the last term in (B.8) to the asymptotic expansion is negligible. Ignoring this term, we get the asymptotic expansion of (B.1) up to the leading order

$$\begin{aligned} I(\beta,t) \approx & e^{\rho t}\int_{\gamma_1} \exp[-t(\frac{x^3}{3} - \gamma^2 x)](a_0 + a_1 x)dx \\ = & 2\pi i e^{\rho t}\left[\frac{a_0}{t^{1/3}}\mathrm{Ai}(t^{2/3}\gamma^2) + \frac{a_1}{t^{2/3}}\mathrm{Ai}'(t^{2/3}\gamma^2)\right] \end{aligned} \tag{B.15}$$

Note that the term $s(z_\pm)$ contributes through a_0 and a_1.

An important feature of this method is that all the quantities defined or calculated above have a well-defined limit as $\gamma \to 0$ ($\beta \to 1$). For example, $a_1 \to G'(0)$. This is a good limit because $z(x)$ is a conformal transformation and $s(z)$ is assumed to be regular, thus $G(x) \equiv \frac{dz}{dx}s(z(x))$ is a regular function. As another example, to get the $\lim_{\gamma\to 0}\frac{dz}{dx}|_{x=\pm\gamma}$, we can apply L'Hospital's rule twice to (B.11) and obtain

$$\left(\frac{dz}{dx}\right)^3\Bigg|_{\substack{x=0 \\ z=z_+=z_-}} = \frac{-2}{\partial_{zzz} w(z_+;\beta)} \tag{B.16}$$

Note that when $z_+ = z_-$, the saddle point is second order: $\partial_{zz} w(z_+;\beta) = 0$, but $\partial_{zzz} w(z_+;\beta) \neq 0$, so the right hand side of the equation above is still finite. In one word, the uniform asymptotic

expansion removes the diverging behavior when the two saddle points collapse as $\beta \to 1$. The decay by different powers of t is partly absorbed into the special function Ai(x), as shown in (B.15).

Next let's discuss the mapping of the integral contours. It turns out that the integral contour in (B.1) cannot be mapped directly to the γ_1 in (B.5). We need to replace it with some combination of other contours, just like what we did in Chapter 6. In particular, for both of the cases $0 < \beta < 1$ and $\beta > 1$, the contour can be divided into two parts C_1 and C_2, defined as

$$C_1 \cong \begin{cases} -D_1 + D_2 & 0 < \beta < 1 \text{ (Fig. 6.1)} \\ -D_1 - D_2 + D_3 & \beta > 1 \text{ (Fig. 6.2)} \end{cases} \tag{B.17}$$

$$C_2 \cong \begin{cases} -D_3 + D_4 & 0 < \beta < 1 \text{ (Fig. 6.1)} \\ -D_3 + D_2 + D_4 & \beta > 1 \text{ (Fig. 6.2)} \end{cases} \tag{B.18}$$

Here the symbol $\cong$ means "asymptotically equivalent to". Note that the D-paths have different definitions for the two cases (see Fig. 6.1 and Fig. 6.2 for details). With this definition, it can be proved that each of C_1 or C_2 can be mapped to γ_1 by a proper choice of the phase of the parameter γ. (This proof is quite involved. One can check Ref. [127] for details.) Let's consider $0 < \beta < 1$ as an example. In this case, from (B.7) we get

$$\gamma^3 = \frac{3i}{2}(\sqrt{1-\beta^2} - \beta \cos^{-1}\beta) \tag{B.19}$$

So there are three possible choices of $\arg(\gamma)$: $\frac{\pi}{6}$, $\frac{5\pi}{6}$ and $-\frac{\pi}{2}$. Let's first map C_1 to γ_1. The second order saddle points on the x-plane and z-plane are $x_o = 0$ and $z_o = \pi/2$, respectively. Let's define $\Delta x = x - x_o$ and $\Delta z = z - z_o$ to be the relative vectors of the contour γ_1 and C_1 with respect to the second order saddle points. As a conformal mapping, when Δz and Δx are small, we have the approximation

$$\Delta z = \frac{dz}{dx}|_{x=x_o} \Delta x \tag{B.20}$$

Making use of (B.11), we get

$$\frac{\Delta z}{\Delta x} = \frac{\gamma^2}{\partial_z w(z_o;\beta)} \tag{B.21}$$

$$\arg(\Delta z) - \arg(\Delta x) = 2\arg(\gamma) - \arg(w(\pi/2;\beta)) \tag{B.22}$$

From Fig. B.5 we see $2\pi/3 < \arg(\Delta x) < 4\pi/3$. When $\Delta z \to 0$, $\arg(\Delta z) = \pi$. It is easy to get $\arg(w(\pi/2;\beta)) = \pi/2$. Making use of these fact, we have

$$-\frac{5\pi}{12} < \arg(\gamma) < -\frac{\pi}{12}, \quad \mod \pi \tag{B.23}$$

So among the three possible phases, $\arg(\gamma) = 5\pi/6$ is the one to give the correct conformal mapping, namely

$$\gamma = e^{5i\pi/6}[\frac{3}{2}(\sqrt{1-\beta^2} - \beta\cos^{-1}\beta)]^{1/3} \tag{B.24}$$

Similarly, if we want to map C_2 to γ_1, the only difference would be $\arg(\Delta z) = 0$, which leads to $\arg(\gamma) = \pi/6$. Generally, by carefully investigating the mapping of contours, all the ambiguous phases of roots can be uniquely determined.

Now let's list the results calculated by the methods above. Note that for different regions of β, the saddle points are different

$$\begin{aligned} z_+ &= \begin{cases} \sin^{-1}\beta, & 0 < \beta < 1 \\ \frac{\pi}{2} + i\cosh^{-1}\beta, & \beta > 1 \end{cases} \\ z_- &= \begin{cases} \pi - \sin^{-1}\beta, & 0 < \beta < 1 \\ \frac{\pi}{2} - i\cosh^{-1}\beta, & \beta > 1 \end{cases} \end{aligned} \tag{B.25}$$

For different contours C_1/C_2, the phases of parameters will be different due to the ambiguous roots. We will denote the integrals of (B.1) over the contour C_1/C_2 as I_1/I_2, and list them separately.

- For the integral over contour C_1,

$$\rho = \frac{i\pi\beta}{2} \tag{B.26}$$

$$\frac{dz}{dx}|_{x=\pm\gamma} = e^{i\pi/6}\frac{\sqrt{2|\gamma|}}{|1-\beta^2|^{1/4}} \tag{B.27}$$

$$\gamma = \begin{cases} e^{5i\pi/6}[\frac{3}{2}(\sqrt{1-\beta^2} - \beta\cos^{-1}\beta)]^{1/3}, & 0 < \beta < 1 \\ e^{i\pi/3}[\frac{3}{2}(\beta\cosh^{-1}\beta - \sqrt{\beta^2-1})]^{1/3}, & \beta > 1 \end{cases} \tag{B.28}$$

$$a_0 = -\frac{s(z_+) + s(z_-)}{2}\frac{e^{i\pi/6}}{2\pi}\frac{\sqrt{2|\gamma|}}{|\beta^2-1|^{1/4}} \tag{B.29}$$

$$a_1 = -\frac{s(z_+) - s(z_-)}{2\gamma}\frac{e^{i\pi/6}}{2\pi}\frac{\sqrt{2|\gamma|}}{|\beta^2-1|^{1/4}} \tag{B.30}$$

$$I_1 = -i^{m+1}\frac{e^{i\pi/6}\sqrt{2|\gamma|}}{|\beta^2-1|^{1/4}}\left[\frac{\mathrm{Ai}(t^{2/3}\gamma^2)}{t^{1/3}}\frac{s(z_+)+s(z_-)}{2} + \frac{\mathrm{Ai}'(t^{2/3}\gamma^2)}{t^{2/3}}\frac{s(z_+)-s(z_-)}{2\gamma}\right] \tag{B.31}$$

- For the integral over contour C_2,

$$\rho = \frac{i\pi\beta}{2} \tag{B.32}$$

$$\frac{dz}{dx}|_{x=\pm\gamma} = -e^{5i\pi/6}\frac{\sqrt{2|\gamma|}}{|1-\beta^2|^{1/4}} \tag{B.33}$$

$$\gamma = \begin{cases} e^{i\pi/6}[\frac{3}{2}(\sqrt{1-\beta^2} - \beta\cos^{-1}\beta)]^{1/3}, & 0<\beta<1 \\ e^{-i\pi/3}[\frac{3}{2}(\beta\cosh^{-1}\beta - \sqrt{\beta^2-1})]^{1/3}, & \beta>1 \end{cases} \tag{B.34}$$

$$a_0 = -\frac{s(z_+)+s(z_-)}{2}\frac{e^{5i\pi/6}}{2\pi}\frac{\sqrt{2|\gamma|}}{|\beta^2-1|^{1/4}} \tag{B.35}$$

$$a_1 = -\frac{s(z_+)-s(z_-)}{2\gamma}\frac{e^{5i\pi/6}}{2\pi}\frac{\sqrt{2|\gamma|}}{|\beta^2-1|^{1/4}} \tag{B.36}$$

$$I_2 = -i^{m+1}\frac{e^{5i\pi/6}\sqrt{2|\gamma|}}{|\beta^2-1|^{1/4}}\left[\frac{\mathrm{Ai}(t^{2/3}\gamma^2}{t^{1/3}}\frac{s(z_+)+s(z_-)}{2} + \frac{\mathrm{Ai}'(t^{2/3}\gamma^2)}{t^{2/3}}\frac{s(z_+)-s(z_-)}{2\gamma}\right] \tag{B.37}$$

Remember what we are looking for finally is $I(\beta,t) = I_1 + I_2$. And we hope to write it in the form

$$I(\beta,t) = I_+(\beta,t)s(z_+) + I_-(\beta,t)s(z_-). \tag{B.38}$$

Namely, we want to separate the contributions of the two saddle points, because this form is easy to be generalized to multi-dimensional integrals. For example, the two dimensional integral can be approximated by

$$\begin{aligned} I(\beta_1,\beta_2,t) =& \int_{-\pi/2}^{3\pi/2}\frac{dz_1}{2\pi}\frac{dz_2}{2\pi}e^{it(\beta_1 z_1+\cos z_1+\beta_2 z_2+\cos z_2)}s(z_1,z_2) \\ =& I_+(z_+(\beta_1))I_+(z_+(\beta_2))s(z_+(\beta_1),z_+(\beta_2)) + I_-(z_-(\beta_1))I_+(z_+(\beta_2))s(z_-(\beta_1),z_+(\beta_2)) \\ &+ I_+(z_+(\beta_1))I_-(z_-(\beta_2))s(z_+(\beta_1),z_-(\beta_2)) + I_-(z_-(\beta_1))I_-(z_-(\beta_2))s(z_-(\beta_1),z_-(\beta_2)) \\ =& \sum_{\delta_1=\pm,\delta_2=\pm} I_{\delta_1}I_{\delta_2}s(z_{\delta_1}(\beta_1),z_{\delta_2}(\beta_2)) \end{aligned} \tag{B.39}$$

To get (B.38) is straightforward: one needs to sum up (B.31) and (B.37), then separate the terms with $s(z_+)$ and $s(z_-)$. The only thing one needs to pay attention is that γ takes different values for both different regions of β, and different contours C_1/C_2. So it is more convenient to define γ to be its absolute value

$$\gamma = \begin{cases} [\frac{3}{2}(\sqrt{1-\beta^2} - \beta\cos^{-1}\beta)]^{1/3}, & 0<\beta<1 \\ [\frac{3}{2}(\beta\cosh^{-1}\beta - \sqrt{\beta^2-1})]^{1/3}, & \beta>1 \end{cases} \tag{B.40}$$

and manually manipulate all the phases. Finally, with the γ defined above, we obtain

$$\begin{aligned} I_{\pm}(0<\beta<1,t) =& -i^{m+1}\frac{\sqrt{2\gamma}}{|1-\beta^2|^{1/4}}\{\frac{1}{2t^{1/3}}\left[e^{i\pi/6}\mathrm{Ai}(e^{-i\pi/3}\gamma^2t^{2/3})+e^{5i\pi/6}\mathrm{Ai}(e^{i\pi/3}\gamma^2t^{2/3})\right] \\ &\pm\frac{1}{2\gamma t^{2/3}}\left[e^{-2\pi/3}\mathrm{Ai}'(e^{-i\pi/3}\gamma^2t^{2/3})+e^{2i\pi/3}\mathrm{Ai}'(e^{i\pi/3}\gamma^2t^{2/3})\right]\} \\ I_{\pm}(\beta>1,t) =& -i^{m+1}\frac{\sqrt{2\gamma}}{|\beta^2-1|^{1/4}}\{\frac{1}{2t^{1/3}}\left[e^{i\pi/6}\mathrm{Ai}(e^{2i\pi/3}\gamma^2t^{2/3})+e^{5i\pi/6}\mathrm{Ai}(e^{-2i\pi/3}\gamma^2t^{2/3})\right] \\ &\pm\frac{1}{2\gamma t^{2/3}}\left[e^{-\pi/6}\mathrm{Ai}'(e^{2i\pi/3}\gamma^2t^{2/3})+e^{-5i\pi/6}\mathrm{Ai}'(e^{-2i\pi/3}\gamma^2t^{2/3})\right]\} \end{aligned} \tag{B.41}$$

We implement (B.25), (B.40) and (B.41) with Mathematica or C++ to get the numerical values of the time-dependent wave functions.